Julius-Maximilians-
UNIVERSITÄT
WÜRZBURG

Phenomenology of electroweak Spin-1 Resonances in Composite Higgs Models

Mass bounds in the coset SU(5)/SO(5)

Jan Hadlik

A thesis presented for the degree of
Master of Science in Physics

Submission: 01.08.2024
Supervisor: Prof. Dr. Werner Porod

Lehrstuhl für Theoretische Physik II
Institut für Theoretische Physik und Astronomie
Julius-Maximilians-Universität Würzburg

Abstract

We investigate electroweak vector and axial-vector resonances in composite Higgs models, concentrating on the phenomenology within the minmal coset SU(5)/SO(5). A comprehensive theoretical background of composite Higgs models is provided and we construct the effective Lagrangian for the Spin-0 and Spin-1 resonances using the Callan-Coleman-Zumino-Wess formalism and the hidden symmetry approach. We identify a subset of vector resonances which can be singly produced in the s-channel, suitable for deriving constraints on the vector mass parameter M_V. Benchmark scenarios for the branching ratios are defined which are used to get very robust exclusion bounds by combining multiple experimental searches from current LHC data. Additionally, we discuss the pair production of a double charged axial vector, from which independent bounds on the axial mass parameter M_A are obtained.

Zusammenfassung

Vektor- und Axialvektor-Resonanzen in "Composite-Higgs-Modellen" werden untersucht mit speziellem Fokus auf Phänomenologie innerhalb der Quotientengruppe SU(5)/SO(5). Wir präsentieren einen umfassenden theoretischen Hintergrund der Composite-Higgs-Modelle und konstruieren die effektive Lagrangedichte für Spin-0- und Spin-1-Resonanzen unter Verwendung des Callan-Coleman-Zumino-Wess-Formalismus und "Hidden Symmetry". Im Folgenden werden Vektorresonanzen identifiziert, welche im s-Kanal einzeln produziert werden können und sich dazu eignen untere Grenzen für den Vektormassenparameter M_V herzuleiten. Benchmarkszenarien für die Zerfallskanäle der Vektoren werden definiert, um sehr robuste Ausschlussgrenzen zu erhalten. Dabei kombinieren wir mehrere experimentelle Limits aus aktuellen LHC-Daten. Zusätzlich diskutieren wir die Paar-Produktion eines doppelt geladenen Axialvektors, aus der unabhängige Grenzen für den Axialmassenparameter M_A abgeleitet werden.

Contents

1 Motivation

In 2012, the Large Hadron Collider (LHC) discovered the Higgs boson [1, 2], the last missing particle of the Standard Model (SM). Its confirmation poses significant questions about the dynamical origin of electroweak (EW) symmetry breaking [3–5]. How is the Higgs mass of 125 GeV stabilized against radiative corrections? Why is there a hierarchy among the fermion masses?
To discuss possible solutions, we first need to take one step back. The SM can not be the ultimate description of nature as it lacks several features, such as neutrino masses, dark matter and a quantum description of gravity. Therefore, the SM must be treated as an effective field theory valid only up to some energy scale Λ_{SM}. Assuming we know the high energy Lagrangian, the effective SM Lagrangian at the scale Λ_{SM} results from integrating out heavy dynamics.
At least above the Planck mass at $E \approx 10^{19}\,\text{GeV}$, new physics must emerge to avoid infinities in a quantum theory of gravity. But more importantly, new physics do not need to arise only at the Planck scale. Instead, there might be an explanation how to dynamically generate the Higgs potential, which leads to EW symmetry breaking, right around the corner.
If we assume to know the full model of EW symmetry breaking the Higgs mass can be calculated as [6]

$$m_H^2 = \int_0^{\Lambda_{SM}} \mathrm{d}E \frac{\mathrm{d}m_H^2}{\mathrm{d}E} + \int_{\Lambda_{SM}}^{\infty} \mathrm{d}E \frac{\mathrm{d}m_H^2}{\mathrm{d}E} = \delta_{\text{SM}} m_H^2 + \delta_{\text{BSM}} m_H^2 \,, \tag{1.1}$$

where E is the energy of virtual particles in loop diagrams contributing to the Higgs mass. The integral is split around the SM cutoff, yielding two completely independent contributions. We can estimate the first part from SM diagrams integrating up to Λ_{SM}, but know nothing about the Beyond the Standard Model (BSM) contributions. The Naturalness problem [7, 8] arises in the following form: We know that the SM contribution are $\propto \Lambda_{\text{SM}}^2$ and get very large for a high cutoff. The BSM contributions must cancel these large contributions with high precision to achieve the measured light Higgs mass. This fine-tuning Δ can be parameterized as [6]

$$\Delta \geq \frac{\delta_{\text{SM}} m_H^2}{m_H^2} = \frac{3 y_t^2}{8\pi^2} \left(\frac{\Lambda_{\text{SM}}}{m_H} \right)^2 \approx \left(\frac{\Lambda_{\text{SM}}}{450\,\text{GeV}} \right)^2 , \tag{1.2}$$

considering only the top loop contribution of the SM. In order to be able to predict the Higgs mass from an underlying UV model, the cutoff scale can not be much above the TeV scale. The Higgs mass has a special role, because it is the only term in the SM where quadratic divergences can appear.
Composite Higgs models offer one solution to stabilize the Higgs mass against higher scales. If the Higgs is a composite particle with size $l_H = 1/m^* \sim 1/\text{TeV}$, the integrand in eq. (1.1) has a natural cutoff.
Loosely speaking, this idea originates from Quantum Chromo Dynamics (QCD), where all known scalars are actually composite states made of two quarks bound by the strong force. Similarly, the Higgs particle might also emerge as a composite state bound by a new strong force with a higher confinement scale m^*.
The earliest models of this type are known as technicolor [8, 9]. These models consist of two sectors:

an elementary sector, which includes matter fermions and gauge bosons, and an additional composite sector, which contains hyperquark fermions. The composite sector shall be invariant under the symmetry group $\mathcal{G}$ in the UV. The condensation of underlying hyperquarks breaks the EW symmetry and gives raise to technipions with a decay constant f_T, giving mass to the gauge bosons $m_W = g f_T/2$. In those models, the decay constant is at the EW scale $f_T \approx \mathrm{v}$. It turns out that the model predicts a scalar resonance significantly heavier than the Higgs and there are also problems explaining the large third generation quark masses [10]. As in QCD, we would also expect further technihadrons and vectorial resonances with masses not too far from the condensation scale [11].
Modern Composite Higgs models (CHM) are based on the same underlying idea, but we will introduce an additional energy scale. At a scale m^* the global group $\mathcal{G}$ spontaneously breaks to $\mathcal{H}$ yielding massless Goldstones with decay constant f in the coset. Gauge interactions of the elementary sector with the composite one explicitly break $\mathcal{G}$ and turn the Goldstones into massive pseudo Nambu–Goldstone Bosons (pNGBs). Loops of SM fermions, gauge bosons and hyperquark mass terms will generate a Higgs potential, which then allows for EW symmetry breaking. Here, the EW scale is generated dynamically and can be smaller than f. The composite Higgs thus can be naturally lighter than the other resonances.
The ratio $\mathrm{v}/f = \sin\theta \ll 1$ is determined by the orientation of the SM vacuum with respect to the "true" vacuum [11]. A very small θ scales up the masses of other resonances and suppresses corrections to EW precision measurements, such as the Peskin–Takeuchi parameters [12]. However, to avoid the Naturalness problem, the misalignment angle θ shouldn't be too small. Today, some degree of fine-tuning seems necessary due to experimental constraints, but new physics may still emerge at the lower multi-TeV scale [12, 13].
There will be further composite resonances besides Spin-0, formed by two or more fermions. In this thesis, we will focus on Spin-1 resonances that emerge in the electroweak sector. These are excited composite states of two hyperfermions, similar to the ρ mesons in QCD. We begin in chapter 2 with a summary of the techniques and methods required to construct the Lagrangian and motivate the minimal coset SU(5)/SO(5), which is discussed in more detail in chapter 3. In chapter 4, constraints on the parameter space are derived by comparison with up-to-date ATLAS and CMS searches.

2 Composite Higgs Models

This chapter shall give an overview on the theoretical background needed to work with a specific CHM. First, the general idea is described before we go into more details on how to construct the Lagrangian involving pNGBs and Spin-1 resonances in sec. 2.2 and sec. 2.3.

2.1 Goldstone boson Higgs

The underlying idea of CHM is to describe the Higgs boson as a Goldstone boson, emerging from spontaneous symmetry breaking of $\mathcal{G}$ to the subgroup $\mathcal{H}$. The breaking shall happen at the confinement scale m^* where, due to the Goldstone theorem [14], for each broken generator in the coset $\mathcal{G}/\mathcal{H}$ one massless scalar forms. As discussed in chapter 1, this confinement scale is bound to the multi-TeV range from below by SM precision measurements and from above by the Naturalness argument.
We call the EW symmetry preserving vacuum Σ_0. It can be used to split the generators T^A of $\mathcal{G}$ into unbroken T^a and broken generators X^j [15, 16]

$$T^a\Sigma_0 + \Sigma_0(T^a)^T = 0, \qquad X^j\Sigma_0 - \Sigma_0(X^j)^T = 0\,. \tag{2.1}$$

With a slight abuse of notation, we define the pNGB matrix as

$$\Pi = \pi^j X^j\,, \tag{2.2}$$

containing one scalar π^j for each broken generator. The global group $\mathcal{G}$ is also explicitly broken due to mass terms of the hyperquarks and gauging the hyperquarks only under the SM subgroup. In consequence, this does also lead to mass terms for the Higgs boson and other scalars. That means we are left with a set of massive pNGBs but can also expect further composite states with higher Spin similar to the Hadrons in QCD. Leading order expressions of the potential and arising mass terms for the pNGBs were discussed e.g. in [16, 17].
In this work, all fields will be defined with respect to the "true" vacuum which is misaligned by the angle θ and breaks the EW symmetry [18]

$$\tilde{\Sigma}_0 = \Omega(\theta)\cdot\Sigma_0\cdot\Omega^T(\theta)\,. \tag{2.3}$$

The misaligned generators still need to fulfill eq. (2.1) from which it's easy to derive

$$\tilde{T}^a = \Omega(\theta)\cdot T^a\cdot\Omega(\theta)^\dagger\,, \qquad \tilde{X}^j = \Omega(\theta)\cdot X^j\cdot\Omega(\theta)^\dagger\,, \tag{2.4}$$

leading to

$$\begin{aligned}
&\tilde{T}^A\tilde{\Sigma}_0 \pm \tilde{\Sigma}_0(\tilde{T}^A)^T \\
&= \Omega(\theta)\cdot T^A\cdot\Omega(\theta)^\dagger\Omega(\theta)\cdot\Sigma_0\cdot\Omega^T(\theta) \pm \Omega(\theta)\cdot\Sigma_0\cdot\Omega^T(\theta)\Omega(\theta)^*\cdot(T^A)^T\cdot\Omega(\theta)^T \\
&= \Omega(\theta)\cdot\left(T^A\Sigma_0 \pm \Sigma_0(T^A)^T\right)\cdot\Omega^T(\theta) = 0\,.
\end{aligned} \tag{2.5}$$

The simplest ansatz of misalignment is given by a rotation along the Higgs generator [19]

$$\Omega(\theta) = \mathrm{e}^{i\sqrt{2}\langle\Pi\rangle/f} = \mathrm{e}^{i\sqrt{2}X_h\theta}\,. \tag{2.6}$$

Here, we assume that only the Higgs develops a non-zero vacuum expectation value (VEV), which encodes EW symmetry breaking. In general, the other pNGBs might also get a non-zero VEV. If this is the case we should choose a more general misalignment in order to minimize the potential and rotate into the "true" vacuum [18].
Studying fluctuations around the misaligned vacuum, we have to consider all degrees of freedom (DOF) of the coset, accumulated by the Goldstone matrix U defined with the misaligned pNGB matrix $\tilde{\Pi}$

$$U = \exp\left(\frac{i\sqrt{2}}{f}\sum \pi_j \tilde{X}^j\right) = \mathrm{e}^{i\sqrt{2}/f\tilde{\Pi}} = \mathrm{e}^{\tilde{\Pi}'}\,, \tag{2.7}$$

which will play a central role in constructing invariant terms for the Lagrangian. Here, f is the decay constant of the pNGBs

$$f = \mathrm{v}\sin\theta\,, \tag{2.8}$$

and the numerical prefactor in the exponent of U is chosen such, that the pNGBs are canonically normalized.

2.2 CCWZ construction

The Callan-Coleman-Wess-Zumino (CCWZ) construction is named after the authors of the two papers [20, 21] from 1969. It can be used for general low-energy effective Lagrangians involving symmetry breaking(s). The benefits include its independence from specific details of the model, such as the representation r_π of the Goldstones. For the following explanations, we will follow roughly chapter 2.3 of [6].
If a global symmetry is spontaneously broken, a massless, scalar Goldstone field occurs for each broken generator. The Goldstone matrix (2.7) does occupy all those physical degrees of freedom with respect to the vacuum.
The underlying high-energy theory must be invariant under transformations of the full symmetry group $\mathcal{G}$. Therefore we take a look at how U transforms under $g \in \mathcal{G}$. The group element can be split into broken X^j and unbroken T^a generators

$$g[\alpha] = \exp\left(i\alpha_A T^A\right) = \exp\left(if_j[\alpha]X^j\right)\cdot\exp\left(if_a[\alpha]T^a\right), \tag{2.9}$$

where the coefficients f_j, f_a are fixed by the commutator relations of the generators. We can decompose their algebra such that

$$[T,T] \sim T\,,\ [X,T] \sim X\,,\ [X,X] \sim T \tag{2.10}$$

where we used the fact that $\mathcal{H}$ is a subgroup for the first two relations and the last one defines the coset to be called symmetric, which is the case for the models we are interested in.
When acting with g on the Goldstone matrix, we can decompose the operator again into two exponentials

$$g\cdot U[\Pi] = U[\Pi^{(g)}]\cdot h[\Pi;g]\,, \tag{2.11}$$

$$U[\Pi^{(g)}] = g\cdot U[\Pi]\cdot h^{-1}[\Pi;g]\,, \tag{2.12}$$

where $h[\Pi; g] \in \mathcal{H}$ is an element of the unbroken subgroup and depends on Π.
$U[\Pi^{(g)}]$ is the exponential of all broken generators which implicitly defines the non-linear transformed Goldstone fields $\Pi^{(g)}$. Their transformation law is in general highly complicated, while the transformation law of $U[\Pi]$ is fairly simple. From eq. (2.12) we can see that U transforms as a tensor with one index in $\mathcal{G}$ and the other in $\mathcal{H}$.
Before going on, we take a look at the appearing representations when breaking $\mathcal{G}$. The generator algebra decomposes under $\mathcal{H}$ as

$$\mathbf{Ad}_{\mathcal{G}} = \mathbf{Ad}_{\mathcal{H}} \oplus \mathbf{r}_{\pi}\,, \tag{2.13}$$

where $\mathbf{r}_{\pi}$ is the representation of the Goldstones under $\mathcal{H}$.
Working out the expanded transformation of Π_j for the broken generators $g_{\mathcal{G}/\mathcal{H}} = \mathbb{1} + i\alpha_j X^j$ leads to [6]

$$\Pi_j^{(g_{\mathcal{G}/\mathcal{H}})} = \Pi_j + \frac{f}{\sqrt{2}}\alpha_j + \mathcal{O}\left(\frac{\Pi^2}{f}\right)\,. \tag{2.14}$$

Due to the constant term α_j, this is called "shift symmetry". To get a Lagrangian invariant under shifts, non-derivative terms of Π, which could lead to potential terms, are forbidden.
With the help of the Goldstone matrix U one can construct the so-called Maurer-Cartan one-form ω_μ

$$\omega_\mu = iU^{-1}\partial_\mu U\,. \tag{2.15}$$

It can be decomposed into so-called d_μ and e_μ symbols, which are the projections to the broken, respectively unbroken generators

$$\omega_\mu = d_{\mu j}X^j + e_{\mu a}T^a = d_\mu + e_\mu\,. \tag{2.16}$$

Following eq. (2.12) their transformation laws are easily worked out

$$\begin{aligned}
\omega_\mu &\to ih[\pi; g]\cdot U^{-1}g^{-1}g\,\partial_\mu\big(Uh^{-1}[\pi; g]\big)\\
&= h[\pi; g]\cdot\omega_\mu\cdot h^{-1}[\pi; g] + ih[\pi; g]\cdot\partial_\mu\cdot h^{-1}[\pi; g]\,, &(2.17)\\
d_\mu &\to h[\pi; g]\cdot d_\mu\cdot h^{-1}[\pi; g]\,, &(2.18)\\
e_\mu &\to h[\pi; g]\cdot(e_\mu + i\partial_\mu)\cdot h^{-1}[\pi; g]\,. &(2.19)
\end{aligned}$$

We see that d_μ transforms linearly with h like the Goldstone fields and expanding d_μ to first order yields $\propto \partial_\mu\Pi$. But in contrast to simple $\partial_\mu\Pi$ the higher orders in d_μ ensure that it transforms as a complete representation r_π under full $\mathcal{G}$. The e_μ symbol transforms in the adjoint representation of $\mathcal{H}$, see eq. (2.13), so it transforms as if it was a gauge field of a local $\mathcal{H}$ symmetry.
For the pNGBs, all Lagrangian terms invariant under $\mathcal{G}$ can be derived by combinations of d_μ, e_μ and derivatives. The only exceptions are the Wess-Zumino-Witten (WZW) terms based on a global anomaly in $\mathcal{G}$.
The picture gets more interesting if we promote $\mathcal{G}$ to be a local symmetry and introduce gauge fields $F_\mu = F_\mu^A T_A = V_{\mu a}T^a + A_{\mu j}X^j$. The generalization is straight forward by substituting the partial derivative with the covariant one

$$\omega_\mu = iU^{-1}D_\mu U = iU^{-1}\left(\partial_\mu - iF_\mu\right)U\,. \tag{2.20}$$

The $d[\pi, F]$ and $e[\pi, F]$ symbols still transform as before but now under the local group $\mathcal{G}$ and contain pNGBs as well as gauge fields.

We can start to identify all possible operators, which transform homogeneously under $\mathcal{H}$. Those are then used to build Lagrangian terms invariant under $\mathcal{G}$. The simplest operator of this kind is given by the d symbol itself. This operator is the only one available at the order of $\mathcal{O}(p)$ and can be used to construct the $\mathcal{O}(p^2)$ operators

$$d^\dagger_{\mu i} d_{\nu j} : \bar{\mathbf{r}}_\pi \otimes \mathbf{r}_\pi = \mathbf{1}_\mathcal{H} + \mathbf{Adj}_\mathcal{H} + \dots \,, \tag{2.21}$$

where the dots indicate further representations depending on the coset. Notice, that d_μ is actually hermitian.
The orders of p refer to the power counting in chiral expansion, equal to the number of derivatives of pNGBs [22]. The simplest invariant is given by the singlet

$$\mathcal{L}^\pi = \frac{f^2}{4} \operatorname{Tr} d_\mu d^\mu \,, \tag{2.22}$$

which does contain the kinetic term of the Goldstone bosons and mass terms of the axial-vector gauge fields $A_{\mu j}$ at lowest order expansion.
Further, we can act with a suitable covariant derivative on the d symbol, given by [6]

$$(D \cdot d)_{\mu\nu j} = \partial_\mu d_{\nu j} - i e_{\mu a} \big(t^a_\pi\big)^i_j d_{\nu i} \in \mathbf{r}_\pi \,, \tag{2.23}$$

$$(D \cdot d)_{\mu\nu j} \to h[\pi; g] \cdot \big(\partial_\mu d_{\nu j} - i e_{\mu a} \big(t^a_\pi\big)^i_j d_{\nu i}\big) \cdot h[\pi; g]^{-1} \tag{2.24}$$

Furthermore, one can use the fact, that the e symbol transforms as a gauge field to construct its field strength tensor [6]

$$E_{\mu\nu} = E_{\mu\nu a} T^a = i[D_\mu, D_\nu] = \partial_\mu e_\nu - \partial_\nu e_\mu - i[e_\mu, e_\nu] \,, \tag{2.25}$$

$$E_{\mu\nu} \to h[\pi; g] \cdot E_{\mu\nu} \cdot h[\pi; g]^{-1} \,. \tag{2.26}$$

Another possibility might be, dressing the field strength tensor of the gauge fields with Goldstone matrices, such that it transforms as a tensor with indices in $\mathcal{H}$

$$\mathcal{F}_{\mu\nu} = U[\Pi]^{-1} \cdot F_{\mu\nu}[F] \cdot U[\Pi] \tag{2.27}$$

$$= U[\Pi]^{-1} \cdot (\partial_\mu F_\nu - \partial_\nu F_\mu - i[F_\mu, F_\nu]) \cdot U[\Pi] \tag{2.28}$$

$$= \big(\mathcal{F}_{\mathbf{Ad}}\big)_{\mu\nu a} T^a + \big(\mathcal{F}_{\mathbf{r}_\pi}\big)_{\mu\nu j} X^j \,. \tag{2.29}$$

But it turns out that d^2, $D \cdot d$ and E are already all possible independent $\mathcal{O}(p^2)$ operators and it is possible to express $\mathcal{F}$ as [6]

$$\big(\mathcal{F}_{\mathbf{Ad}}\big)_{\mu\nu a} = E_{\mu\nu a} + \big(d^2_{\mathbf{Adj}}\big)_{\mu\nu a} \,, \tag{2.30}$$

$$\big(\mathcal{F}_{\mathbf{r}_\pi}\big)_{\mu\nu j} = \big(D \cdot d\big)_{\mu\nu j} - \big(D \cdot d\big)_{\nu\mu j} \,. \tag{2.31}$$

Here, $d^2_{\mathbf{Adj}}$ is the adjoint contraction of eq. (2.21). The invariant Lagrangian term $\operatorname{Tr} \mathcal{F}_{\mu\nu} \mathcal{F}^{\mu\nu}$, can be simplified by using the cyclicity of the trace to get the well-known kinetic gauge terms $\operatorname{Tr} F_{\mu\nu} F^{\mu\nu}$.

2.3 Hidden symmetry formalism

Apart from the pNGBs, there are also Spin-1 resonances expected, similar to the ρ-meson in QCD. To describe those resonances, we will utilize the Hidden symmetry formalism, which was described in [23, 24], see also [25]. It can be shown that any nonlinear sigma model corresponding to the coset

space $\mathcal{G}/\mathcal{H}$ is gauge equivalent to a linear model of the symmetry $\mathcal{G}_{\text{global}} \times \mathcal{G}_{\text{local}}$.
The global group, in the following $\mathcal{G}_0$, will then be partially gauged to contain the SM gauge bosons[1] W_μ, B_μ, while $\mathcal{G}_{\text{local}} = \mathcal{G}_1$ contains a complete set of heavy spin-1 resonances, which transform as the adjoint of $\mathcal{G}$.
We will use the previous described CCWZ formalism to construct the Lagrangian. Therefore, we define for each group $\mathcal{G}_i$ the covariant derivative of their Goldstone matrix

$$\begin{aligned} D_\mu U_0 &= \big(\partial_\mu - igW_\mu - ig' B_\mu\big) U_0 \,, \\ D_\mu U_1 &= \big(\partial_\mu - i\tilde{g}\mathcal{V}_\mu - i\tilde{g}\mathcal{A}_\mu\big) U_1 \,. \end{aligned} \tag{2.32}$$

The SM bosons are defined with their corresponding non-rotated generators, which ensures that the underlying hyperfermions have quantum numbers under $\mathrm{SU}(2)_\mathrm{L}$ and $\mathrm{U}(1)_Y$ hypercharge

$$B_\mu = B_\mu T^3_R \,, \qquad W_\mu = \sum_i^3 W^i_\mu T^i_L \,. \tag{2.33}$$

The composite Spin-1 resonances are divided into vectors $\mathcal{V}_\mu$ associated to unbroken generators $\tilde{T}^a$, and axial-vectors $\mathcal{A}_\mu$ associated to the broken generators $\tilde{X}^j$

$$\mathcal{V}_\mu = \sum_a \mathcal{V}^a_\mu \tilde{T}^a \,, \qquad \mathcal{A}_\mu = \sum_j \mathcal{A}^j_\mu \tilde{X}^j \,. \tag{2.34}$$

Both copies of $\mathcal{G}_i$ are spontaneously broken to $\mathcal{H}_i$ via the two Goldstones U_i. Next, $\mathcal{H}_0 \times \mathcal{H}_1$ is broken to a diagonal $\mathcal{H}$ where another set of Goldstones k emerge

$$K = \exp\Big(i\sqrt{2} k^a \tilde{T}_a / f_K\Big) \,. \tag{2.35}$$

This K field transforms with one index in each subgroup $\mathcal{H}_i$ [26]

$$K \to h(g_0, \pi_0) K h^\dagger(g_1, \pi_1) \,, \tag{2.36}$$

and its covariant derivative reads

$$D_\mu K = \partial_\mu K - i e_{0\mu} K + i K e_{1\mu} \,. \tag{2.37}$$

The Goldstones in K can be gauged away and provide longitudinal DOF for the vector states $\mathcal{V}_\mu$. Further, a linear combination of the pNGBs π_0 and π_1 provide longitudinal DOF for the axials $\mathcal{A}_\mu$. We can now construct an effective Lagrangian involving the field strengths of the SM gauge bosons and Spin-1 resonances eq. (2.27), contractions of $d_{i\mu}$ symbols, a kinetic K field term and a further invariant contraction using the transformation behavior of K [26]. In the following, we normalize all generators to $\operatorname{Tr} T^a T^b = \delta^{ab}$, because in chapter 3 we will work with 5-dimensional matrix representations of SO(5), which have Dynkin[2] index 1. With this convention, the Lagrangian reads

$$\begin{aligned} \mathcal{L} = &-\frac{1}{4} \operatorname{Tr} W_{\mu\nu} W^{\mu\nu} - \frac{1}{4} B_{\mu\nu} B^{\mu\nu} - \frac{1}{4} \operatorname{Tr} \mathcal{F}_{\mu\nu} \mathcal{F}^{\mu\nu} \\ &+ \frac{f_0^2}{4} \operatorname{Tr} d_{0,\mu} d_0^\mu + \frac{f_1^2}{4} \operatorname{Tr} d_{1,\mu} d_1^\mu + \frac{f_K^2}{4} \operatorname{Tr} D^\mu K \, (D_\mu K)^\dagger + \frac{r f_1^2}{2} \operatorname{Tr} d_{0,\mu} K d_1^\mu K^\dagger \,, \end{aligned} \tag{2.38}$$

[1] We restrict the discussion here to the electroweak sector, but the same formalism can be used in the color sector, gauging with Gluons.

[2] The Dynkin index $I(R)$ of a representation R is defined as $\operatorname{Tr} T^a T^b = \delta^{ab}$. We use the same convention as GroupMath [27], which is that the biggest root of a simple algebra has norm 1. This means that the Fundamentals of SU and Sp have $I(F) = 1/2$.

where we defined the field strength tensors as $F_{\mu\nu} = \partial_\mu F_\nu - \partial_\nu F_\mu - i\tilde{g}[F_\mu, F_\nu]$ and $\mathcal{F}_\mu = \mathcal{V}_\mu + \mathcal{A}_\mu$. The kinetic term of K can be simplified in the unitary gauge $K = 1$ to

$$\frac{f_K^2}{4}\mathrm{Tr}\Big(D^\mu K D_\mu K^\dagger\Big) = \frac{f_K^2}{4}\mathrm{Tr}\Big(e_{0\mu}e_0^\mu - 2e_{0\mu}e_1^\mu + e_{1\mu}e_1^\mu\Big)\,, \tag{2.39}$$

where we used the fact that the e_μ symbol is hermitian.

d and e symbols

The Maurer Cartan form eq. (2.20) of the global sector expanded up to three fields reads

$$\begin{aligned}\omega_{0,\mu} = &\Big(i\partial_\mu\tilde{\Pi}_0' + gW_\mu + g'B_\mu\Big)\\ &-\left(\frac{i}{2}\Big[\tilde{\Pi}_0', \partial_\mu\tilde{\Pi}_0'\Big] + g\Big[\tilde{\Pi}_0', W_\mu\Big] + g'\Big[\tilde{\Pi}_0', B_\mu\Big]\right)\\ &+\frac{1}{2}\left(\frac{i}{3}\Big[\tilde{\Pi}_0', \Big[\tilde{\Pi}_0', \partial_\mu\tilde{\Pi}_0'\Big]\Big] + g\Big[\tilde{\Pi}_0', \Big[\tilde{\Pi}_0', W_\mu\Big]\Big] + g'\Big[\tilde{\Pi}_0', \Big[\tilde{\Pi}_0', B_\mu\Big]\Big]\right) + \dots\,,\end{aligned} \tag{2.40}$$

where the Baker–Campbell–Hausdorff formula was used. Using the commutator structure from eq. (2.10), the $d_{0\mu}$ and $e_{0\mu}$ symbols can be written as

$$\begin{aligned}d_{0,\mu} = &\, i\partial_\mu\tilde{\Pi}_0' + g\tilde{X}(W_\mu) + g'\tilde{X}(B_\mu)\\ &- g\Big[\tilde{\Pi}_0', \tilde{T}(W_\mu)\Big] - g'\Big[\tilde{\Pi}_0', \tilde{T}(B_\mu)\Big]\\ &+ \frac{g}{2}\Big[\tilde{\Pi}_0', \Big[\tilde{\Pi}_0', \tilde{X}(W_\mu)\Big]\Big] + \frac{g'}{2}\Big[\tilde{\Pi}_0', \Big[\tilde{\Pi}_0', \tilde{X}(B_\mu)\Big]\Big] + \frac{i}{3!}\Big[\tilde{\Pi}_0', \Big[\tilde{\Pi}_0', \partial_\mu\tilde{\Pi}_0'\Big]\Big] + \dots\,,\end{aligned} \tag{2.41}$$

$$\begin{aligned}e_{0,\mu} = &\, g\tilde{T}(W_\mu) + g'\tilde{T}(B_\mu)\\ &- g\Big[\tilde{\Pi}_0', \tilde{X}(W_\mu)\Big] - g'\Big[\tilde{\Pi}_0', \tilde{X}(B_\mu)\Big] - \frac{i}{2}\Big[\tilde{\Pi}_0', \partial_\mu\tilde{\Pi}_0'\Big]\\ &+ \frac{g}{2}\Big[\tilde{\Pi}_0', \Big[\tilde{\Pi}_0', \tilde{T}(W_\mu)\Big]\Big] + \frac{g'}{2}\Big[\tilde{\Pi}_0', \Big[\tilde{\Pi}_0', \tilde{T}(B_\mu)\Big]\Big] + \dots\,,\end{aligned} \tag{2.42}$$

with the shorthand notations $\tilde{T}(W_\mu) = W_\mu^i\mathrm{Tr}\Big(T_L^i\tilde{T}_a\Big)\tilde{T}_a$ and $\tilde{T}(B_\mu) = B_\mu\mathrm{Tr}\Big(T_R^3\tilde{T}_a\Big)\tilde{T}_a$, respectively $\tilde{X}(W_\mu) = W_\mu^i\mathrm{Tr}\Big(T_L^i\tilde{X}_j\Big)\tilde{X}_j$ and $\tilde{X}(B_\mu) = B_\mu\mathrm{Tr}\Big(T_R^3\tilde{X}_j\Big)\tilde{X}_j$. These are the projections of the SM gauge bosons into the subgroup $\mathcal{H}$, respectively into the coset, with respect to the "true" vacuum. In the local copy the expressions are given by

$$d_{1,\mu} = i\partial_\mu\tilde{\Pi}_1' + \tilde{g}\mathcal{A}_\mu - \tilde{g}\Big[\tilde{\Pi}_1', \mathcal{V}_\mu\Big] + \frac{\tilde{g}}{2}\Big[\tilde{\Pi}_1', \Big[\tilde{\Pi}_1', \mathcal{A}_\mu\Big]\Big] + \frac{i}{3!}\Big[\tilde{\Pi}_1', \Big[\tilde{\Pi}_1', \partial_\mu\tilde{\Pi}_1'\Big]\Big] + \dots\,, \tag{2.43}$$

$$e_{1,\mu} = \tilde{g}\mathcal{V}_\mu - \tilde{g}\Big[\tilde{\Pi}_1', \mathcal{A}_\mu\Big] - \frac{i}{2}\Big[\tilde{\Pi}_1', \partial_\mu\tilde{\Pi}_1'\Big] + \frac{\tilde{g}}{2}\Big[\tilde{\Pi}_1', \Big[\tilde{\Pi}_1', \mathcal{V}_\mu\Big]\Big] + \dots\,. \tag{2.44}$$

2.3.1 Physical Pions

Substituting $\tilde{\Pi}_n' = \sqrt{2}i/f_n\tilde{\Pi}_n$ from eq. (2.7), the kinetic pion terms read

$$\mathcal{L}_\pi^{\mathrm{kin}} = \frac{1}{2}\mathrm{Tr}\left(\partial_\mu\tilde{\Pi}_0\partial_\mu\tilde{\Pi}_0 + \partial_\mu\tilde{\Pi}_1\partial_\mu\tilde{\Pi}_1 + 2r\frac{f_1}{f_0}\partial_\mu\tilde{\Pi}_1\partial_\mu\tilde{\Pi}_0\right)\,. \tag{2.45}$$

Obviously, those are not yet proper kinetic terms due to the $\propto r$ term. This is why one has to redefine the pNGBs into π_A and π_B

$$\begin{aligned}\pi_0^j &= \frac{\pi_A^j}{\sqrt{2}\sqrt{1+rf_1/f_0}} - \frac{\pi_B^j}{\sqrt{2}\sqrt{1-rf_1/f_0}}\,,\\ \pi_1^j &= \frac{\pi_A^j}{\sqrt{2}\sqrt{1+rf_1/f_0}} + \frac{\pi_B^j}{\sqrt{2}\sqrt{1-rf_1/f_0}}\,,\end{aligned} \tag{2.46}$$

to get

$$\begin{aligned}\mathcal{L}_\pi^{\text{kin}} &= \frac{1}{2}\left(\frac{\partial_\mu\pi_A^j\partial_\mu\pi_A^j}{1+rf_1/f_0} + \frac{\partial_\mu\pi_B^j\partial_\mu\pi_B^j}{1-rf_1/f_0} + \frac{rf_1}{f_0}\left[\frac{\partial_\mu\pi_A^j\partial_\mu\pi_A^j}{1+rf_1/f_0} - \frac{\partial_\mu\pi_B^j\partial_\mu\pi_B^j}{1-rf_1/f_0}\right]\right)\\ &= \frac{1}{2}\left(\partial_\mu\pi_A^j\partial_\mu\pi_A^j + \partial_\mu\pi_B^j\partial_\mu\pi_B^j\right)\,.\end{aligned} \tag{2.47}$$

The fields π_A, π_B have potential mixing terms with the axial vectors derived from

$$\begin{aligned}\frac{f_1^2}{4}d_{1\mu}d_1^\mu + \frac{rf_1^2}{2}d_{0\mu}d_1^\mu &\supset -\frac{\tilde{g}}{\sqrt{2}}\left(f_1\,\mathrm{Tr}\,\partial^\mu\tilde{\Pi}_1\mathcal{A}_\mu + \frac{rf_1^2}{f_0}\,\mathrm{Tr}\,\partial^\mu\tilde{\Pi}_0\mathcal{A}_\mu\right)\\ &= -\frac{\tilde{g}f_1}{2}\left(\sqrt{1+rf_1/f_0}\,\mathrm{Tr}\,\partial^\mu\tilde{\Pi}_A\mathcal{A}_\mu + \sqrt{1-rf_1/f_0}\,\mathrm{Tr}\,\partial^\mu\tilde{\Pi}_B\mathcal{A}_\mu\right)\,.\end{aligned} \tag{2.48}$$

For physical pNGBs they have to vanish obviously. As mentioned before, one linear combination π_U are eaten by the longitudinal DOF of the axial vectors, while the set of physical pNGBs π_P remain in the spectrum. With the ansatz

$$\begin{aligned}\pi_A^j &= \cos\alpha\cdot\pi_P^j - \sin\alpha\cdot\pi_U^j\,,\\ \pi_B^j &= \sin\alpha\cdot\pi_P^j + \cos\alpha\cdot\pi_U^j\,,\end{aligned} \tag{2.49}$$

and requiring that the quadratic terms of $\mathcal{A}_\mu$ and π_P vanish, we derive the condition

$$\tan\alpha = -\sqrt{\frac{1+rf_1/f_0}{1-rf_1/f_0}}\,. \tag{2.50}$$

Combining eq. (2.46) and eq. (2.49) gives the final transformation

$$\pi_0^j = \frac{f_0}{f}\pi_P^j\,,\qquad \pi_1^j = \pi_U^j - \frac{rf_1}{f}\pi_P^j\,, \tag{2.51}$$

with the pNGB decay constant

$$f = \sqrt{f_0^2 - r^2f_1^2}\,. \tag{2.52}$$

2.3.2 $\mathcal{V}\pi\pi$ coupling

Having defined the transformation laws for physical pNGBs in eq. (2.51), we can take a look at the coupling parameter $g_{V\pi\pi}$ of the vectors $\mathcal{V}_\mu$ to two physical pNGBs. In principle, this parameter can be calculated on a lattice as it was done for QCD in [28], and it has a physical interpretation.

There is only one independent operator structure in the Lagrangian[3]. Collecting all terms results in

$$\begin{aligned}\mathcal{L}_{\mathcal{V}\pi\pi} &= i\tilde{g}\Big[\mathrm{Tr}\left(\partial_\mu\tilde{\Pi}_1\left[\tilde{\Pi}_1,\mathcal{V}_\mu\right]\right)+\frac{f_K^2}{2f_1^2}\mathrm{Tr}\left(\mathcal{V}_\mu\left[\tilde{\Pi}_1,\partial_\mu\tilde{\Pi}_1\right]\right)\\ &\quad-\frac{f_K^2}{2f_0^2}\,\mathrm{Tr}\left(\mathcal{V}_\mu\left[\tilde{\Pi}_0,\partial_\mu\tilde{\Pi}_0\right]\right)+\frac{rf_1}{f_0}\mathrm{Tr}\left(\partial_\mu\tilde{\Pi}_0\left[\tilde{\Pi}_1,\mathcal{V}_\mu\right]\right)\Big]\\ &= \frac{i\tilde{g}}{f^2}\left[f_1^2r^2+\frac{f_K^2r^2}{2f^2}-\frac{f_K^2}{2f^2}-f_1^2r^2\right]\mathrm{Tr}\left(\mathcal{V}_\mu\left[\tilde{\Pi}_P,\partial_\mu\tilde{\Pi}_P\right]\right)\\ &= \frac{i}{2}g_{V\pi\pi}\cdot\mathrm{Tr}\left(\mathcal{V}_\mu\left[\tilde{\Pi}_P,\partial_\mu\tilde{\Pi}_P\right]\right)=ig_{V\pi\pi}\cdot\frac{f_{ija}}{2}\mathcal{V}_\mu^a\pi_P^i\pi_P^j\,,\end{aligned}\tag{2.53}$$

where f_{ija} is the SU(5) structure constant and we defined the Vector-pNGB-pNGB coupling as

$$g_{V\pi\pi}=\frac{\tilde{g}f_K^2(r^2-1)}{f^2}\,,\tag{2.54}$$

which coincides with the definition in [29].

2.4 Partial Compositeness

An important attribute of the Higgs in the SM is its role in generating the masses of all fermions through Yukawa couplings. We can naively write down an SM inspired operator for the top quark of the form

$$\frac{\lambda_t}{\Lambda_{\mathrm{UV}}^{d-1}}\bar{t}_L\mathcal{O}_S^c t_R\,,\tag{2.55}$$

with $\mathcal{O}_S$ a composite scalar operator with the same quantum numbers as the Higgs field. Examining the prefactor, the interaction strength is determined by the dimension of the scalar operator. The dimensionless coefficient λ_t depends on the underlying microscopic theory and can be expected to be of order one [6]. The corresponding Yukawa coupling below the confinement scale m^* would be given by

$$y_t\simeq\lambda_t[m^*]\simeq\lambda_t\left(\frac{m^*}{\Lambda_{\mathrm{UV}}}\right)^{d-1}\,,\tag{2.56}$$

where d should be at least two to prevent any further Naturalness problem[4]. But now it is difficult to describe a realistic top Yukawa coupling of the order one. We end up with an upper bound on the UV scale[5], which will be far too low to suppress SM operators with dimension > 4.
A solution to generate realistic Yukawas in CHM without relying on special selection rules is the so-called Partial Compositeness hypothesis [30]. The matter fermions are described again external to the composite sector but couple via linear interaction terms of the form

$$\mathcal{L}_{\mathrm{int}}=\frac{\lambda_{t_L}}{\Lambda_{\mathrm{UV}}^{d_L-5/2}}\bar{t}_L\mathcal{O}_F^L+\frac{\lambda_{t_R}}{\Lambda_{\mathrm{UV}}^{d_R-5/2}}\bar{t}_R\mathcal{O}_F^R+\dots\,,\tag{2.57}$$

[3] It is easy to show that $\mathrm{Tr}(\partial_\mu\Pi[\Pi,\mathcal{V}^\mu])=-\mathrm{Tr}(\mathcal{V}^\mu[\Pi,\partial_\mu\Pi])$

[4] A scalar operator with dimension 1 would be an elementary scalar, which we must avoid to get rid of the Naturalness problem.

[5] The confinement scale m^* is already bound to the multi-TeV scale due to Naturalness, see chapter 1.

where "..." includes analogous terms for all other SM quarks. These vertices lead to mass mixing in the Infrared (IR) between the elementary quarks and the fermionic composite resonances $\mathcal{O}_F$. The physical eigenstates are given by a linear combination. If the operator dimensions are $d \sim 5/2$, we can have a large Ultraviolet (UV) scale $\Lambda_{\mathrm{UV}} \gg m^*$ and still get a large top Yukawa coupling

$$\lambda_{t_L}[m^*] \simeq \lambda_{t_L} \left(\frac{m^*}{\Lambda_{\mathrm{UV}}} \right)^{d-5/2} . \tag{2.58}$$

In principle, a fermionic operator is only bound to $d \geq 3/2$ and there is no obstruction against having $d \approx 5/2$.
Our notations used above refers directly to the top quark, because it has by far the largest Yukawa coupling, which might originate from a large mixing with the so-called "top partners" T. In general, the different flavors might couple to operators of different dimensions $d \geq 5/2$, which could explain the mass hierarchy. For all such operators, no further Naturalness problem will be reintroduced, because $|\mathcal{O}_F|^2 \gtrsim 5$.
The top partners T shall be vector-like, such that they can have a Dirac mass term [11]

$$\mathcal{L} = \bar{t}_L i\not{\partial} t_L + \bar{T}_L (i\not{\partial} - m) T_L + \frac{\lambda_{t_L}}{\Lambda_{\mathrm{UV}}^{d_L - 5/2}} \bar{t}_L T_L + \text{h.c.} . \tag{2.59}$$

The mass matrix can be diagonalized yielding (for now) massless SM quarks

$$t_L^{\mathrm{phys}} = \cos\phi_L t_L + \sin\phi_L T_L . \tag{2.60}$$

The mixing angle ϕ_L determines the degree of compositeness. The SM fermions get their mass entirely from their composite components T, which have Yukawa-like interactions with the pNGBs in the composite sector generating Yukawa couplings of the form

$$Y^* \sin\phi_L \sin\phi_R , \tag{2.61}$$

where Y^* is a Yukawa coupling within the composite sector [11]. From here, it is obvious that heavier SM fermions as the top quark can be described with a larger degree of compositeness, while the light quarks and leptons do barely mix.
The standard approach to construct fermionic top partners are baryons built from three hypercolor fermions, which have dimension $9/2$.[6] Those states need to pick up a large anomalous dimension, taking them from $9/2$ towards $5/2$ [31].
Contrary to the considerations in sec. 2.2, the specific implications of partial compositeness depend on the details of the model, how the SM fermions are embedded in $\mathcal{G}$ and under which representation the top partners transform.
With regard to Spin-1 resonances we highlight that there can be partial compositeness contributions to the coupling to $t\bar{t}$, respectively $t\bar{b}$. These are generated by couplings of the Spin-1 resonances to top partner baryons [29].

2.5 Minimal models

In the previous sections the methods to work with CHM were specified in a very general way, applicable for an arbitrary coset. This section shall address the question how to find realistic models.

[6] Depending on the representation, there is also the possibility of constructing fermionic invariants with dimension $7/2$ [31].

Before all, based on the considerations made in [31–33], we will specify the framework in which we are going to work to constrain the class of models of interest to a set of so-called minimal models. First of all, we will assume a purely fermionic UV completion, without introducing elementary scalars again. Further, a simple hypercolor group G_{HC} shall be considered. We work with left-handed Weyl fermions in the representation $n_1R_1 + ... + n_pR_p$, where R_i is an irreducible representation (irrep) of the G_{HC} and n_i is the number of copies, respectively flavors.
For each R_i, the flavor symmetry is given by $\mathrm{U}(n_i) \sim \mathrm{SU}(n_i) \times \mathrm{U}(1)$. One linear combination of all U(1) induces a Adler-Bell-Jackiw (ABJ) anomaly, which can be associated with a very heavy state. Consequently, the anomaly free global symmetry group is given by $\mathrm{G} = \mathrm{SU}(n_1)\times...\times\mathrm{SU}(n_p)\times\mathrm{U}(1)^{p-1}$. For simplicity, we will limit the discussion to the $p = 2$ case in the following, as it already contains all important aspects, yielding $\mathcal{G} = \mathrm{SU}(m) \times \mathrm{SU}(n) \times \mathrm{U}(1)$ with two classes of fermions $\psi \in mR_1$ and $\chi \in nR_2$. The group $\mathrm{SU}(m)$ shall describe the electroweak sector, containing $\mathrm{SU}(2)_L \times \mathrm{SU}(2)_R$, whereas $\mathrm{SU}(n)$ contains the color sector.
Next, we will discuss prerequisites and constraints which need to be fulfilled by this type of models. An important condition is the possibility of allowing a breaking chain via $G_{\mathrm{mid}} = \mathrm{SU}(3)_{\mathrm{c}} \times \mathrm{SU}(2)_{\mathrm{L}} \times \mathrm{SU}(2)_{\mathrm{R}} \times \mathrm{U}(1)_X$ down to the SM group $G_{\mathrm{SM}} = \mathrm{SU}(3)_c \times \mathrm{SU}(2)_{\mathrm{L}} \times \mathrm{U}(1)_{\mathrm{Y}}$. The additional $\mathrm{U}(1)_X$ in G_{mid} is used to obtain the correct hypercharge values $Y = T_R^3 + X$ for the fermions. Further, we demand the existence of a suitable Higgs candidate within the electroweak coset $\mathcal{G}/\mathcal{H} \ni (1, 2, 2)_0$ of G_{mid}. Moreover, G_{SM} shall not contain any 't Hooft anomalies, such that we can gauge it and couple hypercolor fermions to the SM.
We also want to take into account the possibility of top partners to explain the large top quark mass, as briefly oulined in sec. 2.4. This yields restrictions on the representation of three fermion bound states, which will play the role of potential top partners.
As we already mentioned in sec. 2.4, they also need to get a large anomalous dimension. This can be achieved if the theory is conformal in the UV. But in the IR it needs to be strongly interacting, otherwise a condensate can not form. A possible solution are theories which are brought into the conformal window only by adding heavy hyperfermions, which explicitly break conformal invariance at lower energies [32]. This means, we search for an asymptotically free theory, outside of the conformal window. This has to rely on some heuristic arguments, because there is no consensus on how to characterize the conformal region of non-supersymmetric gauge theories outside of the perturbative regime [33].
In the context of minimal models, we are interested only in the smallest n_i such that, for a given set of R_i, all the aforementioned constraints are satisfied.
If we choose R_1 to be a real representation, the condensate $\langle\psi\psi\rangle$, which is proportional to the vacuum of the underlying subgroup, is symmetric. It transforms as the symmetric 2-index representation of $\mathrm{SU}(m)$. This fixes the type of coset to $\mathrm{SU}(m)/\mathrm{SO}(m)$. The smallest subgroup in which the custodial group can be embedded would be $\mathrm{SO}(4) \sim \mathrm{SU}(2) \times \mathrm{SU}(2)$, but the pNGBs of SU(4)/SO(4) would be represented in the 9 of SO(4), equivalent to $(3, 3)$ of $\mathrm{SU}(2)_{\mathrm{L}} \times \mathrm{SU}(2)_{\mathrm{R}}$, which does not contain any Higgs bidoublet. Larger cosets with $m \geq 5$ fulfill the requirements. If R_1 is pseudo-real the condensate is antisymmetric and the coset has to be of the type $\mathrm{SU}(m)/\mathrm{Sp}(m)$ with $m \geq 4$.
For the color sector, the group $\mathrm{SU}(n)$ must contain the subgroup $\mathrm{SU}(3)_c \times \mathrm{U}(1)_X$, which fixes the minimal case to $n = 6$ with subgroups SO(6) or Sp(6).
Further, one is able to restrict the possible hypercolor groups by requiring an asymptotic free theory. It turns out, that the only feasible hypercolor groups are of type $\mathrm{Sp}(N_{\mathrm{HC}})$ or $\mathrm{SO}(N_{\mathrm{HC}})$ [31]. Only if we go to $p > 2$, $\mathrm{SU}(N_{\mathrm{HC}})$ is an option too. The details of these considerations would go beyond the scope of this work and can be found in [31, 33]. In tab. 2.1 all 12 minimal models, classified in [33], are characterized by their hypercolor group G_{HC}, irreps of the underlying Weyl spinors ψ, χ and the

G_{HC}	ψ	χ	EW Coset	Color Coset	Name
SO(7)	$5 \times \mathbf{F}$	$6 \times \mathbf{Spin}$	SU(5)/SO(5)	SU(6)/SO(6)	M1
SO(9)	$5 \times \mathbf{F}$	$6 \times \mathbf{Spin}$			M2
SO(7)	$5 \times \mathbf{Spin}$	$6 \times \mathbf{F}$			M3
SO(9)	$5 \times \mathbf{Spin}$	$6 \times \mathbf{F}$			M4
Sp(4)	$5 \times \mathbf{A}_2$	$6 \times \mathbf{F}$	SU(5)/SO(5)	SU(6)/Sp(6)	M5
SU(4)	$5 \times \mathbf{A}_2$	$3 \times (\mathbf{F}, \overline{\mathbf{F}})$	SU(5)/SO(5)	SU(6)/SO(6)	M6
SO(10)	$5 \times \mathbf{F}$	$3 \times (\mathbf{Spin}, \overline{\mathbf{Spin}})$			M7
Sp(4)	$4 \times \mathbf{F}$	$6 \times \mathbf{A}_2$	SU(4)/Sp(4)	SU(6)/SO(6)	M8
SO(11)	$4 \times \mathbf{Spin}$	$6 \times \mathbf{F}$			M9
SO(10)	$4 \times (\mathbf{Spin}, \overline{\mathbf{Spin}})$	$6 \times \mathbf{F}$	$\text{SU(4)}^2/\text{SU(4)}$	SU(6)/SO(6)	M10
SU(4)	$4 \times (\mathbf{F}, \overline{\mathbf{F}})$	$6 \times \mathbf{A}_2$			M11
SU(5)	$4 \times (\mathbf{F}, \overline{\mathbf{F}})$	$3 \times (\mathbf{A}_2, \overline{\mathbf{A}_2})$	$\text{SU(4)}^2/\text{SU(4)}$	$\text{SU(3)}^2/\text{SU(3)}$	M12

Table 2.1: Classification of minimal CHM structured by their cosets, based on [33]. **F**, **Spin** and $\mathbf{A}_2$ refers to the fundamental, spinor and 2-index antisymmetric hypercolor irrep of the fermions.

corresponding breaking patterns. All listed models are "vector-like" in the way that mass terms can be added for each Spinor and no $\langle\psi\chi\rangle$ condensate will form.
In the following, the electroweak coset SU(5)/SO(5) will be studied in more detail, which is part of the models M1 to M7.

3 Electroweak $SU(5)/SO(5)$ Coset

After providing a brief overview of possible minimal cosets in sec. 2.5, we will now focus on the coset SU(5)/SO(5), which is realized as the electroweak sector in the models M1-M7 according to the classification in [33].

3.1 Vacuum structure & Particle content

Early work on this coset can be found in [34], whereas also more recently the scalars were studied e.g. in [35, 36]. Here, we will follow the presentation given in [18].
The reference vacuum Σ_0 has to transform as a real two-index symmetric representation of SU(5) and shall keep the EW symmetry unbroken

$$\Sigma_0 = \begin{pmatrix} 0 & i\sigma_2 & \\ -i\sigma_2 & 0 & \\ & & 1 \end{pmatrix} = \begin{pmatrix} 0 & 0 & 0 & 1 & 0 \\ 0 & 0 & -1 & 0 & 0 \\ 0 & -1 & 0 & 0 & 0 \\ 1 & 0 & 0 & 0 & 0 \\ 0 & 0 & 0 & 0 & 1 \end{pmatrix}, \tag{3.1}$$

where in general the sign of the entry in the lower right could have been chosen differently. The generators of the custodial symmetry group $\mathrm{SU(2)_L} \times \mathrm{SU(2)_R}$ are embedded into SU(5) as

$$T_L^i = \frac{1}{2}\begin{pmatrix} \mathbb{1}_2 \otimes \sigma^i & \\ & 0 \end{pmatrix}, \qquad T_R^i = \frac{1}{2}\begin{pmatrix} \sigma^i \otimes \mathbb{1}_2 & \\ & 0 \end{pmatrix}, \tag{3.2}$$

with $\mathrm{Tr}\big(T^i T^j\big) = \delta^{ij}$. The unbroken T^a and broken X^j generators can be determined from eq. (2.1). As stated in sec. 2.1, we rotate the vacuum along the Higgs generator X^h with

$$X^h = \frac{1}{2}\begin{pmatrix} & & & & 0 \\ & & & & 1 \\ & & & & -1 \\ & & & & 0 \\ 0 & 1 & -1 & 0 & \end{pmatrix}. \tag{3.3}$$

The rotation matrix $\Omega = \exp\big(i\sqrt{2}X_h\theta\big)$ defined in eq. (2.6), reads

$$\Omega(\theta) = \begin{pmatrix} 1 & 0 & 0 & 0 & 0 \\ 0 & c_{\theta/2}^2 & s_{\theta/2}^2 & 0 & is_\theta/\sqrt{2} \\ 0 & s_{\theta/2}^2 & c_{\theta/2}^2 & 0 & -is_\theta/\sqrt{2} \\ 0 & 0 & 0 & 1 & 0 \\ 0 & is_\theta/\sqrt{2} & -is_\theta/\sqrt{2} & 0 & c_\theta \end{pmatrix}, \tag{3.4}$$

with the shorthand notations $s_\theta = \sin\theta$ and $c_\theta = \cos\theta$. The resulting misaligned vacuum eq. (2.3) is given by

$$\tilde{\Sigma}_0 = \begin{pmatrix} 0 & 0 & 0 & 1 & 0 \\ 0 & -s_\theta^2 & -c_\theta^2 & 0 & is_{2\theta}/\sqrt{2} \\ 0 & -c_\theta^2 & -s_\theta^2 & 0 & -is_{2\theta}/\sqrt{2} \\ 1 & 0 & 0 & 0 & 0 \\ 0 & is_{2\theta}/\sqrt{2} & -is_{2\theta}/\sqrt{2} & 0 & c_{2\theta} \end{pmatrix}. \tag{3.5}$$

Following the prescription in sec. 2.3, the symmetry group gets extended to $\mathrm{SU}(5)_0 \times \mathrm{SU}(5)_1$, where each pNGB matrix $\Pi_{0,1}$ contains $\dim(\mathrm{SU}(5)) - \dim(\mathrm{SO}(5)) = 14$ generators. One linear combination, see eq. (2.51), provides mass terms for the 14 axial vectors $\mathcal{A}_\mu$, whereas the other set are physical pNGBs. Further, we have 10 vector resonances $\mathcal{V}_\mu$ which get their mass from the Goldstones in K, see eq. (2.35).

Embeddings

We embed all states with respect to the non-rotated vacuum Σ_0 for simplicity. The rotated expressions used in the Lagrangian are then easily obtained by acting with Ω as in eq. (2.4). Starting with the scalars, the **14** of SO(5) decomposes to $(\mathbf{3},\mathbf{3}) \oplus (\mathbf{2},\mathbf{2}) \oplus (\mathbf{1},\mathbf{1})$ of $\mathrm{SU}(2)_L \times \mathrm{SU}(2)_R$, which can be parameterized as

$$\Pi = \frac{1}{\sqrt{2}} \begin{pmatrix} \frac{\eta}{\sqrt{10}}\mathbb{1}_2 + \pi_0 & \pi_+ & H \\ \pi_- & \frac{\eta}{\sqrt{10}}\mathbb{1}_2 - \pi_0 & -\tilde{H} \\ H^\dagger & -\tilde{H}^\dagger & -\frac{4}{\sqrt{10}}\eta \end{pmatrix}, \tag{3.6}$$

with $\tilde{H} = i\sigma_2 H^*$ and the bitriplets are given by $\pi_0 = (1/\sqrt{2})\,\pi_0^i\sigma_i$, $\pi_- = \pi_-^i\sigma_i = (\pi_+)^\dagger$.
For further use, it is helpful to decompose the $\mathrm{SU}(2)_L \times \mathrm{SU}(2)_R$ representations into the diagonal $\mathrm{SU}(2)_D$. This is suggested by the fact that it is preserved by the color sector vacuum, whereas the hypercharge $\mathrm{U}(1)_Y$ is constructed from generators of both sectors [36]. The scalar states might undergo mass mixing depending on the details of their potential terms. For simplicity, we will ignore

this possibility and assume similar masses of all the pNGBs.
The Higgs bidoublet[1] is given by

$$H = \begin{pmatrix} \phi^+ \\ 1/\sqrt{2}(h + i\phi^0) \end{pmatrix}. \tag{3.7}$$

The bitriplet decomposes to $(\mathbf{3},\mathbf{3}) \to \mathbf{5} \otimes \mathbf{3} \otimes \mathbf{1}$ of $\mathrm{SU}(2)_D$. The transformation laws are taken from sec. A.1 of [37]

$$\begin{aligned} \pi^+_+ = \eta^{++}_5\,, \quad \pi^0_+ = \frac{i\eta^+_3 - \eta^+_5}{\sqrt{2}}\,, \quad \pi^+_0 = \frac{i\eta^+_3 + \eta^+_5}{\sqrt{2}}\,, \\ \pi^0_0 = \frac{\eta^0_1 - \sqrt{2}\eta^0_5}{\sqrt{3}}\,, \quad \pi^-_+ = \frac{\sqrt{2}\eta^0_1 + \eta^0_5 + i\sqrt{3}\eta^0_3}{\sqrt{6}}\,. \end{aligned} \tag{3.8}$$

We use the custodial generators eq. (3.2) to embed the W_μ triplet as

$$W_\mu = \frac{1}{\sqrt{2}} \begin{pmatrix} \frac{1}{\sqrt{2}}W^3_\mu & \tilde{W}^+_\mu & 0 & 0 & \\ \tilde{W}^-_\mu & \frac{-1}{\sqrt{2}}W^3_\mu & 0 & 0 & \\ 0 & 0 & \frac{1}{\sqrt{2}}W^3_\mu & \tilde{W}^+_\mu & \\ 0 & 0 & \tilde{W}^-_\mu & \frac{-1}{\sqrt{2}}W^3_\mu & \\ & & & & 0 \end{pmatrix}. \tag{3.9}$$

As shown in tab. 3.1, he axial vector $\mathcal{A}_\mu$ decomposes identically to the pNGBs and could be embedded in the same way. But to get a real mass mixing matrix, the triplet a_μ is defined with a different phase compared to the scalar triplet ϕ. The explicit expression in terms of $\mathrm{SU}(2)_D$ fields can be found in appendix A. The vector resonances $\mathcal{V}_\mu$ transform as a **10** of SO(5), which decomposes to $(\mathbf{3},\mathbf{1}) \oplus (\mathbf{1},\mathbf{3}) \oplus (\mathbf{2},\mathbf{2})$ of $\mathrm{SU}(2)_\mathrm{L} \times \mathrm{SU}(2)_\mathrm{R}$, see tab. 3.1. From the $(\mathbf{3},\mathbf{1}) \oplus (\mathbf{1},\mathbf{3})$ representation, two linear combinations can be formed that are triplets of $\mathrm{SU}(2)_D$, namely $v_{1\mu}$ and $v_{2\mu}$. In terms of $\mathrm{SU}(2)_D$ representations the vector matrix can be written as

$$\Omega(\theta)^\dagger \cdot \mathcal{V}_\mu \cdot \Omega(\theta) = \frac{1}{\sqrt{2}} \begin{pmatrix} v^0_{1\mu} & \frac{v^+_{1\mu}+v^+_{2\mu}}{\sqrt{2}} & \frac{v^+_{1\mu}-v^+_{2\mu}}{\sqrt{2}} & 0 & -\hat{r}^+_\mu \\ \frac{v^-_{1\mu}+v^-_{2\mu}}{\sqrt{2}} & -v^0_{2\mu} & 0 & \frac{v^+_{1\mu}-v^+_{2\mu}}{\sqrt{2}} & \frac{\hat{r}^0_\mu - i\hat{x}^0_\mu}{\sqrt{2}} \\ \frac{v^-_{1\mu}-v^-_{2\mu}}{\sqrt{2}} & 0 & v^0_{2\mu} & \frac{v^+_{1\mu}+v^+_{2\mu}}{\sqrt{2}} & \frac{\hat{r}^0_\mu + i\hat{x}^0_\mu}{\sqrt{2}} \\ 0 & \frac{v^-_{1\mu}-v^-_{2\mu}}{\sqrt{2}} & \frac{v^-_{1\mu}+v^-_{2\mu}}{\sqrt{2}} & -v^0_{1\mu} & \hat{r}^-_\mu \\ -\hat{r}^-_\mu & \frac{\hat{r}^0_\mu + i\hat{x}^0_\mu}{\sqrt{2}} & \frac{\hat{r}^0_\mu - i\hat{x}^0_\mu}{\sqrt{2}} & \hat{r}^+_\mu & 0 \end{pmatrix}. \tag{3.10}$$

A more detailed derivation is given in appendix A. The notation of a vector resonance with a hat indicates that it does not have mass mixing terms, while the other states mix with the SM gauge bosons as we will see shortly.

[1] Note, that the $\mathrm{SU}(2)_D$ triplet ϕ will not remain in the scalar spectrum because it provides the longitudinal DOF for the SM gauge bosons.

		$\mathrm{SU}(2)_\mathrm{D}$	$\mathrm{SU}(2)_\mathrm{L} \times \mathrm{SU}(2)_\mathrm{R}$	SO(5)
$\mathcal{V}_\mu$	$v_{1\mu}^{0\pm}$	**3**	$(\mathbf{3},\mathbf{1}) \oplus (\mathbf{1},\mathbf{3})$	**10**
	$v_{2\mu}^{0\pm}$	**3**		
	$\hat{r}_\mu^{0\pm}$	**3**	$(\mathbf{2},\mathbf{2})$	
	$\hat{x}_\mu^0$	**1**		
$\mathcal{A}_\mu$	$a_\mu^{0\pm}$	**3**	$(\mathbf{2},\mathbf{2})$	**14**
	$\hat{y}_{2\mu}^0$	**1**		
	$\hat{a}_{5\mu}^{0,\pm,\pm\pm}$	**5**	$(\mathbf{3},\mathbf{3})$	
	$\hat{a}_{3\mu}^{0\pm}$	**3**		
	$\hat{a}_{1\mu}^0$	**1**		
	$\hat{y}_{1\mu}^0$	**1**	$(\mathbf{1},\mathbf{1})$	

Table 3.1: Classification of spin-1 resonances in the coset SU(5)/SO(5) in terms of their quantum numbers w.r.t. SO(5), $\mathrm{SU}(2)_\mathrm{L} \times \mathrm{SU}(2)_\mathrm{R}$ and $\mathrm{SU}(2)_\mathrm{D}$. Particles denoted as $\hat{p}$ do not mix with the SM gauge bosons.

3.2 Vector mass terms

With the explicit expressions of d_μ and e_μ in eqs. (2.41) to (2.44), the quadratic vector terms of the Lagrangian in eq. (2.38) are given by

$$\begin{aligned}\mathcal{L}_\text{mass} = \mathrm{Tr}\Big[&\frac{f_0^2}{4}\left(g\tilde{X}(W_\mu) + g'\tilde{X}(B_\mu)\right)^2 + \frac{f_K^2}{4}\left(g\tilde{T}(W_\mu) + g'\tilde{T}(B_\mu)\right)^2 \\ &+ \frac{f_1^2}{4}\tilde{g}^2\mathcal{A}_\mu^2 + \frac{f_K^2}{4}\tilde{g}^2\mathcal{V}_\mu^2 \\ &+ \frac{r f_1^2}{2}\left(g\tilde{X}(W_\mu) + g'\tilde{X}(B_\mu)\right)\tilde{g}\mathcal{A}^\mu - \frac{f_K^2}{2}\left(g\tilde{T}(W_\mu) + g'\tilde{T}(B_\mu)\right)\tilde{g}\mathcal{V}^\mu\Big]\,. \end{aligned} \tag{3.11}$$

We define the vector mass parameter M_V and axial-vector mass parameter M_A as

$$M_V^2 = \frac{f_K^2\tilde{g}^2}{2}\,, \qquad M_A^2 = \frac{f_1^2\tilde{g}^2}{2}\,. \tag{3.12}$$

The mass entries of the Spin-1 resonances denoted with a hat are diagonal. The vectors have mass M_V coming from the kinetic K term and axial-vectors get mass M_A from the $d_{1\mu}d_1^\mu$ term.
However, the two vector triplets $v_{1\mu}$, $v_{2\mu}$ as well as the axial triplet a_μ mix with the SM gauge

bosons

$$\mathcal{L}^{(\text{mix})}_{\text{mass}} = \left(\tilde{W}^+_\mu,\, a^+_\mu,\, v^+_{1\mu},\, v^+_{2\mu}\right)\mathcal{M}^2_C \begin{pmatrix} \tilde{W}^+_\mu \\ a^+_\mu \\ v^+_{1\mu} \\ v^+_{2\mu} \end{pmatrix} + \frac{1}{2}\left(B_\mu,\, W^3_\mu,\, a^0_\mu,\, v^0_{1\mu},\, v^0_{2\mu}\right)\mathcal{M}^2_N \begin{pmatrix} B_\mu \\ W^3_\mu \\ a^0_\mu \\ v^0_{1\mu} \\ v^0_{2\mu} \end{pmatrix}. \tag{3.13}$$

Using the vector state embeddings in eqs. (3.10) and (A.2) the charged non-diagonal mass matrix reads

$$\mathcal{M}^2_C = \begin{pmatrix} \frac{1}{4}g^2\left(f_0^2 s_\theta^2 + 2\frac{M_V^2}{\tilde{g}^2}(2-s_\theta^2)\right) & g\frac{r s_\theta M_A^2}{\sqrt{2}\tilde{g}} & -g\frac{M_V^2}{\sqrt{2}\tilde{g}} & -g\frac{M_V^2 c_\theta}{\sqrt{2}\tilde{g}} \\ g\frac{r s_\theta M_A^2}{\sqrt{2}\tilde{g}} & M_A^2 & & \\ -g\frac{M_V^2}{\sqrt{2}\tilde{g}} & & M_V^2 & \\ -g\frac{M_V^2 c_\theta}{\sqrt{2}\tilde{g}} & & & M_V^2 \end{pmatrix}, \tag{3.14}$$

and the neutral mass mixing is given by

$$\mathcal{M}^2_N = \begin{pmatrix} \frac{1}{4}g'^2\left(f_0^2 s_\theta^2 + 2\frac{M_V^2}{\tilde{g}^2}(2-s_\theta^2)\right) & \frac{1}{4}gg'\left(\frac{2M_V^2}{\tilde{g}^2} - f_0^2\right)s_\theta^2 & -g'\frac{r s_\theta M_A^2}{\sqrt{2}\tilde{g}} & -g'\frac{M_V^2}{\sqrt{2}\tilde{g}} & g'\frac{M_V^2 c_\theta}{\sqrt{2}\tilde{g}} \\ \frac{1}{4}gg'\left(\frac{2M_V^2}{\tilde{g}^2} - f_0^2\right)s_\theta^2 & \frac{1}{4}g^2\left(f_0^2 s_\theta^2 + 2\frac{M_V^2}{\tilde{g}^2}(2-s_\theta^2)\right) & g\frac{r M_A^2 s_\theta}{\sqrt{2}\tilde{g}} & -g\frac{M_V^2}{\sqrt{2}\tilde{g}} & -g\frac{M_V^2 c_\theta}{\sqrt{2}\tilde{g}} \\ -g'\frac{r s_\theta M_A^2}{\sqrt{2}\tilde{g}} & g\frac{r M_A^2 s_\theta}{\sqrt{2}\tilde{g}} & M_A^2 & & \\ -g'\frac{M_V^2}{\sqrt{2}\tilde{g}} & -g\frac{M_V^2}{\sqrt{2}\tilde{g}} & & M_V^2 & \\ g'\frac{M_V^2 c_\theta}{\sqrt{2}\tilde{g}} & -g\frac{M_V^2 c_\theta}{\sqrt{2}\tilde{g}} & & & M_V^2 \end{pmatrix}. \tag{3.15}$$

We define the orthogonal rotation matrices $\mathcal{C}$ and $\mathcal{N}$ to get the physical mass eigenstates denoted with upper case letters

$$\begin{pmatrix} \tilde{W}^+_\mu \\ a^+_\mu \\ v^+_{1\mu} \\ v^+_{2\mu} \end{pmatrix} = \mathcal{C}\begin{pmatrix} W^+_\mu \\ A^+_\mu \\ V^+_{1\mu} \\ V^+_{2\mu} \end{pmatrix} = \mathcal{C}R^+_\mu\,, \qquad \begin{pmatrix} B_\mu \\ W^3_\mu \\ a^0_\mu \\ v^0_{1\mu} \\ v^0_{2\mu} \end{pmatrix} = \mathcal{N}\begin{pmatrix} A_\mu \\ Z_\mu \\ A^0_\mu \\ V^0_{1\mu} \\ V^0_{2\mu} \end{pmatrix} = \mathcal{N}R^0_\mu\,, \tag{3.16}$$

where we defined the mass eigenstate vectors R^+_μ, R^0_μ.
In $\mathcal{M}^2_N$ we find an eigenstate with mass eigenvalue 0, identified as the photon γ_μ with eigenvector

$$\gamma_\mu = \frac{1/g}{\sqrt{\frac{1}{g^2}+\frac{1}{g'^2}+\frac{2}{\tilde{g}^2}}}W^3_\mu + \frac{1/g'}{\sqrt{\frac{1}{g^2}+\frac{1}{g'^2}+\frac{2}{\tilde{g}^2}}}B_\mu + \sqrt{2}\frac{1/\tilde{g}}{\sqrt{\frac{1}{g^2}+\frac{1}{g'^2}+\frac{2}{\tilde{g}^2}}}v^0_{1\mu}\,. \tag{3.17}$$

Using this result to express the gauge interaction of photon to W^+W^-, the coupling constant is given by

$$\frac{\mathcal{C}_{11}^2+\mathcal{C}_{21}^2+\mathcal{C}_{31}^2+\mathcal{C}_{41}^2}{\sqrt{2/\tilde{g}^2+1/g^2+1/g'^2}} \equiv e\,, \tag{3.18}$$

where we used unitarity of the charged diagonalization matrix $\mathcal{C}$ and define the electric charge e as

$$\frac{1}{e^2}=\frac{1}{g^2}+\frac{1}{g'^2}+\frac{2}{\tilde{g}^2}\,. \tag{3.19}$$

The photon eigenvector can then be written in the following form

$$\gamma_\mu = \frac{e}{g}W_\mu^3+\frac{e}{g'}B_\mu+\sqrt{2}\frac{e}{\tilde{g}}v_\mu^0\,. \tag{3.20}$$

Taking a closer look at the Lagrangian terms in eq. (3.11), the term proportional to r is the only possible contribution for mixing of the SM bosons with $\mathcal{A}_\mu$, coming from the fact that the SM gauge boson generators are not misaligned and have non-vanishing contributions in the coset $\sim \tilde{X}^j$. Since they are induced from misalignment their contribution is suppressed by $\sim s_\theta$.
Further, we chose the misalignment eq. (2.6) rotating only along the Higgs bidoublet. Therefore, the only axial triplet which mixes is a_μ of the axial bidoublet. The mass mixing matrices given in [26], describing the coset SU(4)/Sp(4), are exactly the same up to sign differences coming from different parameterization. This is not surprising, noting that SO(5) is isomorphic to Sp(4) and the misalignment is along the same direction.

3.2.1 Approximate diagonalization

Although we will diagonalize the mass matrices numerically in chapter 4, an approximate diagonalization remains useful for identifying the primary contributions of couplings and vector masses.
In the appendix of [26], solutions for the transformation matrices $\mathcal{C}$, $\mathcal{N}$ are given in expansion for $\tilde{g}\gg 1$ and $\theta\to 0$, which coincide with the ones we will use. For illustrative purposes, in the following we give some intermediate results and explanation on how to derive them.
In the charged sector it is easy to see that one eigenstate $V_2^+=v_2^+-c_\theta v_1^+$ decouples. To partially diagonalize the matrix we need to find the orthogonal complement $W^\perp$ of the V_2^+ eigenvector space, which can be seen as a linear combination of the remaining 3 Eigenvectors. The transformation matrix $\mathcal{C}_a$ is easily constructed and reads

$$\mathcal{C}_a=(W^\perp,\vec{V}_2^+)=\begin{pmatrix} 1 & 0 & 0 & 0\\ 0 & 1 & 0 & 0\\ 0 & 0 & \frac{1}{\sqrt{1+\cos^2\theta}} & \frac{-\cos\theta}{\sqrt{1+\cos^2\theta}}\\ 0 & 0 & \frac{\cos\theta}{\sqrt{1+\cos^2\theta}} & \frac{1}{\sqrt{1+\cos^2\theta}}\end{pmatrix}, \tag{3.21}$$

which reduces the charged mass matrix to an effective 3×3 problem

$$\mathcal{C}_a^{-1}\cdot\mathcal{M}_C^2\cdot\mathcal{C}_a=\begin{pmatrix} \frac{g^2M_V^2\left(1+\omega\sin^2(\theta)\right)}{\tilde{g}^2} & \frac{gM_A^2 r\sin(\theta)}{\sqrt{2}\tilde{g}} & -\frac{gM_V^2\sqrt{3+\cos(2\theta)}}{2\tilde{g}} & 0\\ \frac{gM_A^2 r\sin(\theta)}{\sqrt{2}\tilde{g}} & M_A^2 & 0 & 0\\ -\frac{gM_V^2\sqrt{3+\cos(2\theta)}}{2\tilde{g}} & 0 & M_V^2 & 0\\ 0 & 0 & 0 & M_V^2\end{pmatrix}. \tag{3.22}$$

For the purpose of the expansion we assume that the parameters r, f_1 and f_K are of order one. Further, we fix the ratio f_0/f_K and define the parameter $\omega = \frac{1}{2}(f_0^2/f_K^2 - 1)$. With those assumptions, in the above result there is a mass hierarchy between the gauge boson W^+ and the heavy resonances A^+, V_1^+, visible in form of orders of $g/\tilde{g}$. In sec. 3.3 we will change the set of parameters, but this will not affect the validity of the following considerations, as the parameters r, f_1, f_K and f_0 do not depend on $g/\tilde{g}$.
Exploiting the mass hierarchy, it is possible to use the Seesaw mechanism as explained in [38]. The idea is to get a unitary transformation $\mathcal{C}_b$ such that

$$\mathcal{C}_b^T \cdot \begin{pmatrix} M_L & M_D^T \\ M_D & M_R \end{pmatrix} \cdot \mathcal{C}_b = \begin{pmatrix} M_{\text{light}} & 0 \\ 0 & M_{\text{heavy}} \end{pmatrix}, \tag{3.23}$$

with the following Ansatz [38]

$$\mathcal{C}_b = \begin{pmatrix} \sqrt{1 - BB^\dagger} & B \\ -B^\dagger & \sqrt{1 - B^\dagger B} \end{pmatrix}, \tag{3.24}$$

where B is a 1×2 matrix in this example. Vanishing off-diagonal entries lead us to a condition for B which can be solved as a power series in $g^2/\tilde{g}^2$ up to arbitrary order. In [38], the general solution is stated explicitly up to second order. Apply the first order solution to eq. (3.22), we get the following Seesaw transformation

$$\mathcal{C}_b = \begin{pmatrix} 1 + \frac{-3g^2 - g^2\cos(2\theta) - 2g^2r^2\sin^2(\theta)}{8\tilde{g}^2} & \frac{gr\sin(\theta)}{\sqrt{2}\tilde{g}} & -\frac{g\sqrt{3+\cos(2\theta)}}{2\tilde{g}} & 0 \\ -\frac{gr\sin(\theta)}{\sqrt{2}\tilde{g}} & 1 - \frac{g^2r^2\sin^2(\theta)}{4\tilde{g}^2} & \frac{g^2r\sqrt{3+\cos(2\theta)}\sin(\theta)}{4\sqrt{2}\tilde{g}^2} & 0 \\ \frac{g\sqrt{3+\cos(2\theta)}}{2\tilde{g}} & \frac{g^2r\sqrt{3+\cos(2\theta)}\sin(\theta)}{4\sqrt{2}\tilde{g}^2} & 1 - \frac{g^2(3+\cos(2\theta))}{8\tilde{g}^2} & 0 \\ 0 & 0 & 0 & 1 \end{pmatrix}. \tag{3.25}$$

This yields a light eigenvalue for the W boson expanded in terms of $g/\tilde{g}$, using $\xi = M_A/M_V$

$$(\mathcal{C}_a\mathcal{C}_b)^{-1} \cdot \mathcal{M}_C^2 \cdot \mathcal{C}_a\mathcal{C}_b = \begin{pmatrix} \frac{1}{4}(f_0^2 - r^2f_1^2)g^2s_\theta^2 & 0 & 0 & 0 \\ 0 & M_A^2(1 + \frac{g^2r^2s_\theta^2}{2\tilde{g}^2}) & -\frac{g^2M_V^2r(\xi^2+1)\sqrt{3+c_{2\theta}}s_\theta}{4\sqrt{2}\tilde{g}^2} & 0 \\ 0 & -\frac{g^2M_V^2r(\xi^2+1)\sqrt{3+c_{2\theta}}s_\theta}{4\sqrt{2}\tilde{g}^2} & M_V^2(1 + \frac{g^2(3+c_{2\theta})}{4\tilde{g}^2}) & 0 \\ 0 & 0 & 0 & M_V^2 \end{pmatrix}. \tag{3.26}$$

The remaining non diagonal 2×2 matrix can be diagonalized with a suitable ansatz in the limit $\sin(\theta) \to 0$

$$\mathcal{C}_c = \mathbb{1}_4 + s_\theta \begin{pmatrix} 0 & 0 & 0 & 0 \\ 0 & 0 & -a & 0 \\ 0 & a & 0 & 0 \\ 0 & 0 & 0 & 0 \end{pmatrix}, \qquad a = \frac{g^2r(1+\xi^2)}{2\sqrt{2}(g^2 + \tilde{g}^2(1-\xi^2))} \tag{3.27}$$

Putting all steps together, we get the total transformation $\mathcal{C} = \mathcal{C}_a\mathcal{C}_b\mathcal{C}_c$, explicitly stated in appendix C. Including the second order Seesaw formula as well, it is possible to derive the mass eigenvalues

$$M_W^2 = \frac{1}{4}g^2\left(f_0^2 - f_1^2 r^2\right)\sin^2(\theta)\left(1 - \frac{1}{2}\left(\frac{g}{\tilde{g}}\right)^2\left(\left(r^2-1\right)\sin^2(\theta)+2\right) + \mathcal{O}(\tilde{g}^{-4})\right), \tag{3.28}$$

$$M_{A^+}^2 = M_A^2\left(1 + \frac{1}{2}r^2\left(\frac{g}{\tilde{g}}\right)^2\sin^2(\theta) + \mathcal{O}(\tilde{g}^{-4})\right), \tag{3.29}$$

$$M_{V_1^+}^2 = M_V^2\left(1 + \frac{1}{2}\left(\frac{g}{\tilde{g}}\right)^2\left(2 - \sin^2(\theta)\right) + \mathcal{O}(\tilde{g}^{-4})\right), \tag{3.30}$$

$$M_{V_2^+}^2 = M_V^2\,. \tag{3.31}$$

The higher order corrections of M_W^2 can be absorbed in the definition of the "physical" coupling constant

$$g_{\text{phys}}^2 = g^2\left(1 - \frac{1}{2}\left(\frac{g}{\tilde{g}}\right)^2\left(\left(r^2-1\right)\sin^2(\theta)+2\right) + \mathcal{O}(\tilde{g}^{-4})\right), \tag{3.32}$$

which simplifies to g^2 in the SM limit $\tilde{g} \to \infty$, where the heavy resonances decouple completely for fixed f_1, f_K. In this limit we require the M_W^2 expression to match with the definition of the VEV, $\mathrm{v}^2 = (246\,\text{GeV})^2$. Using eq. (2.8), we recall the definition of the pNGB decay constant in eq. (2.52) derived from

$$\mathrm{v}^2 = \frac{4}{g^2}M_W^2 \overset{\tilde{g}\to\infty}{=} \left(f_0^2 - f_1^2 r^2\right)s_\theta^2 \tag{3.33}$$

$$= f^2 s_\theta^2\,. \tag{3.34}$$

In the neutral sector it is actually easier to start directly with a Seesaw approximation using the hierarchy between the two light SM bosons and three heavy resonances. Therefore, we omit the exact photon vector for this purpose to get

$$\mathcal{N}_a^{-1}\cdot\mathcal{M}_N^2\cdot\mathcal{N}_a = \begin{pmatrix} M_{\text{light}}^2 & 0 \\ 0 & M_{\text{heavy}}^2 \end{pmatrix}, \tag{3.35}$$

$$M_{\text{light}}^2 = \frac{(M_V^2(1+2\omega) - M_A^2 r^2)s_\theta^2}{2\tilde{g}^2}\begin{pmatrix} g^2 & -gg' \\ -gg' & g'^2 \end{pmatrix}. \tag{3.36}$$

The upper 2×2 block matrix M_{light}^2 contains the light gauge bosons and can be diagonalized easily, while we can do another Seesaw in

$$\mathcal{M}_{\text{heavy}}^2 - M_A^2\cdot\mathbb{1}_3 = \begin{pmatrix} \frac{1}{2}M_A^2\frac{(g'^2+g^2)r^2\sin^2(\theta)}{\tilde{g}^2} & \frac{(g'^2-g^2)(M_A^2+M_V^2)r\sin(\theta)}{4\tilde{g}^2} & \frac{(g'^2+g^2)(M_A^2+M_V^2)r\sin(2\theta)}{8\tilde{g}^2} \\ \frac{(g'^2-g^2)(M_A^2+M_V^2)r\sin(\theta)}{4\tilde{g}^2} & -M_A^2 + \frac{(g'^2+g^2+2\tilde{g}^2)M_V^2}{2\tilde{g}^2} & \frac{(g'^2-g^2)M_V^2\cos(\theta)}{2\tilde{g}^2} \\ \frac{(g'^2+g^2)(M_A^2+M_V^2)r\sin(2\theta)}{8\tilde{g}^2} & \frac{(g'^2-g^2)M_V^2\cos(\theta)}{2\tilde{g}^2} & -M_A^2 + \frac{(2\tilde{g}^2+(g'^2+g^2)\cos^2(\theta))M_V^2}{2\tilde{g}^2} \end{pmatrix}, \tag{3.37}$$

using the Seesaw transformation

$$\mathcal{N}_b = \begin{pmatrix} 1 & 0 & 0 & 0 & 0 \\ 0 & 1 & 0 & 0 & 0 \\ 0 & 0 & 1 & \frac{r\left(g'^2-g^2\right)\left(M_A^2+M_V^2\right)s_\theta}{4\tilde{g}^2\left(M_V^2-M_A^2\right)} & \frac{r\left(g'^2+g^2\right)\left(M_A^2+M_V^2\right)s_{2\theta}}{8\tilde{g}^2\left(M_V^2-M_A^2\right)} \\ 0 & 0 & \frac{r\left(g'^2-g^2\right)\left(M_A^2+M_V^2\right)s_\theta}{4\tilde{g}^2\left(M_A^2-M_V^2\right)} & 1 & 0 \\ 0 & 0 & \frac{r\left(g'^2+g^2\right)\left(M_A^2+M_V^2\right)s_{2\theta}}{8\tilde{g}^2\left(M_A^2-M_V^2\right)} & 0 & 1 \end{pmatrix} . \tag{3.38}$$

In the end we get the following neutral mass eigenvalues, where we used $\theta \to 0$ to diagonalize the 2×2 block of V_1^0 and V_2^0

$$M_A^2 = 0\,, \tag{3.39}$$

$$M_Z^2 = \frac{1}{4}\left(g'^2+g^2\right)v^2\left(1+\frac{\left(1-r^2\right)\left(g'^2+g^2\right)^2\sin^2(\theta)-2\left(g'^4+g^4\right)}{2\tilde{g}^2\left(g'^2+g^2\right)}+\mathcal{O}(\tilde{g}^{-4})\right), \tag{3.40}$$

$$M_{A^0}^2 = M_A^2\left(1+\frac{r^2\left(g'^2+g^2\right)\sin^2(\theta)}{2\tilde{g}^2}+\mathcal{O}(\tilde{g}^{-4})\right), \tag{3.41}$$

$$M_{V^0/S^0}^2 = M_V^2\left(1+\frac{\left(g'^2+g^2\right)\left(\pm\sqrt{\frac{2(-6g^2g'^2+g'^4+g^4)\cos^2(\theta)}{(g'^2+g^2)^2}+\cos^4(\theta)+1}+\cos^2(\theta)+1\right)}{4\tilde{g}^2}+\mathcal{O}(\tilde{g}^{-4})\right). \tag{3.42}$$

In fig. 3.1, the numerically calculated vector masses of $V_{1\mu}^{0\pm}$, $V_{2\mu}^0$ are shown as contour lines in the $M_V - \tilde{g}$ plane. As the charged state $V_{2\mu}^+$ is a linear combination only of $v_{1\mu}^+$ and $v_{2\mu}^+$ its mass does

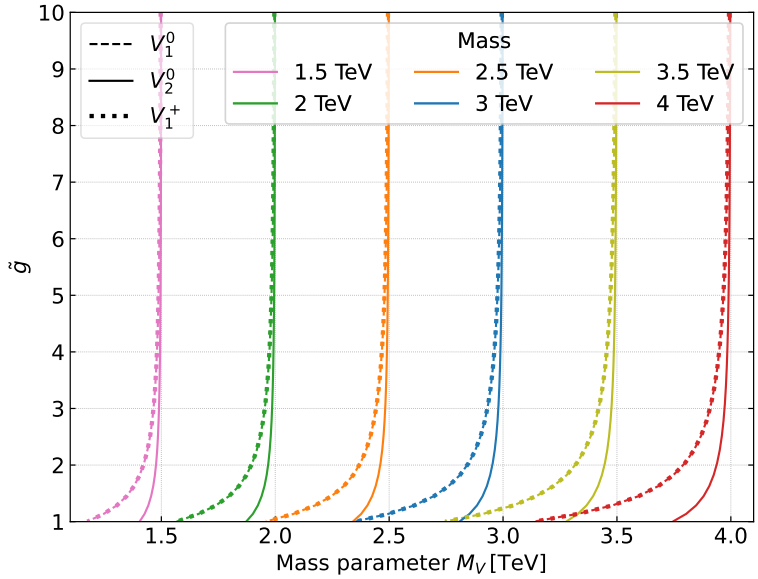

Figure 3.1: Mass contour lines in the $M_V - \tilde{g}$ plane for fixed $g_{V\pi\pi} = 0$, $f = 1\,\text{TeV}$, $\xi = 1.4$. Shown are the numerically calculated mass terms of the vector resonances $V_{1\mu}^{0\pm}$ and $V_{2\mu}^0$.

not have further corrections. The neutral and charged states of the triplet $V_{1\mu}$ behave very similar

to each other with a mass difference of less than 0.1%. As can be seen in fig. 3.1, their masses get very large corrections from M_V at smaller $\tilde{g}$, which leads to a significant mass splitting between $V_{1\mu}$ and $V_{2\mu}$.

3.3 Model parameters

The effective Lagrangian eq. (2.38) was defined with five independent parameters f_1, f_K, r, θ, $\tilde{g}$. For Phenomenology we wish to use a set of parameters which can be interpreted in a physical context. We keep $\tilde{g}$ as independent parameter, and use eq. (3.12) to exchange f_K and f_1 in favor of the vector mass parameter M_V, respectively axial vector mass parameter M_A. As stated before, these mass parameters describe the mass terms of the non-mixing resonances, while the others get further corrections. Further, instead of M_A, the ratio $\xi = M_A/M_V$ will be used, as it can be estimated in holographic models of a composite Higgs. The parameter r can be replaced by the Vector-pNGB-pNGB coupling constant, defined in eq. (2.54). Moreover, the pion decay constant f eq. (2.8) will be fixed to 1 TeV, which corresponds to $\theta \approx 0.25$, which matches to the current lower bounds [18]. Varying f has only very small effects on the decay channels of interest if we keep $g_{V\pi\pi}$ constant. But significantly larger values of f would lead to stronger fine tuning to get the measured Higgs mass and is therefore not interesting. In summary, the input model parameters are

$$\tilde{g}\,, \quad M_V\,, \quad \xi\,, \quad g_{V\pi\pi}\,, \quad f\,. \tag{3.43}$$

Using this set of parameters, one can express the remaining Lagrangian parameters as

$$f_1 = \frac{\sqrt{2}}{\tilde{g}} M_V \xi\,, \tag{3.44}$$

$$r = \sqrt{1 + \frac{f^2 g_{V\pi\pi}\tilde{g}}{2M_V^2}}\,, \tag{3.45}$$

$$f_0 = \sqrt{f^2 + r^2 f_1^2} = \sqrt{f^2 + \frac{2M_V^2\xi^2}{\tilde{g}^2} + \frac{\xi^2 f^2 g_{V\pi\pi}}{\tilde{g}}}\,. \tag{3.46}$$

Additionally, we use the SM values of the electric charge e and mass of the Z boson M_Z as input parameters to get an output expression for the coupling constants g, g' derived from the conditions

$$\frac{1}{e^2} = \frac{1}{g^2} + \frac{1}{g'^2} + \frac{2}{\tilde{g}^2}\,, \qquad \det\left(M_N^2 - M_Z^2 \mathbb{1}_5\right) = 0\,. \tag{3.47}$$

3.4 Couplings

In this section we will go into details about relevant vertices involving production and decay of the Spin-1 resonances. This does also include additional terms not yet involved in eq. (2.38) like the couplings to SM fermions explored in sec. 3.4.1. Note, that we will work in unitary gauge in the following.

3.4.1 Standard Model Fermions

In the SM, we have couplings of gauge bosons to fermions via charged and neutral currents, which makes it possible to have Drell-Yan single production of vector bosons. Through those terms, couplings to heavy Spin-1 resonances are generated due to the mass mixing of B_μ and W_μ. With $P_{\mathrm{L,R}} = (1 \pm \gamma_5)/2$, the fermion currents can be written as

$$\mathcal{L}_{\mathrm{CC}} = \frac{g}{\sqrt{2}} \sum_{i,f} \mathcal{C}_{1i} R^+_{i\mu} \bar{\psi}_f \gamma^\mu P_{\mathrm{L}} \psi_{f'} + \mathrm{h.c.}\,, \tag{3.48}$$

$$\mathcal{L}_{\mathrm{NC}} = \sum_{i,f} R^0_{i\mu} \bar{\psi}_f \gamma^\mu \left(g^f_{\mathrm{L}i} P_{\mathrm{L}} + g^f_{\mathrm{R}i} P_{\mathrm{R}} \right) \psi_f \tag{3.49}$$

$$= \sum_{i,f} R^0_{i\mu} \bar{\psi}_f \gamma^\mu \left(\left[g T^3 \mathcal{N}_{2i} + g' Y_L \mathcal{N}_{1i} \right] P_{\mathrm{L}} + g' Y_R \mathcal{N}_{1i} P_{\mathrm{R}} \right) \psi_f\,, \tag{3.50}$$

with the weak isospin T^3 and hypercharge $Y_{\mathrm{L,R}}$ of the left-chiral doublets and right-chiral singlets. Note that eq. (3.19) implies that

$$g_{\mathrm{phys}} s_{\mathrm{W}} = g'_{\mathrm{phys}} c_{\mathrm{W}} = e = g \cdot \mathcal{N}_{21} = g' \cdot \mathcal{N}_{11}\,. \tag{3.51}$$

Further contributions can be expected from couplings of the baryonic top-partners to vector resonances in the partial compositeness framework. For the top quark these couplings can be large compared to the SM expression. Therefore, the total top coupling will be parameterized in a simplified manner with generic coupling constants as

$$\mathcal{L}^{\mathrm{PC}} = \bar{t} V^0_\mu \gamma^\mu \left(g_{t,L} P_L + g_{t,R} P_R \right) t + \bar{t} V^+_\mu \gamma^\mu g_{tb,L} P_L b\,, \tag{3.52}$$

for $V_\mu = A_\mu, V_{1\mu}, V_{2\mu}$. Some details about the structure and origin of these couplings in the color sector are given in A.5 of [29].

3.4.2 Higgs & Gauge Bosons

Three-Vector vertices involving mass mixing resonances can be relevant for Di-Vector Drell-Yan production. One interesting aspect are couplings of single produced resonances decaying into two SM gauge bosons. In terms of gauge eigenstates the non-vanishing commutator structure for those vertices reads

$$\begin{aligned}\mathcal{L} \supset -i\Big(& g \tilde{W}^{+\nu} \tilde{W}^-_\mu \partial^\mu W^3_\nu + \frac{\tilde{g}}{\sqrt{2}} \Big((a^{+\nu} v^-_{1\mu} + v^{+\nu}_1 a^-_\mu) \partial^\mu a^0_\nu + (v^{+\nu}_1 v^-_{2\mu} + v^{+\nu}_2 v^-_{1\mu}) \partial^\mu v^0_{2\nu} \Big) \\ & + \frac{\tilde{g}}{\sqrt{2}} \left(a^{+\nu} a^-_\mu + v^{+\nu}_1 v^-_{1\mu} + v^{+\nu}_2 v^-_{2\mu} \right) \partial^\mu v^0_{1\nu} \Big) + \text{permutations}\,. \end{aligned} \tag{3.53}$$

Replacing the gauge eigenstates with their mass mixing eigenvectors, one can easily derive a generic expression in terms of $\mathcal{C}$ and $\mathcal{N}$ entries.
Decay channels into hZ and $hW^\pm$ do also emerge from the pNGB Lagrangian eq. (2.38). The coupling of two mass eigenstate vectors to the Higgs h can be written as

$$\mathcal{L} \supset c^{\mathrm{gauge}}_{hR^+R^-} \cdot h \left(\mathcal{C} R^+_\mu \right)_i \left(\mathcal{C}^* R^{-\mu} \right)_j + \frac{1}{2} c^{\mathrm{gauge}}_{hR^0R^0} \cdot h \left(\mathcal{N} R^0_\mu \right)_i \left(\mathcal{N} R^{0\mu} \right)_j \tag{3.54}$$

$$= c_{hR^+R^-} \cdot h R^+_{i\mu} R^{-\mu}_j + \frac{1}{2} c_{hR^0R^0} \cdot h R^0_{i\mu} R^{0\mu}_j\,. \tag{3.55}$$

In the gauge eigenbasis the couplings read

$$\frac{1}{2}c^{\text{gauge}}_{hR^0R^0} = \begin{pmatrix} \frac{g'^2(f^2\tilde{g}^2-2M_V^2+2M_A^2r^2)s_{2\theta}}{8f\tilde{g}^2} & -\frac{gg'(f^2\tilde{g}^2-2M_V^2+2M_A^2r^2)s_{2\theta}}{8f\tilde{g}^2} & -\frac{g'(M_A^2-M_V^2)rc_\theta}{\sqrt{2}f\tilde{g}} & 0 & -\frac{g'(M_V^2-r^2M_A^2)s_\theta}{\sqrt{2}f\tilde{g}} \\ -\frac{gg'(f^2\tilde{g}^2-2M_V^2+2M_A^2r^2)s_{2\theta}}{8f\tilde{g}^2} & \frac{g^2(f^2\tilde{g}^2-2M_V^2+2M_A^2r^2)s_{2\theta}}{8f\tilde{g}^2} & \frac{g(M_A^2-M_V^2)rc_\theta}{\sqrt{2}f\tilde{g}} & 0 & \frac{g(M_V^2-r^2M_A^2)s_\theta}{\sqrt{2}f\tilde{g}} \\ -\frac{g'(M_A^2-M_V^2)rc_\theta}{\sqrt{2}f\tilde{g}} & \frac{g(M_A^2-M_V^2)rc_\theta}{\sqrt{2}f\tilde{g}} & 0 & 0 & \frac{r(M_V^2-M_A^2)}{f} \\ 0 & 0 & 0 & 0 & 0 \\ -\frac{g'(M_V^2-r^2M_A^2)s_\theta}{\sqrt{2}f\tilde{g}} & \frac{g(M_V^2-r^2M_A^2)s_\theta}{\sqrt{2}f\tilde{g}} & \frac{r(M_V^2-M_A^2)}{f} & 0 & 0 \end{pmatrix}, \tag{3.56}$$

$$c^{\text{gauge}}_{hR^+R^-} = \begin{pmatrix} \frac{g^2(f^2\tilde{g}^2-2M_V^2+2M_A^2r^2)s_{2\theta}}{4f\tilde{g}^2} & -\frac{g(M_V^2-M_A^2)rc_\theta}{\sqrt{2}f\tilde{g}} & 0 & \frac{g(M_V^2-r^2M_A^2)s_\theta}{\sqrt{2}f\tilde{g}} \\ -\frac{g(M_V^2-M_A^2)rc_\theta}{\sqrt{2}f\tilde{g}} & 0 & 0 & \frac{r(M_V^2-M_A^2)}{f} \\ 0 & 0 & 0 & 0 \\ \frac{g(M_V^2-r^2M_A^2)s_\theta}{\sqrt{2}f\tilde{g}} & \frac{r(M_V^2-M_A^2)}{f} & 0 & 0 \end{pmatrix}. \tag{3.57}$$

3.4.3 Decays into two pNGBs

In the gauge eigenbasis, only the vectors $\mathcal{V}_\mu$ can decay into two pNGBs given by the structure in eq. (2.53), whereas the axials have only couplings to three scalars. Due to the mass mixing, there are in principal also discalar decay channels for the axial triplet a_μ. However, they are suppressed by $1/\tilde{g}$ and s_θ.
The vector states, which mix with W_μ, B_μ, get corrections to $g_{V\pi\pi}$ from the $\tilde{T}^a$ projections of the gauge bosons. Collecting the terms, the corresponding expression is

$$\begin{aligned}\mathcal{L}_{W\pi\pi} &= \frac{i}{f^2}\Big[f_0^2\,\mathrm{Tr}\left(\partial_\mu\tilde{\Pi}_P\left[\tilde{\Pi}_P, g\tilde{T}(W_\mu)+g'\tilde{T}(B_\mu)\right]\right) - r^2f_1^2\,\mathrm{Tr}\left(\partial_\mu\tilde{\Pi}_P\left[\tilde{\Pi}_P, g\tilde{T}(W_\mu)+g'\tilde{T}(B_\mu)\right]\right) \\ &\quad + \frac{f_K^2}{2}\,\mathrm{Tr}\left(\left(g\tilde{T}(W_\mu)+g'\tilde{T}(B_\mu)\right)\left[\tilde{\Pi}_P, \partial_\mu\tilde{\Pi}_P\right]\right) - \frac{f_K^2r^2}{2}\,\mathrm{Tr}\left(\left(g\tilde{T}(W_\mu)+g'\tilde{T}(B_\mu)\right)\left[\tilde{\Pi}_P, \partial_\mu\tilde{\Pi}_P\right]\right)\Big] \\ &= i\Big[\frac{f_K^2}{2f^2}(1-r^2)-1\Big]\,\mathrm{Tr}\left(\left(g\tilde{T}(W_\mu)+g'\tilde{T}(B_\mu)\right)\left[\tilde{\Pi}_P, \partial_\mu\tilde{\Pi}_P\right]\right) \\ &= -i\frac{g_{V\pi\pi}+2\tilde{g}}{2\tilde{g}}\,\mathrm{Tr}\left(\left(g\tilde{T}(W_\mu)+g'\tilde{T}(B_\mu)\right)\left[\tilde{\Pi}_P, \partial_\mu\tilde{\Pi}_P\right]\right). \end{aligned} \tag{3.58}$$

The total discalar decay constant of $V_{1\mu}$, $V_{2\mu}$ can be derived through insertion of the mass eigenstates eq. (3.16) into the $g_{V\pi\pi}$ term eq. (2.53) and the above Lagrangian.
In fig. D.5, we show the relative decay widths of the pNGB channels among themselves for the mass eigenstates $V_1^{0\pm}$, $V_{2\mu}^0$, which barely scale with $\tilde{g}$. Taking into account decay modes into the pNGBs, we need to discuss their subsequent decay channels into SM particles. A possibility already mentioned are the anomaly induced WZW terms.

3.4.4 WZW anomaly terms

As discussed in sec. 2.5, the axial combination of the two U(1) induces a so-called ABJ anomaly of the axial current when we go from the classical to the quantized model. Therefore extra terms are

needed, which were described in [39, 40] and named Wess-Zumino-Witten (WZW) after the authors. For some further details, see also section 1.3 of [41]. Those anomaly terms involve two orders of Goldstones U and two orders of electroweak gauge bosons. Expanded to first order of pNGBs for the SU(5)/SO(5) coset they read [37]

$$\begin{aligned}
\mathcal{L}_{\mathrm{WZW}} = \frac{e^2 \dim(\psi)}{48\pi^2 f} \Bigg[& \\
& \eta \left(\frac{3\sqrt{2}}{\sqrt{5}} F_{\mu\nu}\tilde{F}^{\mu\nu} + \frac{6\sqrt{2}c_{2W}}{\sqrt{5}s_{2W}} F_{\mu\nu}\tilde{Z}^{\mu\nu} + \frac{3(3c_\theta^2 + c_{4W})}{4\sqrt{10}c_W^2 s_W^2} Z_{\mu\nu}\tilde{Z}^{\mu\nu} + \frac{3(3_{2\theta}+5)}{4\sqrt{10}s_W^2} W^+_{\mu\nu}\tilde{W}^{-\mu\nu} \right) + \\
& \eta_1^0 \left(\sqrt{6}F_{\mu\nu}\tilde{F}^{\mu\nu} + \frac{2\sqrt{6}c_{2W}}{s_{2W}} F_{\mu\nu}\tilde{Z}^{\mu\nu} + \frac{1 - 7c_{2\theta} + 6c_{4W}}{2\sqrt{6}s_{2W}^2} Z_{\mu\nu}\tilde{Z}^{\mu\nu} + \frac{7s_\theta^2}{2\sqrt{6}s_W^2} W^+_{\mu\nu}\tilde{W}^{-\mu\nu} \right) + \\
& \eta_5^0 \left(-2\sqrt{3}F_{\mu\nu}\tilde{F}^{\mu\nu} + \frac{-4\sqrt{3}c_{2W}}{s_{2W}} F_{\mu\nu}\tilde{Z}^{\mu\nu} + \frac{1 + 2c_{2\theta} - 3c_{4W}}{\sqrt{3}s_{2W}^2} Z_{\mu\nu}\tilde{Z}^{\mu\nu} + \frac{s_\theta^2}{\sqrt{3}s_W^2} W^+_{\mu\nu}\tilde{W}^{-\mu\nu} \right) + \\
& \eta_3^+ \left(\frac{-3c_\theta}{s_W} F_{\mu\nu}\tilde{W}^{-\mu\nu} + \frac{3c_\theta}{c_W} Z_{\mu\nu}\tilde{W}^{-\mu\nu} \right) + \mathrm{h.c.} + \\
& \eta_5^+ \left(\frac{3i}{s_W} F_{\mu\nu}\tilde{W}^{-\mu\nu} + \frac{i(3c_{2W} - c_{2\theta} - 2)}{2c_W s_W^2} Z_{\mu\nu}\tilde{W}^{-\mu\nu} \right) + \mathrm{h.c.} + \\
& \eta_5^{++} \frac{-s_\theta^2}{\sqrt{2}s_W^2} W^-_{\mu\nu}\tilde{W}^{-\mu\nu} + \mathrm{h.c.} \Bigg] .
\end{aligned} \tag{3.59}$$

The combination of field strength tensor and its dual can couple only to CP-uneven scalars. Note that there is no such term for η_3^0. Further, the couplings of the Z boson (CP uneven) to $\eta_1^0\eta_3^0$ and $\eta_5^0\eta_3^0$ do exist in the Lagrangian. It follows, that η_3^0 has to be a CP-even scalar, while all other pNGBs are pseudoscalars.

The overall prefactor $\dim(\psi)$ is given by the dimension of the hypercolor irrep of ψ. In this work we can keep in unspecified as we will be only interested in the branching ratios. Notice, that the couplings to two W bosons are suppressed by s_θ^2 and can be neglected for the neutral scalars, but are the only decay channel for η_5^{++}. Calculation of the corresponding Feynman rules can be found in appendix B.

The resulting two-body branching ratios for the neutral and single charged pNGBs are shown in fig. 3.2 as function of the particles mass M_η. As we can see, the branching ratios remain stable over a wide mass range. The three decay channels of the neutral pNGBs roughly have the same partial widths, whereas the charged pNGBs decay primarily into $W^+\gamma$ with $\approx 78\%$.

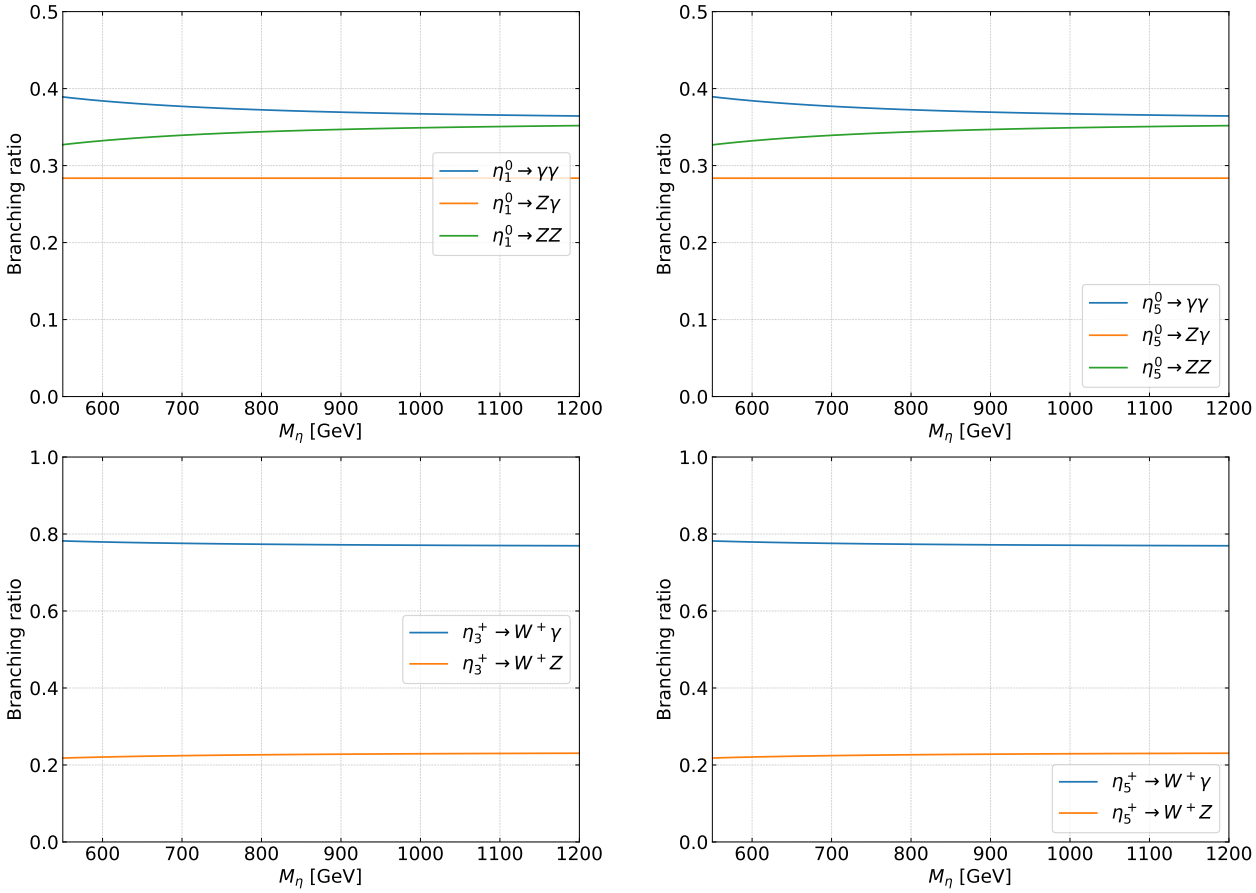

Figure 3.2: Branching ratios as function of the scalar mass M_η for $\eta_3^\pm$, $\eta_5^\pm$, η_1^0 and η_5^0 assuming only WZW induced decay channels in the limit $\theta \to 0$ as described in sec. 3.4.4.

3.5 Three-body decay of η_3^0

In this section we take a closer look on the decay channels of η_3^0 into gauge bosons. As we have seen in sec. 3.4.4, the CP-even η_3^0 has no anomaly induced decay channel into two gauge bosons. But it can decay into 3-body final states. Given the assumption that η_3 is the lightest multiplet and there is only a small mass splitting $\Delta < 30\,\text{GeV}$ between η_3 and the other multiplets, the neutral component η_3^0 will decay predominantly via an off-shell pNGB [36] as shown in the Feynman diagrams fig. 3.3. For its calculation one needs the WZW terms and couplings of two scalars to Z or W, which are stated in [36]. In their paper the scalar sector was studied without taking into account vector mixing, which will modify the couplings to the SM gauge bosons. Nonetheless, those modifications can be expected to be suppressed by small misalignment and large $\tilde{g}$.
In the following, we highlight a few key points on how to analytically calculate the 3-body decay cross section, where we follow the ansatz in [42]. The five different decay channels are shown in fig. 3.3, where we neglected the $\sim s_\theta^2$ suppressed couplings $\eta_{1,5}^0 \to W^+W^-$.
The total width is then the sum of all partial widths $\Gamma = \sum_{j=1}^5 \Gamma_j$, with

$$\Gamma_j = \frac{S}{2m_{\eta_3^0}} \int |\mathcal{M}_j|^2 (2\pi)^4 \delta^4(p_1 - p_2 - p_3 - p_4) \prod_{i=2}^{4} \frac{\mathrm{d}^4 p_i}{(2\pi)^3} \Theta(p_i^0) \delta(p_i^2 - m_i^2)\,, \tag{3.60}$$

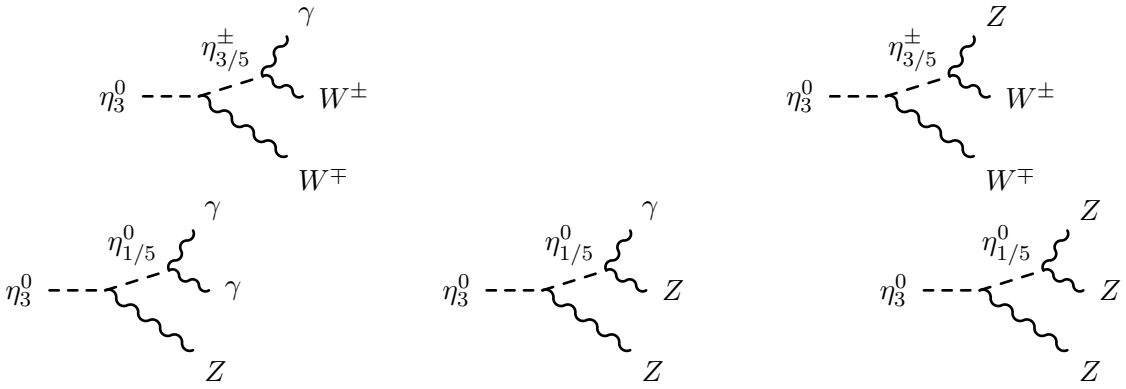

Figure 3.3: All relevant fermiophobic 3-body decay channels of the CP-even pNGB η_3^0.

where $S = \frac{1}{n!}$ is the symmetry factor with n the number of identical final states.
The decay is mediated through an off-shell pNGB with finite width, so we use the Breit-Wigner propagator of the form

$$\frac{\mathrm{i}}{q_\eta^2 - M_\eta^2 + \mathrm{i}\Gamma_\eta M_\eta}\,. \tag{3.61}$$

It's handy to define the Mandelstam variables as

$$\begin{aligned} \bar{t} &= (p_3 + p_4)^2 = (p_1 - p_2)^2\,, \\ \bar{u} &= (p_2 + p_4)^2 = (p_1 - p_3)^2\,, \\ \bar{s} &= (p_2 + p_3)^2 = (p_1 - p_4)^2\,, \\ \sum_{i=1}^{4} m_i^2 &= \bar{t} + \bar{u} + \bar{s}\,. \end{aligned} \tag{3.62}$$

Working in the rest frame of η_3^0 and using the identities

$$\begin{aligned} \int_{(m_3+m_4)^2}^{(m_1-m_2)^2} \mathrm{d}\bar{t}\,\delta\left(\bar{t} - (p_1 - p_2)^2\right) &= 1\,, \\ \int_{(m_2+m_3)^2}^{(m_1-m_4)^2} \mathrm{d}\bar{s}\,\delta\left(\bar{s} - (p_1 - p_4)^2\right) &= 1\,, \end{aligned} \tag{3.63}$$

the partial width from eq. (3.60) can be simplified to

$$\Gamma_j = \frac{S}{m_{\eta_3^0}} \frac{1}{2^8\pi^3} \int_{(m_2+m_3)^2}^{(m_1-m_4)^2} \mathrm{d}\bar{s} \int_{t_-(\bar{s})}^{t_+(\bar{s})} \mathrm{d}\bar{t} |\mathcal{M}_j|^2(\bar{t},\bar{s}) \frac{\pi^2}{4m_1^2}\,, \tag{3.64}$$

with $t_\pm$ being the $\bar{s}$ dependent integral bounds

$$t_\pm = \frac{1}{2}\left(m_1^2 + m_2^2 + m_3^2 + m_4^2 - \bar{s}\right) - \frac{1}{2\bar{s}}\left(m_1^2 - m_4^2\right)\left(m_2^2 - m_3^2\right) \pm \frac{1}{2\bar{s}}\sqrt{\lambda(\bar{s}, m_2^2, m_3^2)}\sqrt{\lambda(\bar{s}, m_1^2, m_4^2)}\,, \tag{3.65}$$

and

$$\lambda(\bar{s}, y, z) = \bar{s}^2 + y^2 + z^2 - 2\bar{s}y - 2\bar{s}z - 2yz\,. \tag{3.66}$$

The form of the Feynman rules and squared matrix elements $|\mathcal{M}_j|^2$ needed for the calculation are derived in appendix B.
We will fix the scalar masses of the different multiplets to

$$M(\eta_3) = M_\eta - \Delta\,, \qquad M(\eta_5) = M_\eta\,, \qquad M(\eta_1) = M_\eta + \Delta\,, \tag{3.67}$$

such that the triplet is always the lightest. For small mass splitting $\Delta = 2\,\text{GeV}$, all pNGBs except η_3^0 will decay directly into two gauge bosons and the neutral triplet η_3^0 has to decay via an off-shell pNGB.
For $M_\eta = 700\,\text{GeV}$, we calculate a total width of $6.49 \cdot 10^{-10}\,\text{GeV}$ with branching ratios as in tab. 3.2.

channel	$W^+W^-\gamma$	W^+W^-Z	$Z\gamma\gamma$	$ZZ\gamma$	ZZZ
BR [%]	4.3	70.7	1.5	1.0	22.5

Table 3.2: The branching ratios (BR) of three-body decays via WZW terms of η_3^0 using $M_\eta = 700\,\text{GeV}$ and a mass splitting of $\Delta = 2\,\text{GeV}$. The total width is $6.49 \cdot 10^{-10}\,\text{GeV}$.

4 Phenomenology

In this chapter, we want to make quantitative predictions about the parameter space in the coset SU(5)/SO(5). To this end, we compare simulated collider events with current experimental data to derive lower limits on the mass parameters and coupling constants. Ultimately, we aim to determine the extent of the parameter space that remains viable, despite the absence of evidence for new heavy resonances at the LHC so far.

In sec. 4.1, we focus on single production of vector resonances suited to derive bounds on the vector mass parameter M_V. Following, we will take a look at pair production of the double charged axial resonance $\hat{a}_5^{++}$ in sec. 4.2 and constrain its mass M_A.

For the simulation of signal events all relevant couplings were implemented as a `FeynRules` [43] model. The model was built upon the existing SM implementation [44] version 1.4.7, therein the fine structure constant was used at the Z pole, $\alpha = 1/127.9$, the Z mass $m_Z = 91.1876\,\text{GeV}$ and Fermi constant $G_f = 1.16637 \cdot 10^{-5}\,\text{GeV}^{-2}$. `FeynRules` then generates Universal FeynRules Output (UFO), a set of Python files readable to all common event generators.

Proton-proton collision events at $\sqrt{s} = 13\,\text{TeV}$ are then simulated with the Monte Carlo generator `MadGraph5aMC@NLO` [45] version 3.5.1, with parton densities from NNPDF 2.3 [46, 47].

`MadGraph5` does rely on the Narrow-Width-Approximation (NWA) approximation. Including a proper treatment of large widths would require further work. In general, the validity for a narrow width in this context is given up to $\approx 10\%$ of its mass.

Further decay into detectable final states, showering and hadronization, is done with `Pythia8` [48]. For several $2 \to 2$ scattering processes we are able to compare the calculated cross section of 10^4 events directly to upper limits of searches of the same signatures. Whereas for more complex final states we simulate 10^5 events which are then analyzed by Recasting tools.

The term "Recasting" needs a little bit of an explanation. The collaborations ATLAS and CMS are known for frequently publishing searches for BSM physics hidden in up-to-date LHC data. First, the measured detector signatures have to be used to reconstruct the actual scattering events. To this end, the so-called anti-kT algorithm is used to identify jets. Depending on the details of the process interested in, the events will be filtered by some criteria (cuts) like number of jets or minimal transverse momentum. Events which satisfy certain bounds are sorted into predefined signal regions (SR) [49]. By comparing the observed number of events in one SR with the expected number from SM plus BSM, one can derive limits on the masses and coupling constants of predicted new particles. Within such a published search limits are usually set specifically for one BSM model. However, the cuts and signal regions used for the analysis of LHC data can be implemented and applied to simulated events of different models. In this way, searches are said to be recasted and limits can be obtained for an arbitrary model [49]. Obviously, Recasting will yield only powerful results if the signatures analyzed in a search match to the ones expected for processes in our model.

To have a wide variety of already recasted searches, we use `MadAnalysis5` [50–53] and `CheckMate2` [54], which use the detector simulation `Delphes3` [55] and the anti-kT algorithm [56] implemented in `FastJet` [57, 58]. Furthermore, the generated events are compared to searches implemented in `Rivet` [59] and evaluated with `Contur` [60, 61].

The exclusion of the calculated events at a given parameter point is then calculated with the CLs

technique [62]. For the presentation, we choose to show exclusion lines at 95% CL, interpolated on the scanned grid using Pythons `matplotlib` and the `Scipy` module `interpolate`.

4.1 Single Production

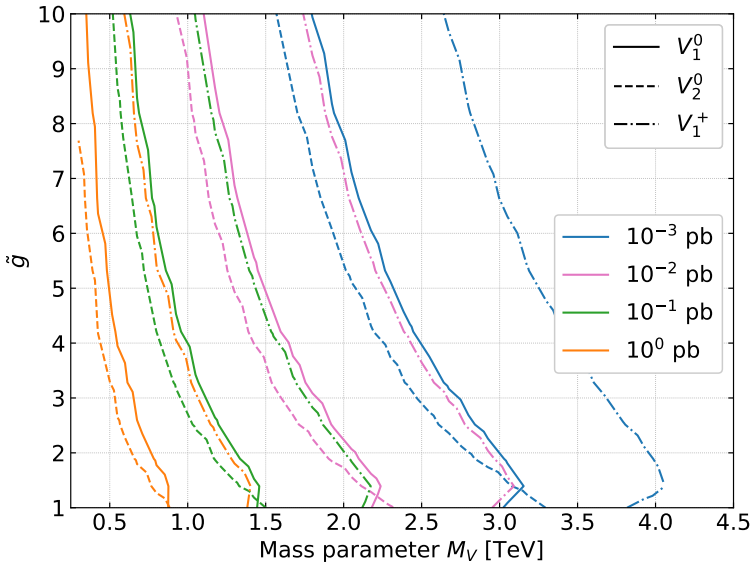

Figure 4.1: Shown are the single production cross sections at $\sqrt{s} = 13\,\text{TeV}$ of the heavy vector states $V_{1\mu}^{0\pm}$, $V_{2\mu}^{0}$ assuming a small $g_{V\pi\pi}$ and SM-like couplings to the top quarks such that we can safely assume a narrow width.

Single Production via Drell-Yan processes are in general expected to yield large cross sections. We saw in sec. 3.4.1, that some resonances have couplings to the SM quarks and therefore they can be single produced in proton-proton collisions. A CHM compatible with LHC bounds must have a relatively small misalignment angle θ. That's why we will take into account only those vectors for which the mass mixing with the SM gauge bosons does not vanish as θ approaches zero. In this limit, the eigenvectors expanded up to $(g^{(\prime)}/\tilde{g})^2$ read

$$B_\mu = \frac{g\left(1-\frac{g'^2}{2\tilde{g}^2}\right)}{\sqrt{g^2+g'^2}}\gamma_\mu + \frac{g'\left(1-\frac{g'^2}{2\tilde{g}^2}\right)}{\sqrt{g^2+g'^2}}Z_\mu + \frac{g'}{\tilde{g}}V_{2\mu}^0\,, \tag{4.1}$$

$$W_\mu^3 = \frac{g'\left(1-\frac{g^2}{2\tilde{g}^2}\right)}{\sqrt{g^2+g'^2}}\gamma_\mu - \frac{g\left(1-\frac{g^2}{2\tilde{g}^2}\right)}{\sqrt{g^2+g'^2}}Z_\mu - \frac{g}{\tilde{g}}V_{1\mu}^0\,, \tag{4.2}$$

$$\tilde{W}_\mu^+ = \left(1-\frac{g^2}{2\tilde{g}^2}\right)W_\mu^+ + \frac{g}{\tilde{g}}V_{1\mu}^+\,. \tag{4.3}$$

This is an important result for the following analysis as we will focus only on single production of $V_{1\mu}^{0\pm}$ and $V_{2\mu}^0$ because here we can expect the largest cross sections. The charged state $V_{2\mu}^+$ does not mix with the gauge bosons at all and the couplings of A_μ are suppressed by s_θ.
Notice, that in the limit $g^{(\prime)}/\tilde{g} \to 0$, we recall the SM expressions of photon and Z boson in terms of the Weinberg angle.
In the following, we will not use the expanded diagonalization results but calculate for each parameter point the matrices $\mathcal{C}$, $\mathcal{N}$ numerically with the `linalg` module of `numpy` to have exact results also

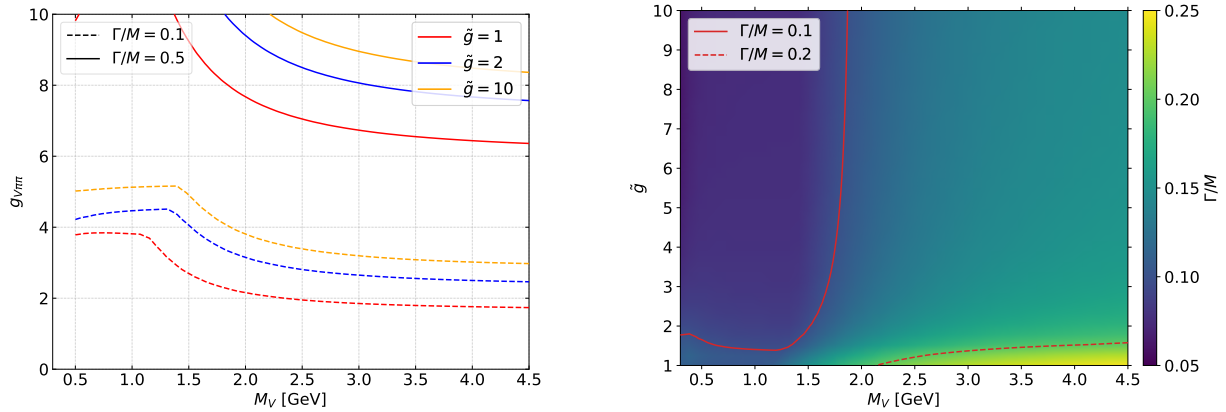

(a) Contour lines of $\Gamma/M = 0.1, 0.5$ in the $M_V - g_{V\pi\pi}$ plane for different values of $\tilde{g}$.

(b) Γ/M in the $M_V - \tilde{g}$ plane as colormap for fixed $g_{V\pi\pi} = 4$.

Figure 4.2: Width Γ over mass M for the vector resonance $V^0_{1\mu}$ in the scenario of partial compositeness top coupling. The scalar masses are set as in eq. (4.7).

where $\tilde{g} \approx 1$.
As noted in sec. 3.3, there are 5 independent model parameters coming from the pNGB Lagrangian eq. (2.38) from which we will fix the decay constant to the current lower limit $f = 1\,\text{TeV}$ [18] and the mass ratio $\xi = 1.4$. The latter is motivated by [63], where a holographic model of chiral symmetry breaking is used to calculate several observables in CHM.
The greatest impact on the production of $V^{0\pm}_{1\mu}$, $V^0_{2\mu}$ have the vector mass parameter M_V and the coupling constant $\tilde{g}$. In fig. 4.1 we show the production cross section in a zero width approximation of the vector resonances. One can see, that the cross section of the charged resonance is an order of magnitude larger compared to the neutral resonances.
Because M_V and $\tilde{g}$ have the greatest impact on the production we are interested in exclusion bounds in the $M_V - \tilde{g}$ plane, while the subsequent decay depends heavily on the top coupling g_t and pNGB coupling $g_{V\pi\pi}$. To make that point more explicit, the decay channels can be divided into three groups

$$\begin{aligned} &V^0_{1,2} \to q\bar{q},\, l^+l^-,\, \nu\bar{\nu}, && V^0_{1,2} \to t\bar{t}, && V^0_{1,2} \to \pi\pi,\, HZ,\, W^+W^-\,, \\ &V^+_1 \to q\bar{q}',\, l^+\nu, && V^+_1 \to t\bar{b}, && V^+_1 \to \pi\pi,\, W^+Z,\, W^+H\,, \end{aligned} \tag{4.4}$$

where q are all light quarks u, d, s, c, b and l, ν are the three lepton generations. The first group of channels arises out of the SM fermion couplings in eq. (3.50) and scale primarily with $1/\tilde{g}$, see eq. (4.3). The second channel is described by the partial compositeness term eq. (3.52). It depends on the coupling constant g_t, which can not specified further. Therefore, we will look at two edge cases: either large contributions from partial compositeness (PC) or only SM contributions as for the lighter quarks and leptons. The two scenarios are denoted as

$$\begin{aligned} \textbf{SM } \boldsymbol{t}: &\quad g_{t,L/R} = g^{(\text{SM})}_{t,L/R}\,, && g_{tb,L} = g^{(\text{SM})}_{tb,L}\,, \\ \textbf{PC } \boldsymbol{t}: &\quad g_{t,L} = g_{t,R} = 1/\sqrt{2}\,, && g_{tb,L} = 1\,. \end{aligned} \tag{4.5}$$

The third group of decay channels was explored in secs. 3.4.2 and 3.4.3. The leading order behavior for all three channels is determined by $g_{V\pi\pi}$, whereas only for $g_{V\pi\pi} \approx 0$ corrections from mass mixing

$\propto 1/\tilde{g}$ get important. We will study again only two different scenarios, divided into

$$\begin{aligned} \textbf{weak } \boldsymbol{\pi}: &\quad g_{V\pi\pi} = 0\,, \\ \textbf{strong } \boldsymbol{\pi}: &\quad g_{V\pi\pi} = 4\,. \end{aligned} \tag{4.6}$$

Combining the top and pNGB edge cases, we have four independent scenarios which will be studied. Exclusion bounds depend further on the subsequent decay of the scalars. Additionally to the WZW terms in sec. 3.4.4 there might also be the option for couplings to top quarks. It depends on the spurion representation in which the SM quarks are embedded if these couplings exist. These terms were classified e.g. in [18] for the SU(5)/SO(5) coset. In particular, there might be also possibilities in which all couplings vanish at tree level. If this is not the case, they can be expected to be significantly larger than the anomaly terms. For this reason, we split the analysis of the pNGB pair production into two scenarios: Either all scalars decay dominantly into third generation quarks (fermiophilic) or all of them decay only via the WZW terms into gauge bosons (fermiophobic). The two pNGB scenarios were already studied in [36], where bounds on the scalar masses were derived. We will assume only a small mass splitting $\Delta = 2\,\text{GeV}$ among the scalar multiplets and stick to the parameterization as in eq. (3.67), which matches with the scenario "S-eq" in [36]. In the fermiophobic model the scalar mass M_η is excluded below $\approx 660\,\text{GeV}$, see fig. 8 of [36]. We fix the masses a bit above to

$$M(\eta_3) = 698\,\text{GeV}\,, \qquad M(\eta_5) = 700\,\text{GeV}\,, \qquad M(\eta_1) = 702\,\text{GeV}\,. \tag{4.7}$$

In the fermiophilic model the current mass bounds are only around 500 GeV [36]. For simplicity, as the scalar mass (slightly) influences the branching ratio of all other channels, we will use the same mass parameterization for comparison.
To justify, that we work in a regime of NWA for all scenarios, figs. 4.2, D.1 and D.2 show the total width over vector mass as function of M_V, $\tilde{g}$ and $g_{V\pi\pi}$ for all three vector resonances in a scenario of PC t. In the left hand plot one can clearly see that the decay into two pNGBs drops out if the vector mass approaches $2M_\eta$. As the vector mass depends also on $\tilde{g}$, this drop out shifts with smaller $\tilde{g}$ to smaller values of M_V. Admittedly, the total decay width of $V_{1\mu}^{0\pm}$ can exceed 10% for very small values of $\tilde{g}$. That means, results above 1.5 TeV and $\tilde{g} \lesssim 2$ have to be treated with caution.
The branching ratios in each scenario for the vector states $V_{1\mu}^0$, $V_{2\mu}^0$ and $V_{1\mu}^+$ are shown in figs. 4.3, D.3 and D.4 for $M_V = 3\,\text{TeV}$. In the scenarios with PC t or strong π, the channel with the strong coupling is the dominant decay channel. For two strong couplings, called PC t, strong π, the sum of all pNGB channels has roughly the same decay width as the partial compositeness top coupling. If we choose at least one channel to be dominant, the SM fermion couplings are always suppressed by $\tilde{g}$. Only for SM like top coupling and $g_{V\pi\pi} = 0$, the partial widths of all channels scale the same in terms of $\tilde{g}$ and the branching ratios are nearly constant.

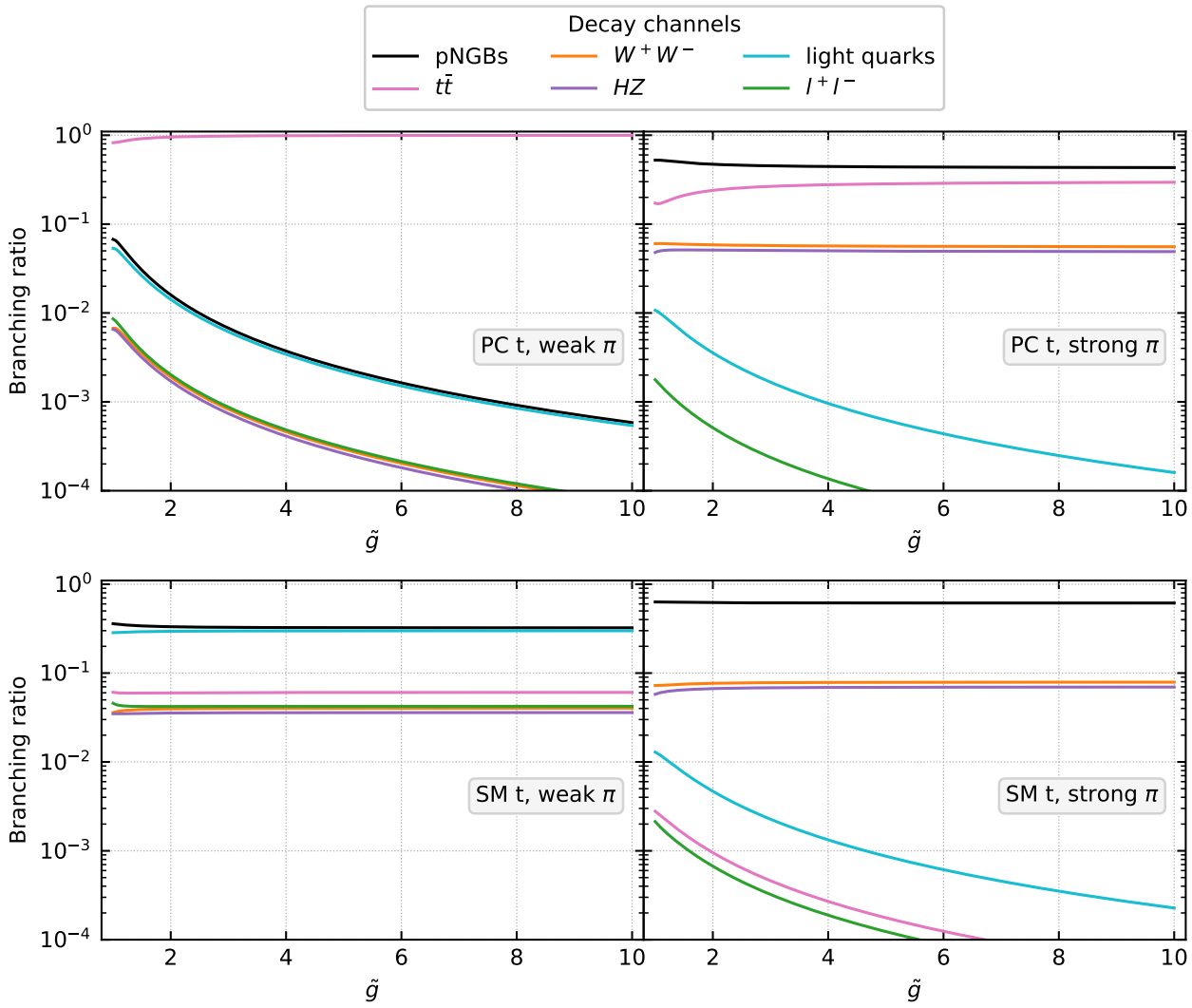

Figure 4.3: Relevant branching ratios of $V^0_{1\mu}$ for $M_V = 3\,\text{TeV}$, $M_A/M_V = 1.4$ and $f = 1\,\text{TeV}$ in four benchmark scenarios defined in eqs. (4.5) and (4.6). The scalar masses are set as in eq. (4.7). We use here $l = e, \mu$ and the light quarks are u, d, s, c, b. The channel pNGB is the sum of all decays into two pNGBs.

4.1.1 Decay channels

In the following, we derive bounds in the $M_V - \tilde{g}$ plane for all four benchmark scenarios by analyzing numerous decay channels sorted by their origin in eq. (4.4).

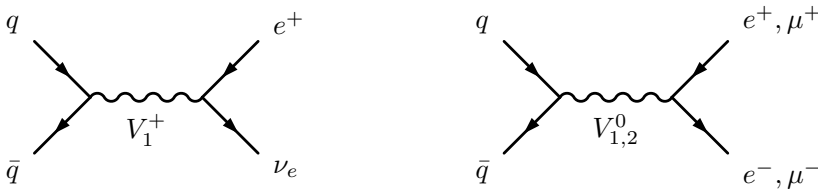

Figure 4.4: Feynman diagrams for Drell-Yan production of charged and neutral vector resonance and subsequent decay into leptons.

Leptonic final states

We start with the final state $e^{\pm}\nu$, shown on the left in fig. 4.4, for which experimental upper limits on the cross section σ_{95} can be found in [64], published by the ATLAS collaboration. A search for a heavy charged vector resonance decaying into electron and neutrino is presented therein, using the LHC dataset of proton-proton collisions with an integrated luminosity of $139\,\text{fb}^{-1}$. To be able to compare the data with our model, we calculate the cross section of $p\,p \to V_{1\mu}^{+} \to e^{+}\nu_e$ on a fine grid in the $M_V - \tilde{g}$ plane. For the event simulation in `MadGraph5`, we take into account off-shell effects of the vector resonance within the NWA. The colormap in fig. 4.5 shows the cross section as a function of $\tilde{g}$ and the actual vector mass. Note, that the latter differs clearly from the mass parameter M_V for small values of $\tilde{g}$, see also fig. 3.1. Next, we interpolate the simulated cross section σ to the mass values given in the observed 95 % CL upper limit σ_{95} and calculate the ratio σ/σ_{95} as a function of vector mass and $\tilde{g}$. An exclusion line is then drawn where this ratio is interpolated to be $\sigma/\sigma_{95} = 1$. In fig. 4.5 the results are shown for each of the four benchmark scenarios. As we would expect from the branching ratios in fig. D.4, the strongest bounds in this process are given for weak π and SM top coupling. In dependence of $\tilde{g}$, the excluded $V_{1\mu}^{+}$ mass ranges up to 5.1 TeV. We fixed the maximal $\tilde{g}$ value for our scans to 10. In general, the perturbation theory approach becomes invalid for coupling constants exceeding $4\pi \approx 12.6$. Nevertheless, reaching this limit is unlikely to yield additional insights. For the other scenarios, the bounds depend more on $\tilde{g}$ because not only the production coupling, but also the branching ratio into $e^{\pm}\nu_e$ is affected. The results all the other three scenarios are roughly in the same range, excluding vector masses up to 4.7 TeV at $\tilde{g} = 1$, whereas masses around 1 TeV are still possible at $\tilde{g} \gtrsim 5$. We conclude the analysis by presenting the exclusion lines as functions of the mass parameter M_V in one combined figure, see fig. 4.6. The combined presentation makes it easy to compare the different scenarios within one channel. But it particularly enables one to compare the results of different processes more easily.
The benefits are more apparent when we study the final state $e^{+}e^{-} + \mu^{+}\mu^{-}$. In [65], a search for high-mass dielectron and dimuon resonances is presented and upper limits on the cross section are stated for different widths of the resonance in terms of a fiducial cross section. The search aims for a single neutral vector resonance Z', whereas in our model we can have two neutral resonances $V_{1\mu}^{0}$, $V_{2\mu}^{0}$ in the s-channel, as in fig. 4.4.
The main concern is the large mass splitting of both states at smaller $\tilde{g}$ values. This makes it challenging to compare a process involving $V_{1\mu}^{0}$ and $V_{2\mu}^{0}$ with upper limits on the cross section at a given Z' mass. Therefore, we analyze the two neutral resonances individually. With this approach, we neglect interference effects of the vector resonances, but checked that those are below 10% anyways. Further, we were able to implement the same cuts used by the ATLAS Collaboration within `MadGraph5`. Each muon (electron) candidate needs to have transverse momentum $p_T > 30\,\text{GeV}$ ($E_T > 30\,\text{GeV}$) and a pseudorapidity of $|\eta| < 2.5$. Also, there is a criteria for the dilepton mass to satisfy $m_{ll}^{\text{true}} > M_x - 2\Gamma_x$, where M_x, Γ_x are the mass and width of the s-channel vector resonance. For comparison with simulated data, we used the upper limits for a fixed width of 6%. In general the upper limits would be larger for larger widths, but overall it has only a minor influence on our results.
The exclusion plots in terms of the actual vector masses can be found in appendix D.2, while we present here only the final result in terms of the mass parameter M_V, see fig. 4.7. In the $M_V - \tilde{g}$ plane it is possible to show the bounds of both resonances, despite their mass splitting. As one can see, the individual bounds from $V_{1\mu}^{0}$ and $V_{2\mu}^{0}$ do not differ much. Overall, in comparison with the bounds of $e^{\pm}\nu_e$, the bounds of $e^{+}e^{-} + \mu^{+}\mu^{-}$ are a bit weaker besides some exceptions at very small or very large M_V.

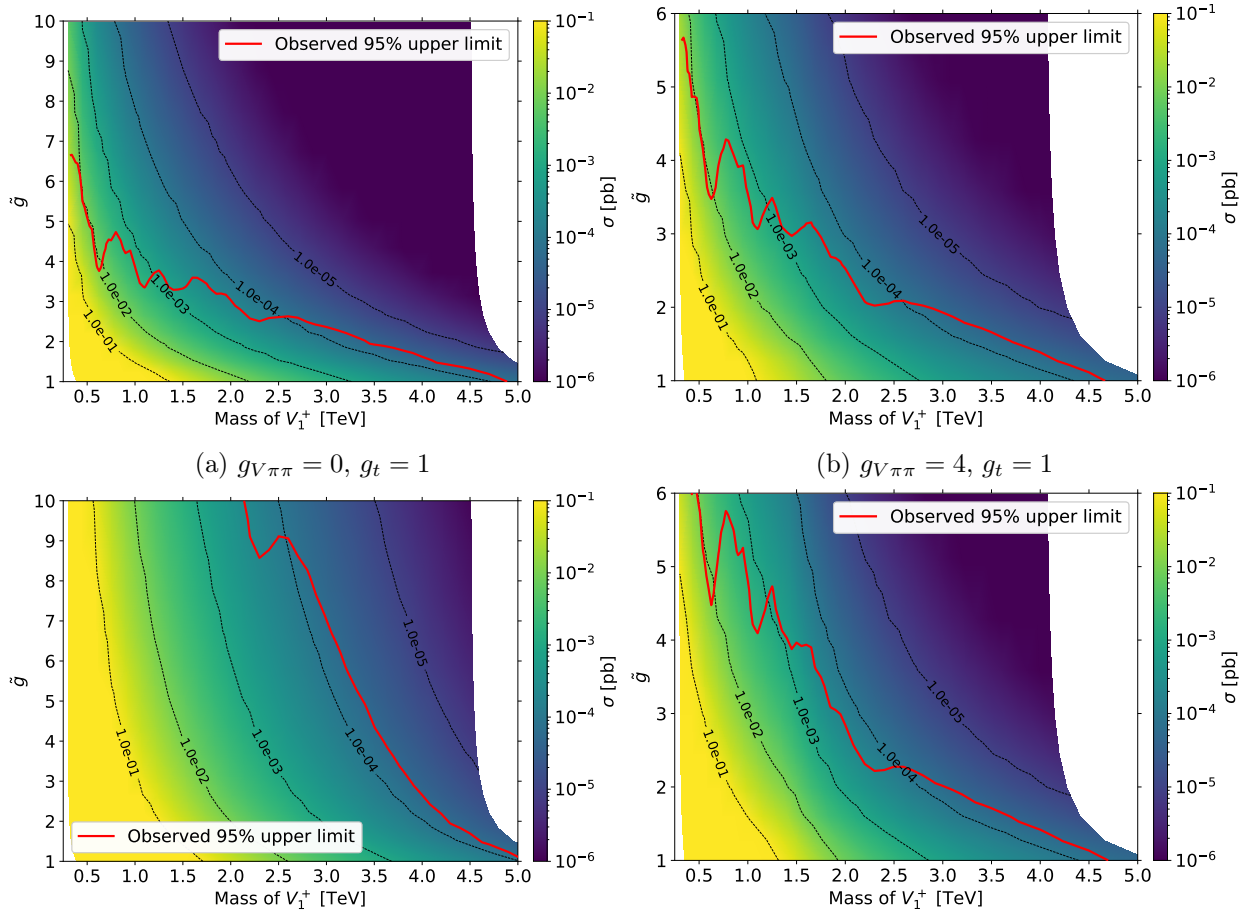

(a) $g_{V\pi\pi} = 0$, $g_t = 1$

(b) $g_{V\pi\pi} = 4$, $g_t = 1$

(c) $g_{V\pi\pi} = 0$, $g_t = g_t^{(\mathrm{SM})}$

(d) $g_{V\pi\pi} = 4$, $g_t = g_t^{(\mathrm{SM})}$

Figure 4.5: Shown are the 95% CL exclusion lines derived from the channel $pp \to V_{1\mu}^{\pm} \to e^{\pm}\nu$ for $M_A/M_V = 1.4$, $f = 1\,\mathrm{TeV}$. The area below the red line is excluded, which was calculated from the upper limits on the cross section in [64]. The pNGB masses are defined as in eq. (4.7).

Aside from the leptons, the light quarks q correspond to the same group of decay channels. However, we compared simulated cross section to [66] and found that bounds would be considerably weaker compared to the leptonic channels.

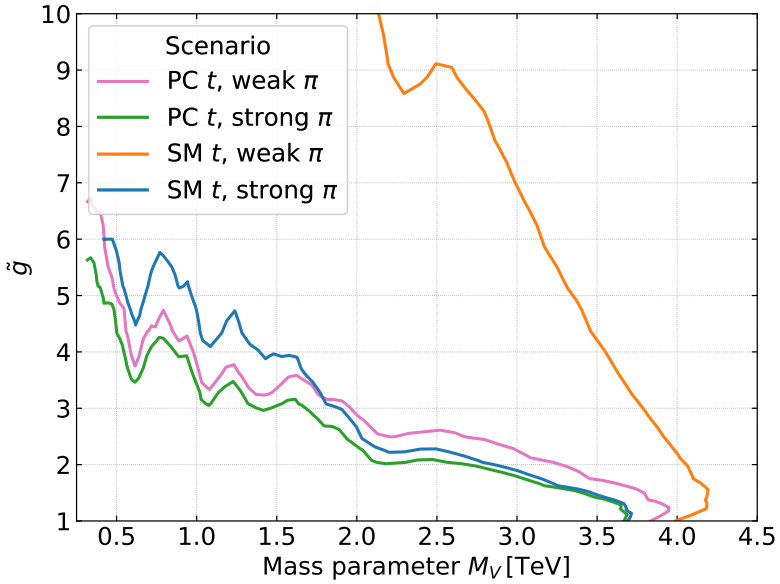

Figure 4.6: Combined presentation the results in fig. 4.5 as function of the mass parameter M_V. The benchmark scenarios were defined in eqs. (4.5) and (4.6).

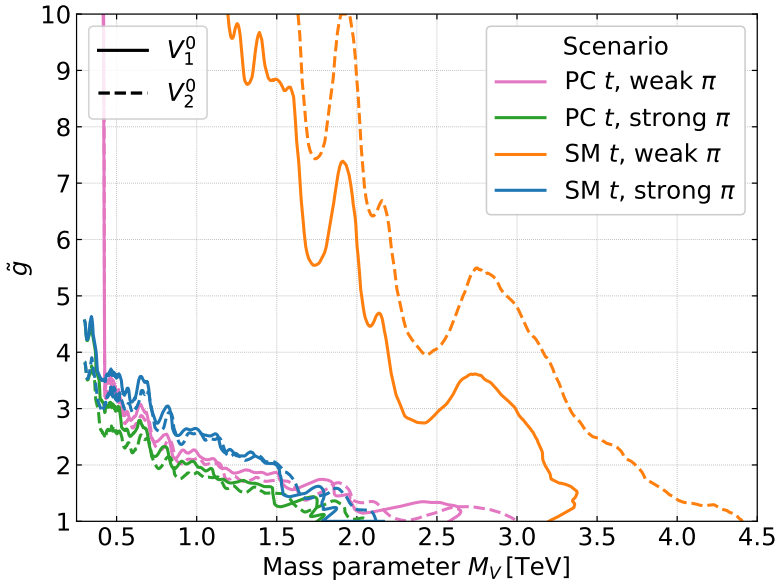

Figure 4.7: Shown are the 95% CL exclusion lines derived from the channel $pp \to V_{i\mu}^0 \to l^+l^-$ with $i = 1, 2$ and $l = e, \mu$ for fixed $M_A/M_V = 1.4$, $f = 1\,\text{TeV}$. The area below the lines is excluded, calculated from the upper limits on the cross section in [65]. The pNGB masses are defined as in eq. (4.7) and the benchmark scenarios are defined in eqs. (4.5) and (4.6).

Top quark final states

The second group of eq. (4.4) are the final states $t\bar{b}$ and $t\bar{t}$. For the scenario of a large partial compositeness coupling and a rather weak pNGB channel, this would be the dominant decay mode. We compared our model to the cross section limits in [67], where we explicitly use the bounds from

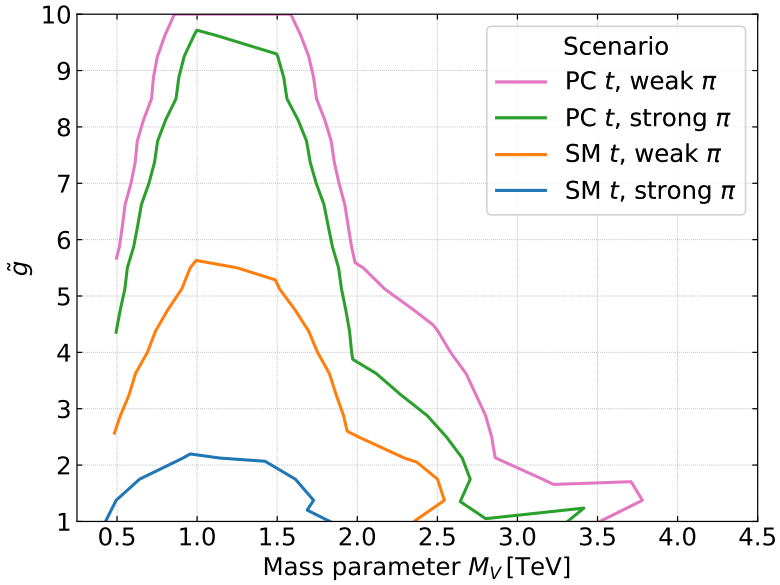

Figure 4.8: Shown are the 95% CL exclusion lines derived from the channel $pp \to V_{1\mu}^{+} \to t\bar{b}$ for $M_A/M_V = 1.4$, $f = 1\,\text{TeV}$. The area below the lines is excluded, calculated from the upper limits on the cross section in [67]. The pNGB masses are defined as in eq. (4.7) and the benchmark scenarios are defined in eqs. (4.5) and (4.6).

fig. 13a for a heavy charged resonance coupling to the left handed fermions of the standard model. The upper limits stem from the LHC data set with integrated luminosity of $139\,\text{fb}^{-1}$ analyzed by the ATLAS collaboration. The upper limits were derived for a resonance with narrow width $\sim 3\%$. Available bounds stated for a larger width are substantially weaker. This means we will overestimate bounds in scenarios with at least one strong coupling, because the actual widths are larger.
We show our results in form of a combined plot in the $M_V - \tilde{g}$ plane in fig. 4.8. For the case of a dominant decay $V_{1\mu}^{+} \to t\bar{b}$ we can exclude the model parameters up to $M_V \sim 3.7\,\text{TeV}$. For relatively small masses of $M_V < 1\,\text{TeV}$ the SM background from W^{+} becomes stronger and it becomes more difficult to detect BSM effects.
We did also compare our model against limits stated in [68] for $t\bar{t}$ signatures. But derived bounds are significantly weaker compared to the charged vector resonance.

pNGB pair production

The branching ratios into the pNGBs depend heavily on the value of $g_{V\pi\pi}$. Their subsequent decay yields numerous final states, therefore Recasting is suited well to get exclusion values. In the following we analyze the combination of the two neutral and the charged vector resonances. In our `MadGraph5` setup, we neglect interference between the pNGBs as their width is much smaller than their mass. This can be expected also for the fermiophilic model because the couplings scale as $m_t/f \sim s_\theta$ [36] For the fermiophobic model, the final states are made up of four to six gauge bosons. An example is

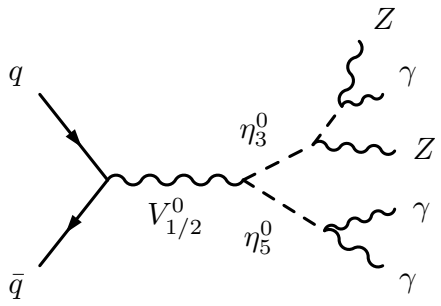

Figure 4.9: Single Production of neutral vector decaying into a pair of pNGBs in a fermiophobic model.

shown in fig. 4.9. Here, we make use of the analytic results for the three-body decay of η_3^0, see the explicit branching ratios in tab. 3.2. It turns out, that the `CheckMate2` recast of `atlas_1802_03158` [69] yields the strongest bounds in the scanned parameter space. It searches for gauge-mediated supersymmetry in final states containing at least two photons and some jets. Therefore, it is especially sensitive for final states containing multiple photons and W or Z bosons, which decay hadronically. There are numerous combinations of this kind possible for the process under study.
We choose our scanning grid to start at $M_V = 2 \cdot M_\eta = 1.4\,\text{TeV}$ and interpolate between the grid points a 95% CL exclusion bound. The result for each scenario is shown in fig. 4.10. The figure does show additional information like the exclusion of each point indicated by color and the signal region (SR), in which the exclusion value was calculated. As we would expect, the bounds get weak if we approach $M_V = 2 \cdot M_\eta$, as the branching ratio into pNGBs is kinematically suppressed. This effect does also depend on $\tilde{g}$, as the actual vector masses are significantly larger than M_V at smaller $\tilde{g}$. The total cross section, shown as dotted black lines, shows a further notability at small $\tilde{g}$ due to the same reason. With very small $\tilde{g}$ the vector masses get so much larger than M_V which then even exceeds the effect of a larger production coupling to the light quarks. We unite these results in fig. D.9, which can be compared easily to the channels analyzed before. In the fermiophilic model all single charged and neutral pNGBs will decay into top-bottom or top-top pairs, as shown on the left hand side of fig. 4.11. The double charged η_5^{++} can not decay into two SM quarks but undergoes a three-body decay via an off-shell pNGB into W^+ and two fermions

$$\eta_5^{++} \to W^+ \eta_{3,5}^{+*} \to W^+ t\bar{b}\,. \tag{4.8}$$

We found multiple recasts are sensible for these signatures. Within `CheckMate2`, we used the searches `atlas_2106_09609` [70] and `atlas_2101_01629` [71]. The first paper deals with R-parity-violating supersymmetry searching for final states containing many jets and at least one lepton. The latter searches for gluino and squark pair production decaying into exactly one isolated lepton, further jets and missing transverse momentum. In `MadAnalysis5` the searches `cms_sus_19_006` [72] and `cms_sus_16_033` [73] are giving the strongest bounds. Both search for supersymmetric particles decaying into final states with multiple jets and large missing transverse momentum.
Detailed exclusion plots for each scenario can be found in appendix D.2, whereas we state here only the combination in fig. 4.11. The exclusion bounds for $M_\eta = 700\,\text{GeV}$ are shown as solid lines. For comparison, we also show the results for the case of lighter pNGBs as dotted contours. The shapes of the exclusion bounds for $M_\eta = 700\,\text{GeV}$ seem to be a bit unusual, but this might be because of the various different searches which contribute.

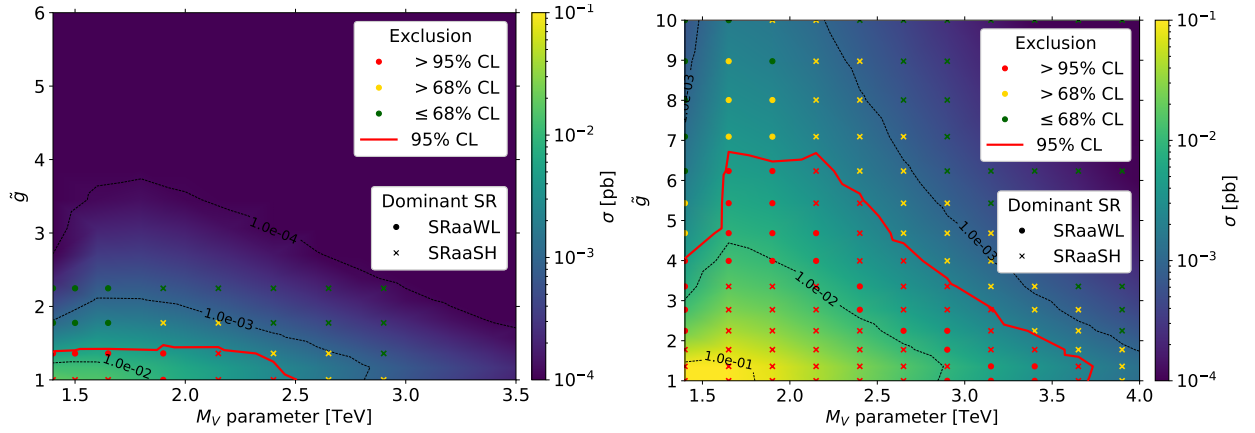

(a) $g_{V\pi\pi} = 0$, $g_t = 1$

(b) $g_{V\pi\pi} = 4$, $g_t = 1$

(c) $g_{V\pi\pi} = 0$, $g_t = g_t^{(\mathrm{SM})}$

(d) $g_{V\pi\pi} = 4$, $g_t = g_t^{(\mathrm{SM})}$

Figure 4.10: Shown are the 95% CL exclusion lines derived from single produced vector resonances decaying into a pair of pNGBs in a fermiophobic model with pNGB masses as in eq. (4.7). The bounds were derived using the recasted search [69] for $M_A/M_V = 1.4$ and $f = 1\,\mathrm{TeV}$. The cross section is shown as a colormap in the background and we state the exclusion values and the dominant signal region (SR) for each recasted grid point.

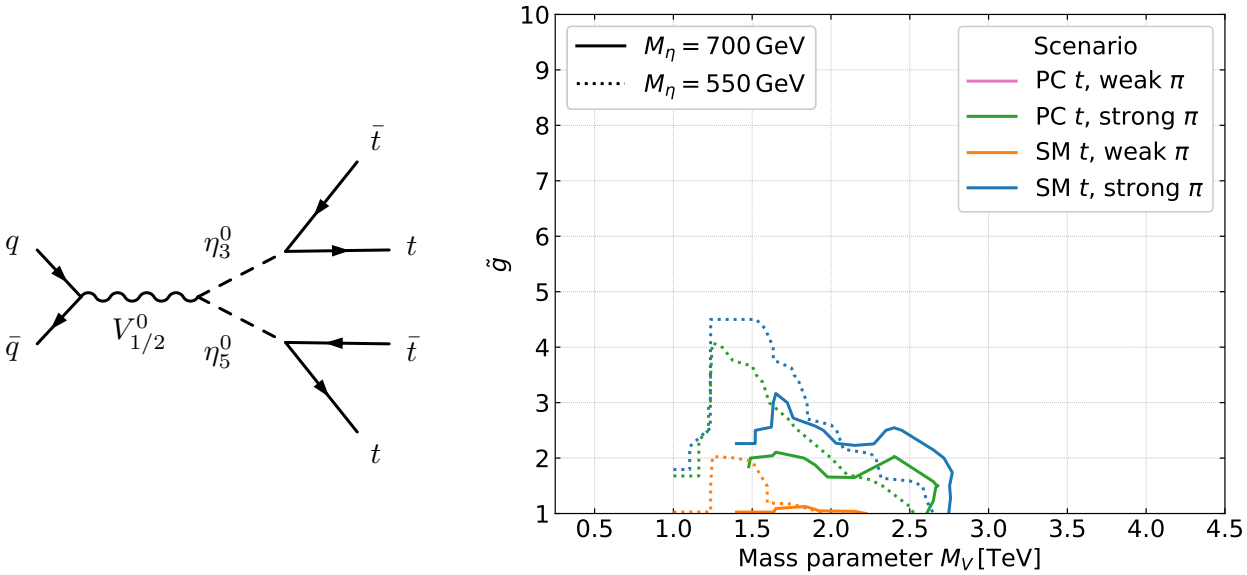

Figure 4.11: The left hand side shows an example for single production of vector resonances decaying into a pair of pNGBs in a fermiophilic model. On the right hand side the 95% CL exclusion lines are shown, derived from single produced vector resonances decaying into a pair of pNGBs in a fermiophilic model with pNGB masses as in eq. (4.7). The bounds of four scenarios, defined in eqs. (4.5) and (4.6) are combined into one plot for $M_A/M_V = 1.4$ and $f = 1\,\text{TeV}$. More information about the single results can be found in fig. D.10.

4.1.2 Discussion

The results of all analyzed decay channels are summarized in fig. 4.12. All exclusion bounds of one scenario are taken together and the interpolated envelope is drawn. The solid lines correspond to the fermiophobic model, while the dashed lines show the fermiophilic model, both with $M_\eta = 700\,\text{GeV}$. In the latter case, the bounds from vector decays into two pNGBs do not contribute to the envelopes as they are weaker than the bounds from leptonic or top quark decay.
As we have briefly mentioned before, in a fermiophilic model the scalar masses are not bound to $M_\eta = 700\,\text{GeV}$. However, for a proper treatment with lower M_η, one would have to run the direct decays into leptons and top quarks again, as their branching ratios depend also on the scalar mass. In particular, M_η determines where the decay into two pNGBs drops out of the branching ratios. In the end it would effect the final results only slightly. In fig. 4.11, we present the bounds for $M_\eta = 700\,\text{GeV}$ and $550\,\text{GeV}$ for the decay channel into pNGBs. Also in this case, the scalar mass does not affect the results that much.
Further, we rely heavily on the assumption $M_A/M_V > 1$, which is motivated by [63]. However, if we drop this assumption, further decay channels of the type $V \to A\pi$ could be possible.
We want to emphasize, that neither of the presented scenarios will represent the true model, but we can expect the model to be realized somewhere in between. The scenario of SM t and weak π stands out as its bounds are a bit stronger, predicting $M_V \gtrsim 2.2 - 4.4\,\text{TeV}$ if we bound $\tilde{g} < 10$. But this scenario has to be seen as a rather unrealistic realization of a CHM. The composite sector is a strong coupling sector, so we would typically expect $g_{V\pi\pi}$ to be larger than one. We can compare the situation with QCD, where the ρ meson decays mainly into two pions with $g_{\rho\pi\pi} \approx 6$. Additionally, to explain the quark mass hierarchy within CHM, contributions from partial compositeness to the top quark coupling are strongly anticipated.
The predictions for the other scenarios do not differ that much especially at smaller $\tilde{g}$. We highlight, that the exact value of $g_{V\pi\pi}$ is not that important, as long as it is a strong coupling. Larger or a bit smaller values than $g_{V\pi\pi} = 4$ would not change the branching ratios substantially. Its effect might even be balanced by a different choice of g_t.
As mentioned before, we actually overestimated the bounds for some channels as we compared our model to experimental upper limits, which were derived for resonances with narrower widths. Despite that, vector resonances around $2 - 2.5\,\text{TeV}$ are still realizable for medium large $\tilde{g}$ in all scenarios except for the case of SM t and weak π. But we want to highlight, that we can not even exclude vector masses of around $\sim 1\,\text{TeV}$ in all scenarios, which is barely above the current scalar mass bounds.
In conclusion, the lower multi-TeV range is still acceptable for vector resonances in the model under study. Next-to-Leading-Order effects could strengthen or weaken the derived bounds, but will not change the overall picture.
We can not compare our results directly to the bounds in [26] from 2016 for the electroweak SU(4)/Sp(4) coset, as they used a different set of parameters. Further, they did not take into account the possibility of a partial compositeness coupling to the top quarks. Nonetheless, it seems that our bounds on M_V are at least $1\,\text{TeV}$ stronger for small $\tilde{g}$, which might be due to the larger LHC data set we had access to.

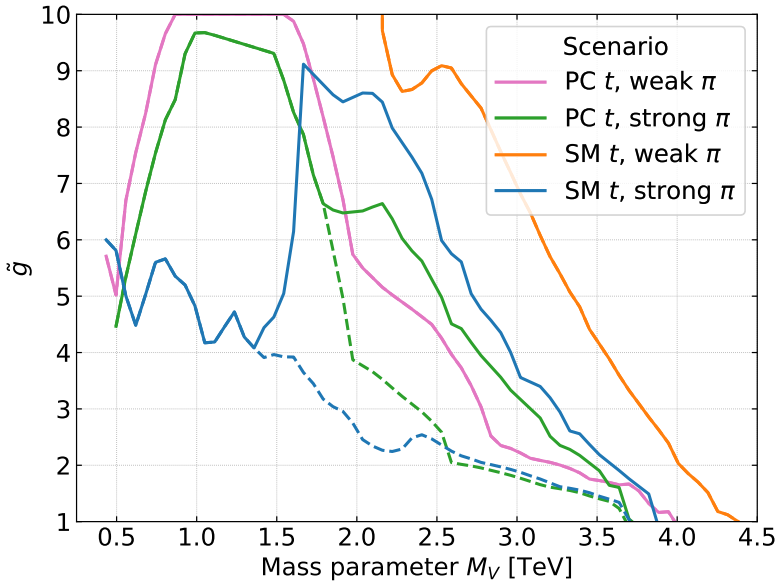

Figure 4.12: The envelopes of multiple exclusion bounds derived from different decay channels of single produced vector resonances presented in sec. 4.1.1. The dashed lines correspond to the fermiophilic, the solid lines to fermiophobic pNGBs. In all cases the masses are defined as in eq. (4.7). The scenarios were defined in eqs. (4.5) and (4.6) and we fixed $M_A/M_V = 1.4$ and $f = 1\,\text{TeV}$.

4.2 Pair Production of $\hat{a}_5^{++}$

The single production in sec. 4.1 is suitable for processes which are sensitive on the vector mass parameter M_V. In the following, we will study those kind of channels which yield independent bounds on the axial-vector mass parameter M_A.
As we have seen, the single production of the mass mixing axial vector $A^{0,\pm}$ is suppressed. Therefore, we decided to look at pair production of the double charged axial $\hat{a}_5^{++}$, because it is a unique prediction of the SU(5)/SO(5) coset within the minimal models. There is no $W^+ \to \hat{a}_5^{++}W^-$ vertex allowed because $\mathbf{3}_0 \times \mathbf{3}_0 \times \mathbf{3}_1$ has no singlet. But the gauge couplings to photon and Z give rise to Drell-Yan pair production $pp \to \hat{a}_5^{--}\hat{a}_5^{++}$. For production, the most relevant coupling is given by the gauge interaction to the photon $2e$, while the coupling to Z in general is a function of all independent model parameters. Nevertheless, its value converges for larger $\tilde{g}$ very fast and we fixed the coupling to 0.4.
Contrary to the previous scans in sec. 4.1 we will vary the masses of the pNGBs too, respecting a lower limit of $M_\eta \gtrsim 700\,\text{GeV}$. Further, to get independent bounds on M_A, we will loosen up the fixation of the mass parameter ratio to $\xi \gtrsim 1$ with $M_V > M_\eta$. In this setting the decay channels of an axial into a vector resonance and scalar is kinematically still suppressed for lower multi-TeV axial masses M_A and we will neglect this possibility. Therefore, the double charged $\hat{a}_5^{++}$ can undergo only three-body decays via η_5^{++} or $\eta_{3/5}^{+}$, where we will assume that the pNGBs decay into gauge bosons through the WZW terms. This results in three different signatures $W^+W^-W^+W^-\gamma\gamma$, $W^+W^-W^+W^-Z\gamma$ and $W^+W^-W^+W^-ZZ$. An example of the process is shown in fig. 4.13.
It turns out that the η_3^+ and η_5^+ channel differ only by $\cos\theta$ in terms of expanded coupling constants. Fixing the decay constant f, there are only two independent couplings with an arbitrary ratio depending on M_V, ξ, $g_{V\pi\pi}$, $\tilde{g}$. We decide to study two edge cases, dominance of the $\eta^{++}Z$ or $\eta_{3/5}^{+}W^+$ channel, and a 50% branching ratio for each. In this way we can derive exclusion limits in the plane $M_A - M_\eta$.

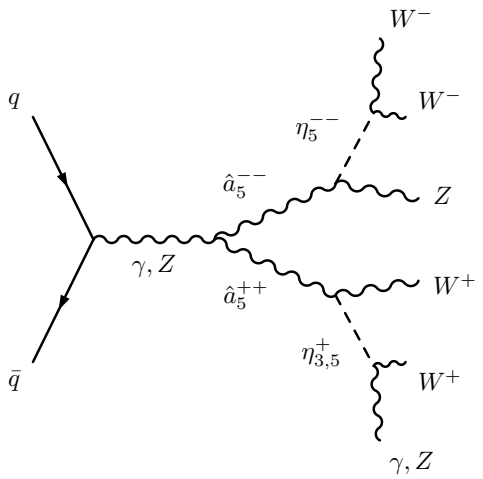

Figure 4.13: Feynman diagram for pair production of the double charged axial $\hat{a}_5^{++}$ and subsequent decay in a fermiophobic model.

4.2.1 Results

Starting with $\eta_5^{++}Z$ dominance, the final state is always given by four W and two Z bosons. In this case, it turns out that the `MadAnalysis5` recast `cms_exo_19_002` [74] is most sensible. They search for BSM physics in final states with at least three charged leptons (electrons or muons). The results of the recast are summarized in fig. 4.14. Shown is the cross section as heatmap background, the dominant signal region (SR) and the exclusion value of each scan point.
As one can see, the bounds on M_A lie around 860 GeV, which is barely above the scalar mass bounds. The mass bounds in the η^+W^+ channel are slightly stronger, stated in fig. 4.15. As it was shown in

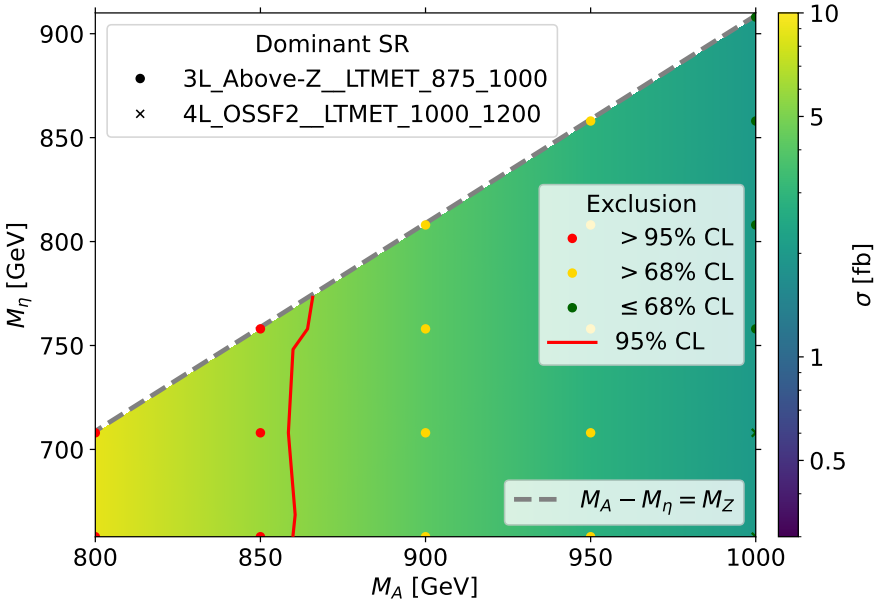

Figure 4.14: The exclusion bound in the $M_A - M_\eta$ plane for pair production of $\hat{a}_5^{++}$ in the scenario of $\eta_5^{++}Z$ dominance. Shown are also the grid points with dominant signal regions (SR) of the scan, which were evaluated with `cms_exo_19_002` [74] implemented in `MadAnalysis5`.

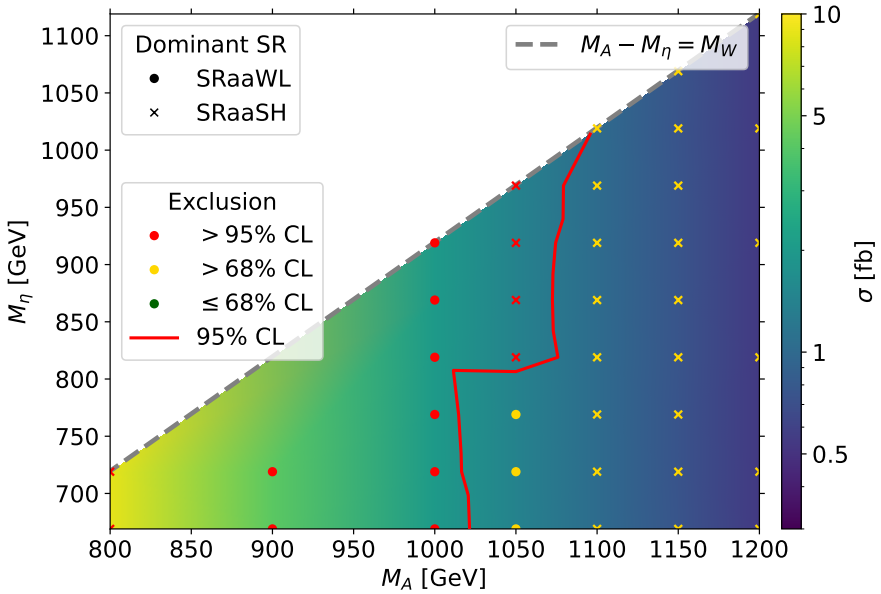

Figure 4.15: The exclusion bound in the $M_A - M_\eta$ plane for pair production of $\hat{a}_5^{++}$ in the scenario of $\eta^+ W^+$ dominance. Shown are also the grid points with dominant signal regions (SR) of the scan, which were evaluated with `atlas_1802_03158` [69] implemented in `CheckMATE`.

fig. 3.2, η_3^+ and η_5^+ decay most likely to at least one photon, which is why we get in total $\approx 60\%$ of diphoton final state. For this type of signature, the search `atlas_1802_03158` [69] implemented in `CheckMATE` gives strong bounds, as we have seen already in sec. 4.1.1.

For the case of 50% branching ratio for both decay channels, the diphotonic final state does only contribute with $\approx 15\%$, but mixed ZA signatures get more important. It turns out, that besides `atlas_1802_03158` two other searches are useful. The `MadAnalysis5` recast `cms_exo_20_004` [75], which searches for energetic jets and large missing transverse momentum, and at smaller masses we found that `ATLAS_13_LL_GAMMA` implemented in `Contur` using the search `ATLAS_2019_I1764342` [76] gives the strongest bounds. The latter analysis explicitly searches for a prompt photon in association with a Z boson. The results are shown in fig. 4.16. The `MadAnalysis5` recast `cms_exo_20_004` combines multiple signal regions to state a significantly stronger bound. Consequently, it is nearly impossible to retrace the impact of a single signal region to the final exclusion value. As the efficiency of most signal regions is very small there are only a few events getting through the cuts, even with 10^5 events. The combination with a rather small SM background leads to larger fluctuations between neighbored grid points.

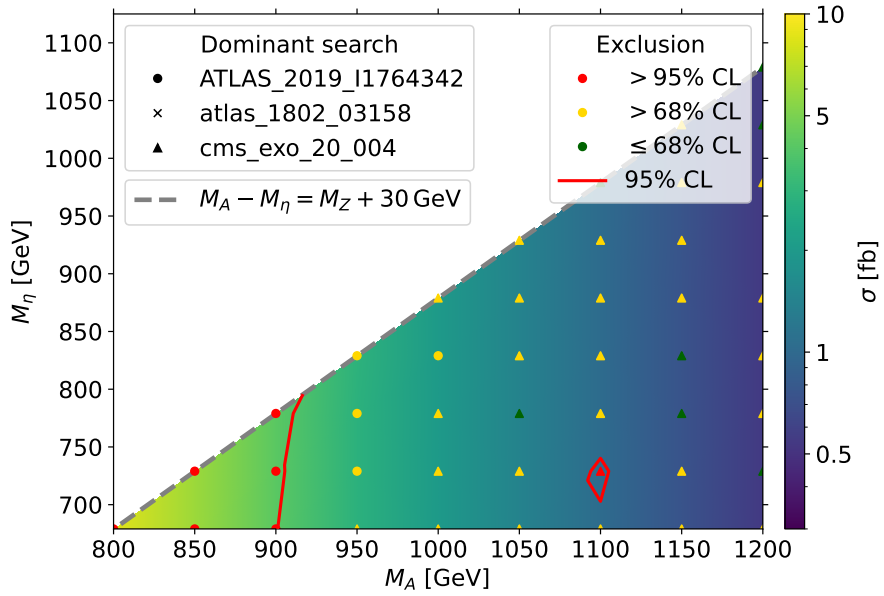

Figure 4.16: The exclusion bound in the $M_A - M_\eta$ plane for pair production of $\hat{a}_5^{++}$ in the scenario of 50% branching ratio of $\eta_5^{++}Z$ and η^+W^+. Shown are also the grid points and the corresponding search which gave the strongest bounds.

4.2.2 Discussion

Compared to the bounds on M_V in the previous section, the mass of the axial vectors is only barely constrained by current LHC data. The results can be interpreted in two ways. If we trust the holographic model calculations [63], the bound on axial mass parameter is simply $M_A \gtrsim 1.4 \cdot M_V$, predicting axial-vectors to be in the lower to mid multi-TeV range. On the other hand, if we do not rely on this type of predictions, the parameter space along M_A is wide open and allows for $M_A \gtrsim 1\,\mathrm{TeV}$.

We motivated the analysis of the double charged vector, as it leads to special signatures involving pairs of same charged W bosons. However, it turned out that the recastings with the strongest bounds are not sensitive to this feature. Therefore, we should take into account pair production involving other states of the axial multiplet, which will contribute to the same signal regions.

Furthermore, looking at the vertices $ZW^+\hat{a}^-_{3,5}$, $ZZ\hat{a}^0_{1,3,5}$ $W^+W^-\hat{a}^0_{1,3,5}$, there is a variety of different diagrams producing a SM boson plus an axial resonance. As they lead to completely different final states, it would be worth exploring their implications.

Aside from that, we did not yet discuss the scenario of fermiophilic scalars, where the pNGBs decay mainly into top quarks. As we have seen in sec. 4.1, the bounds coming from the diphoton final states are much stronger than from the quarks searches. In our pair production scenarios, the strongest bounds do also come from the diphoton search and we expect, that in a fermiophilic model the bounds on M_A will stay below that. This means, we expect the bounds to be $M_A \lesssim 1\,\mathrm{TeV}$ at scalar masses $M_\eta \gtrsim 700\,\mathrm{GeV}$ and therefore they would not add any new insights. Admittedly, the scalar mass is not bound to 700 GeV in a fermiophilic model, but we have seen so far that it doesn't have a great impact on the M_A bounds. In conclusion, there are still some possibilities unexplored for further analysis of the axial vector resonances. Nevertheless, our results indicate that with the currently available recasting tools the bounds can be expected to be significantly weaker compared to the bounds on the vector mass parameter M_V from single production.

5 Conclusion & Outlook

In this thesis we explored Composite Higgs Models with a focus on phenomenology of Spin-1 resonances emerging from the electroweak coset SU(5)/SO(5). The motivation for this study stems from the limitations of the Standard Model to explain a dynamical origin of the electroweak symmetry breaking.

We built the pNGB Lagrangian, including vector and axial vector resonances following CCWZ and hidden symmetry formalism. Further, we discussed the decomposition of the vector representations into the custodial group $\mathrm{SU}(2)_L \times \mathrm{SU}(2)_R$ and its diagonal $\mathrm{SU}(2)_D$ and gave explicit embeddings in the subgroup SO(5). Furthermore, we investigated the mass mixing among the Spin-1 resonances with the SM gauge bosons. In that regard, approximated solutions to diagonalize the mass matrices were given. These were then used to identify three vector resonances $V_{1\mu}^{0\pm}$, $V_{2\mu}^{0}$, which have non-vanishing couplings to SM fermions even in the SM limit of zero misalignemnt $\theta \to 0$. This implies that these states can be single produced in the s-channel, which is suited to derive bounds on their mass parameter M_V. Their decay channels were studied intensively, taking into account the pNGB Lagrangian, SM fermions and contributions from partial compositeness.

The remainder of this thesis was dedicated to LHC phenomenology of the model. First, we studied single production of the resonances mentioned. Therefore, four benchmark scenarios were defined which fix the Vector-pNGB-pNGB coupling $g_{V\pi\pi}$ and partial compositeness contributions to the coupling of a top pair to vector resonances. Each benchmark scenario has a huge impact on the branching ratio hierarchy, but we find that the final mass bounds do not differ much. Using `MadGraph5_aMC@NLO` we were able to compare simulated events with experimental data from ATLAS and CMS. Bounds were derived from numerous different decay channels in each benchmark scenario. We stated the final result in fig. 4.12, where we combined multiple direct searches for lepton and quark final states with recasting results used for more complex signatures. The resulting bounds are very robust and do not depend much on the exact values chosen for the benchmark scenarios. We highlight, that there is still the possibility for Spin-1 resonances in the lower multi-TeV range or even around 1 TeV in some scenarios for reasonable values of their coupling constant $\tilde{g}$.

Furthermore, we looked into pair production of the double charged axial resonance $\hat{a}_5^{++}$, which is a unique prediction for SU(5)/SO(5) within the set of minimal models. We derived bounds on the axial mass parameter M_A independently from our analysis before. With currently available recasting tools, we got a bound of $M_A \gtrsim 860 - 1100\,\mathrm{GeV}$. Investigation of interactions involving other states of the axial multiplet might strengthen those bounds.

Also, taking into account Next-to-Leading-Order effects might have a significant impact on the cross sections under study. However, our Leading-Order estimates of lower limits of M_V and M_A suggest that there is still a wide-open parameter space for new discoveries. Future collider experiments, with increased energy and luminosity, could provide potential discoveries or more stringent constraints of the predicted resonances. In this thesis we have limited ourselves to the coset SU(5)/SO(5), which is one of three minimal EW cosets besides SU(4)/Sp(4) and $\mathrm{SU}(4) \times \mathrm{SU}(4)/\mathrm{SU}(4)$. As each coset predicts a different BSM particle content, it would be interesting to explore the differences and similarities with regard to the phenomenological considerations made in this work.

Last but not least we point out that these models contain an additional spin-1 resonance, not considered here, stemming from the inclusion of the QCD sector and which mixes with the $U(1)_Y$ boson. We expect that the impact of this state is weak if it is heavier than the other spin-1 resonances. However, there are scenarios in which this state could be lighter which deserve further investigations.

A Explicit Embeddings

The 14 axial vectors are embeded similiar to the pNGBs. We start with eq. (3.6) and transform into $\mathrm{SU}(2)_D$ using eq. (3.8) where η is replaced by $\hat{a}_\mu$. The bidoublet components are parameterized with a different phase compared to eq. (3.7) as

$$H_{\mathcal{A}} = \begin{pmatrix} i a_\mu^+ \\ 1/\sqrt{2}(\hat{y}_{2\mu}^0 - i a_\mu^0) \end{pmatrix}. \tag{A.1}$$

With this convention the axial vector matrix reads

$$\Omega(\theta)^\dagger \cdot \mathcal{A}_\mu \cdot \Omega(\theta) =$$

$$\frac{1}{\sqrt{2}} \begin{pmatrix} \frac{\sqrt{3}\hat{y}_{1\mu}^0 + \sqrt{5}\hat{a}_{1\mu}^0 - \sqrt{10}\hat{a}_{5\mu}^0}{\sqrt{30}} & \frac{i\hat{a}_{3\mu}^+ + \hat{a}_{5\mu}^+}{\sqrt{2}} & \frac{-i\hat{a}_{3\mu}^+ + \hat{a}_{5\mu}^+}{\sqrt{2}} & \sqrt{2}\hat{a}_{5\mu}^{++} & i a_\mu^+ \\ \frac{-i\hat{a}_{3\mu}^- + \hat{a}_{5\mu}^-}{\sqrt{2}} & \frac{\sqrt{3}y_{1\mu}^0 - \sqrt{5}\hat{a}_{1\mu}^0 + \sqrt{10}\hat{a}_{5\mu}^0}{\sqrt{30}} & \frac{i\sqrt{3}\hat{a}_{3\mu}^0 + \hat{a}_{5\mu}^0 + \sqrt{2}\hat{a}_{1\mu}^0}{\sqrt{3}} & \frac{i\hat{a}_{3\mu}^+ - \hat{a}_{5\mu}^+}{\sqrt{2}} & \frac{-i a_\mu^0 + \hat{y}_{2\mu}^0}{\sqrt{2}} \\ \frac{i\hat{a}_{3\mu}^- + \hat{a}_{5\mu}^-}{\sqrt{2}} & \frac{-i\sqrt{3}\hat{a}_{3\mu}^0 + \hat{a}_{5\mu}^0 + \sqrt{2}\hat{a}_{1\mu}^0}{\sqrt{3}} & \frac{\sqrt{3}\hat{y}_{1\mu}^0 - \sqrt{5}\hat{a}_{1\mu}^0 + \sqrt{10}\hat{a}_{5\mu}^0}{\sqrt{30}} & \frac{-i\hat{a}_{3\mu}^+ - \hat{a}_{5\mu}^+}{\sqrt{2}} & \frac{-i a_\mu^0 - \hat{y}_{2\mu}^0}{\sqrt{2}} \\ \sqrt{2}\hat{a}_{5\mu}^{--} & \frac{-i\hat{a}_{3\mu}^- - \hat{a}_{5\mu}^-}{\sqrt{2}} & \frac{i\hat{a}_{3\mu}^- - \hat{a}_{5\mu}^-}{\sqrt{2}} & \frac{\sqrt{3}y_{1\mu}^0 + \sqrt{5}\hat{a}_{1\mu}^0 - \sqrt{10}\hat{a}_{5\mu}^0}{\sqrt{30}} & -i a_\mu^- \\ -i a_\mu^- & \frac{i a_\mu^0 + \hat{y}_{2\mu}^0}{\sqrt{2}} & \frac{i a_\mu^0 - \hat{y}_{2\mu}^0}{\sqrt{2}} & i a_\mu^+ & \frac{-4}{\sqrt{10}}\hat{y}_{1\mu}^0 \end{pmatrix}. \tag{A.2}$$

The vector resonances $\mathcal{V}_\mu$ can be decomposed to $(\mathbf{3},\mathbf{1}) \oplus (\mathbf{1},\mathbf{3}) \oplus (\mathbf{2},\mathbf{2})$ of $\mathrm{SU}(2)_D$, which can be parameterized as

$$\Omega(\theta)^\dagger \cdot \mathcal{V}_\mu \cdot \Omega(\theta) =$$

$$\frac{1}{\sqrt{2}} \begin{pmatrix} \frac{1}{\sqrt{2}}(t_{L\mu}^0 + t_{R\mu}^0) & t_{L\mu}^+ & t_{R\mu}^+ & 0 & d_\mu^{++} \\ t_{L\mu}^- & \frac{-1}{\sqrt{2}}(t_{L\mu}^0 - t_{R\mu}^0) & 0 & t_{R\mu}^+ & d_\mu^{-+} \\ t_{R\mu}^- & 0 & \frac{1}{\sqrt{2}}(t_{L\mu}^0 - t_{R\mu}^0) & t_{L\mu}^+ & (d_\mu^{-+})^\dagger \\ 0 & t_{R\mu}^- & t_{L\mu}^- & \frac{-1}{\sqrt{2}}(t_{L\mu}^0 + t_{R\mu}^0) & -(d_\mu^{++})^\dagger \\ (d_\mu^{++})^\dagger & (d_\mu^{-+})^\dagger & d_\mu^{-+} & -d_\mu^{++} & 0 \end{pmatrix}, \tag{A.3}$$

where $t_{L/R}$ denotes the $\mathrm{SU}(2)_{L/R}$ triplet. The bidoublet d_μ is decomposed further into $(\mathbf{2},\mathbf{2}) \to \mathbf{3} \oplus \mathbf{1}$ of $\mathrm{SU}(2)_D$, parameterized as

$$d_\mu^{++} = -\hat{r}_\mu^+, \qquad d_\mu^{-+} = \frac{1}{\sqrt{2}}(\hat{r}_\mu^0 - i\hat{x}_\mu^0). \tag{A.4}$$

From $(\mathbf{3},\mathbf{1}) \oplus (\mathbf{1},\mathbf{3})$ two linear combinations can be formed to be triplets of $\mathrm{SU}(2)_D$

$$t_{L\mu}^{0\pm} = \frac{1}{\sqrt{2}}(v_{1\mu}^{0\pm} + v_{2\mu}^{0\pm}), \qquad t_{R\mu}^{0\pm} = \frac{1}{\sqrt{2}}(v_{1\mu}^{0\pm} - v_{2\mu}^{0\pm}). \tag{A.5}$$

Inserting the above transformations yields eq. (3.10).

B Details of the pNGB decay channels

B.1 Two-body decays

Here, the 2-body decays of $\eta_3^\pm$, $\eta_5^\pm$, η_1^0, η_5^0 into EW bosons are calculated

$$\Gamma_i = \frac{S p_0}{8\pi m_1^2} |\mathcal{M}_i|^2 \,, \tag{B.1}$$

with $p_0 = \frac{1}{2m_1}\sqrt{\lambda(m_1^2, m_2^2, m_3^2)}$, where λ was defined in eq. (3.66), m_1 is the mass of the decaying scalar and m_2, m_3 are the masses of the final vector bosons.
In order to derive the Feynman rules, the following sign convention for inward and outgoing momentum

$$\eta_{\text{in}} \sim \mathrm{e}^{+ip\cdot x} \,, \qquad \eta_{\text{out}} \sim \mathrm{e}^{-ip\cdot x} \,, \tag{B.2}$$

is used. Following, the structure of the Feynman rules of the WZW terms is worked out in detail for $\eta^+ A W^-$

$$\begin{aligned}
iL_{WZW} \supset\; & iK_{\gamma W}^{\eta^+} \cdot \eta^+ F_{\mu\nu} \tilde{W}^{-\mu\nu} + \text{h.c.} \\
&= \frac{i}{2} K_{\gamma W}^{\eta^+} \cdot \eta^+ \left(\partial_\mu A_\nu - \partial_\nu A_\mu\right) \varepsilon^{\mu\nu\rho\delta} \left(\partial_\rho W_\delta^- - \partial_\delta W_\rho^-\right) + \text{h.c.} \\
&= \frac{-i}{2} K_{\gamma W}^{\eta^+} \cdot \eta^+ \left(p_\mu^A A_\nu - p_\nu^A A_\mu\right) \varepsilon^{\mu\nu\rho\delta} \left(p_\rho^W W_\delta^- - p_\delta^W W_\rho^-\right) + \text{h.c.} \\
&= \frac{-i}{2} K_{\gamma W}^{\eta^+} \cdot \eta^+ \varepsilon^{\mu\nu\rho\delta} \left(p_\mu^A A_\nu p_\rho^W W_\delta^- - p_\nu^A A_\mu p_\rho^W W_\delta^- - p_\mu^A A_\nu p_\delta^W W_\rho^- + p_\nu^A A_\mu p_\delta^W W_\rho^-\right) + \text{h.c.} \\
&= 2iK_{\gamma W}^{\eta^+} \varepsilon^{\mu\nu\rho\delta} p_\mu^A p_\nu^W \cdot \eta^+ A_\rho W_\delta^- + 2i \left(K_{\gamma W}^{\eta^+}\right)^* \varepsilon^{\mu\nu\rho\delta} p_\mu^A p_\nu^W \cdot \eta^- A_\rho W_\delta^+ \,, \qquad \text{(B.3)} \\
&\to 2iK_{VV}^{\eta} \cdot p_{2\mu} p_{3\nu} \varepsilon^{\mu\nu\rho\delta} \,, \qquad \text{(B.4)}
\end{aligned}$$

where the associated K_{VV}^η parameters can be read of from eq. (3.59)

$$K_{\gamma W}^{\eta_5^+} = \frac{e^2 \dim(\psi)}{48\pi^2 f_\pi} \cdot \frac{3i}{s_W} \,, \qquad K_{\gamma W}^{\eta_3^+} = \frac{e^2 \dim(\psi)}{48\pi^2 f_\pi} \cdot \frac{-3c_\theta}{s_W} \,.$$

Using the above form of the Feynman rule, the spin-averaged product of the squared amplitude can be calculated to

$$|\mathcal{M}|^2 = \sum_{s_2, s_3} 4 \left|K_{VV}^\eta\right|^2 p_{2\rho} p_{3\sigma} \varepsilon^{\rho\sigma\mu\nu} \epsilon_\mu^*(s_2) \epsilon_\nu^*(s_3) p_2^\chi p_3^\lambda \, \varepsilon_{\chi\lambda}{}^{\alpha\beta} \epsilon_\alpha(s_2) \epsilon_\beta(s_3) \,, \tag{B.5}$$

using the polarization completeness relation [77]

$$\sum_s \epsilon_\mu^*(s) \epsilon_\nu(s) = -\eta_{\mu\nu} + \frac{p_\mu p_\nu}{m^2} \,, \tag{B.6}$$

we get

$$|\mathcal{M}|^2 = -8\left|K_{VV}^{\eta}\right|^2 p_{2\rho}p_{3\sigma}p_2^{\chi}p_3^{\lambda}\left(\delta_{\chi}^{\rho}\delta_{\lambda}^{\sigma}-\delta_{\lambda}^{\rho}\delta_{\chi}^{\sigma}\right) = 8\left|K_{VV}^{\eta}\right|^2\left((p_2\cdot p_3)^2-m_2^2m_3^2\right)$$
$$= 8\left|K_{VV}^{\eta}\right|^2\left(\frac{1}{4}\left(m_1^2-m_2^2-m_3^2\right)^2-m_2^2m_3^2\right), \tag{B.7}$$

where in the last step the rest frame of η was used.

B.2 Three-body decay

For the three-body decay channels we do need in addition the Feynman rules for $\eta\eta V$ vertices

$$iL_{\eta\eta V} \supset i\left(K_W^{\eta^0\eta^+}\right)\cdot W^{-\mu}\eta^0\overleftrightarrow{\partial_\mu}\eta^+ + \text{h.c.}$$
$$= i\left(K_W^{\eta^0\eta^+}\right)\cdot W^{-\mu}\left(\eta^0\partial_\mu\eta^+-\eta^+\partial_\mu\eta^0\right)+\text{h.c.}$$
$$= K_W^{\eta^0\eta^+}\cdot W^{-\mu}\left(p_\mu^{\eta^+}\eta^+\eta^0+p_\mu^{\eta^0}\eta^+\eta^0\right)+\text{h.c.}$$
$$= K_W^{\eta^0\eta^+}\left(p_\mu^{\eta^+}+p_\mu^{\eta^0}\right)\cdot W^{-\mu}\eta^+\eta^0+\left(K_W^{\eta^0\eta^+}\right)^*\left(p_\mu^{\eta^+}+p_\mu^{\eta^0}\right)\cdot W^{+\mu}\eta^-\eta^0\,, \tag{B.8}$$
$$\to K_V^{\eta\eta}\cdot(q+p_1)_\mu\,. \tag{B.9}$$

Applying the Feynman rules for the t-channel $q=p_1-p_2$, we get

$$-i\mathcal{M}_t = (2\pi)^4\delta\left(\textstyle\sum_i p_i\right)\cdot 4K_{VV}^{\eta}K_V^{\eta\eta}\cdot p_1^{\tau}\epsilon_\tau^*(s_2)\frac{1}{\bar{t}-M^2+i\Gamma M}p_{3\rho}p_{4\sigma}\varepsilon^{\rho\sigma\mu\nu}\epsilon_\mu^*(s_3)\epsilon_\nu^*(s_4)\,. \tag{B.10}$$

For the expressions of u and s-channel one just has to rename indices.
The spin-average of two t-channels with different virtual scalars η, η' is given by

$$M_{tt}(\eta,\eta') = \left\langle\mathcal{M}_t\mathcal{M}_t'^*\right\rangle = \sum_{s_2,s_3,s_4}16K_{V_2V_3}^{\eta}K_{V_1}^{\eta_0^3\eta}(K_{V_2V_3}^{\eta'})^*(K_{V_1}^{\eta_3^0\eta'})^*\frac{1}{\bar{t}-M^2+i\Gamma M}\frac{1}{\bar{t}-M'^2-i\Gamma'M'}$$
$$\cdot p_1^{\tau}p_1^{\gamma}\epsilon_\tau(s_2)\epsilon_\gamma^*(s_2)p_{3\rho}p_{4\sigma}p_{3\delta}p_{4\lambda}\varepsilon^{\delta\lambda\alpha\beta}\varepsilon^{\rho\sigma\mu\nu}\epsilon_\alpha(s_4)\epsilon_\mu^*(s_4)\epsilon_\beta(s_3)\epsilon_\nu^*(s_3)$$
$$= 32K_{V_2V_3}^{\eta}K_{V_1}^{\eta_0^3\eta}(K_{V_2V_3}^{\eta'})^*(K_{V_1}^{\eta_3^0\eta'})^*\frac{1}{\bar{t}-M^2+i\Gamma M}\frac{1}{\bar{t}-M'^2-i\Gamma'M'}$$
$$\cdot\left(\frac{1}{4m_2^2}\left(m_1^2+m_2^2-\bar{t}\right)^2-m_1^2\right)\cdot\left(\frac{1}{4}\left(\bar{t}-m_3^4-m_4^2\right)^2-m_3^2m_4^2\right). \tag{B.11}$$

Note that the same result can be achieved for M_{uu}, M_{ss} by replacing $\bar{t}$ with the corresponding Mandelstam variable in the above expression.
Interference terms involving the combination of different momenta channel can be worked out in the same way using

$$\epsilon^{\rho\delta\tau\mu}\epsilon_{\chi\lambda\beta\mu} = -\left(\delta_\chi^\rho\delta_\lambda^\delta\delta_\beta^\tau-\delta_\chi^\delta\delta_\lambda^\rho\delta_\beta^\tau+\delta_\chi^\delta\delta_\lambda^\tau\delta_\beta^\rho-\delta_\chi^\tau\delta_\lambda^\delta\delta_\beta^\rho+\delta_\chi^\tau\delta_\lambda^\rho\delta_\beta^\delta-\delta_\chi^\rho\delta_\lambda^\tau\delta_\beta^\delta\right)$$

to get

$$M_{tu} = 2K_{V_2V_3}^{\eta}K_{V_1}^{\eta_0^3\eta}(K_{V_2V_3}^{\eta'})^*(K_{V_1}^{\eta_3^0\eta'})^*\cdot\frac{1}{\bar{t}-M^2+i\Gamma M}\frac{1}{\bar{u}-M'^2-i\Gamma'M'}$$
$$\cdot\Big[(\bar{u}-m_1^2-m_3^2)\cdot\Big((\bar{t}-m_1^2-m_2^2)(\bar{t}-m_3^2-m_4^2)+(\bar{s}-m_1^2-m_4^2)(\bar{s}-m_2^2-m_3^2)$$
$$-(\bar{u}-m_1^2-m_3^2)(\bar{u}-m_2^2-m_4^2)\Big)$$
$$-2m_1^2(\bar{s}-m_2^2-m_3^2)(\bar{t}-m_3^2-m_4^2)-2m_3^2(\bar{s}-m_1^2-m_4^2)(\bar{t}-m_1^2-m_2^2)$$
$$+4m_1^2m_3^2(\bar{u}-m_2^2-m_4^2)\Big]. \tag{B.12}$$

One can use these results to express the squared matrix elements $|\mathcal{M}|^2$ in terms of only two independent functions M_{xx}, M_{xy}. Starting with the channels $\eta_3^0 \to W^+ + W^- + \gamma/Z$, one gets

$$\begin{aligned}\left|\mathcal{M}_{1/2}\right|^2 &= \left\langle \left|\mathcal{M}_t(\eta_3^+) + \mathcal{M}_u(\eta_3^-) + \mathcal{M}_t(\eta_5^+) + \mathcal{M}_u(\eta_5^-)\right|^2 \right\rangle \\ &= M_{tt}(\eta_3^+,\eta_3^+) + M_{uu}(\eta_3^-,\eta_3^-) + M_{tt}(\eta_5^+,\eta_5^+) + M_{uu}(\eta_5^-,\eta_5^-) \\ &+ 2\mathrm{Re}\Big[M_{tu}(\eta_3^+,\eta_3^-) + M_{tt}(\eta_3^+,\eta_5^+) + M_{tu}(\eta_3^+,\eta_5^-) + M_{tu}(\eta_3^-,\eta_5^+) \\ &\quad + M_{uu}(\eta_3^-,\eta_5^-) + M_{tu}(\eta_5^+,\eta_5^-)\Big] .\end{aligned} \tag{B.13}$$

Following the expressions for $\eta_3^0 \to Z + \gamma + \gamma$

$$\begin{aligned}|\mathcal{M}_3|^2 &= \left\langle \left|2\mathcal{M}_t(\eta_1^0) + 2\mathcal{M}_t(\eta_5^0)\right|^2 \right\rangle \\ &= 4\left(M_{tt}(\eta_1^0,\eta_1^0) + 2\mathrm{Re}\left[M_{tt}(\eta_1^0,\eta_5^0)\right] + M_{tt}(\eta_5^0,\eta_5^0)\right) ,\end{aligned} \tag{B.14}$$

and $\eta_3^0 \to Z + Z + \gamma$

$$\begin{aligned}|\mathcal{M}_3|^2 &= \left\langle \left|\mathcal{M}_t\left(\eta_1^0\right) + \mathcal{M}_t\left(\eta_5^0\right) + \mathcal{M}_u\left(\eta_1^0\right) + \mathcal{M}_u\left(\eta_5^0\right)\right|^2 \right\rangle \\ &= M_{tt}\left(\eta_1^0,\eta_1^0\right) + M_{tt}\left(\eta_5^0,\eta_5^0\right) + M_{uu}\left(\eta_1^0,\eta_1^0\right) + M_{uu}\left(\eta_5^0,\eta_5^0\right) \\ &+ 2\mathrm{Re}\Big[M_{tt}\left(\eta_1^0,\eta_5^0\right) + M_{uu}\left(\eta_1^0,\eta_5^0\right) \\ &\quad + M_{tu}\left(\eta_1^0,\eta_1^0\right) + M_{tu}\left(\eta_5^0,\eta_5^0\right) + M_{tu}\left(\eta_1^0,\eta_5^0\right) + M_{tu}\left(\eta_5^0,\eta_1^0\right)\Big] .\end{aligned} \tag{B.15}$$

The last channel $\eta_3^0 \to Z + Z + Z$ involves a lot of permutations and comes with symmetry factor $S = \frac{1}{3!}$

$$\begin{aligned}|\mathcal{M}_5|^2 &= \left\langle \left|2\mathcal{M}_t\left(\eta_1^0\right) + 2\mathcal{M}_t\left(\eta_5^0\right) + 2\mathcal{M}_u\left(\eta_1^0\right) + 2\mathcal{M}_u\left(\eta_5^0\right) + 2\mathcal{M}_s\left(\eta_1^0\right) + 2\mathcal{M}_s\left(\eta_5^0\right)\right|^2 \right\rangle \\ &= 4\Big(\mathcal{M}_{tt}\left(\eta_1^0,\eta_1^0\right) + \mathcal{M}_{tt}\left(\eta_5^0,\eta_5^0\right) + 2\mathrm{Re}\left[\mathcal{M}_{tt}\left(\eta_1^0,\eta_5^0\right)\right] \\ &\quad + \mathcal{M}_{uu}\left(\eta_1^0,\eta_1^0\right) + \mathcal{M}_{uu}\left(\eta_5^0,\eta_5^0\right) + 2\mathrm{Re}\left[\mathcal{M}_{uu}\left(\eta_1^0,\eta_5^0\right)\right] \\ &\quad + \mathcal{M}_{ss}\left(\eta_1^0,\eta_1^0\right) + \mathcal{M}_{ss}\left(\eta_5^0,\eta_5^0\right) + 2\mathrm{Re}\left[\mathcal{M}_{ss}\left(\eta_1^0,\eta_5^0\right)\right] \\ &\quad + 2\mathrm{Re}\left[\mathcal{M}_{tu}\left(\eta_1^0,\eta_1^0\right) + \mathcal{M}_{tu}\left(\eta_5^0,\eta_5^0\right) + \mathcal{M}_{tu}\left(\eta_1^0,\eta_5^0\right) + \mathcal{M}_{tu}\left(\eta_5^0,\eta_1^0\right)\right] \\ &\quad + 2\mathrm{Re}\left[\mathcal{M}_{ts}\left(\eta_1^0,\eta_1^0\right) + \mathcal{M}_{ts}\left(\eta_5^0,\eta_5^0\right) + \mathcal{M}_{ts}\left(\eta_1^0,\eta_5^0\right) + \mathcal{M}_{ts}\left(\eta_5^0,\eta_1^0\right)\right] \\ &\quad + 2\mathrm{Re}\left[\mathcal{M}_{us}\left(\eta_1^0,\eta_1^0\right) + \mathcal{M}_{us}\left(\eta_5^0,\eta_5^0\right) + \mathcal{M}_{us}\left(\eta_1^0,\eta_5^0\right) + \mathcal{M}_{us}\left(\eta_5^0,\eta_1^0\right)\right]\Big) .\end{aligned} \tag{B.16}$$

C Approximate Diagonalization of Mass Matrices

The expressions for the components of the transformation $\mathcal{C} = \mathcal{C}_a\mathcal{C}_b\mathcal{C}_c$ were already given in the main text, see sec. 3.2.1. Here we state the resulting total transformation in the same basis as in eq. (3.16)

$$\mathcal{C} = \begin{pmatrix} 1 - \frac{g^2(1+c_\theta^2+r^2s_\theta^2)}{4\tilde{g}^2} & \frac{grs_\theta}{\sqrt{2}\tilde{g}} & \frac{g\sqrt{3+c_{2\theta}}}{2\tilde{g}} & 0 \\ \frac{-grs_\theta}{\sqrt{2}\tilde{g}} & 1 - \frac{g^2r^2s_\theta^2}{4\tilde{g}^2} & -\frac{g^2M_A^2r\sqrt{1+c_\theta^2}s_\theta}{2\tilde{g}^2(M_A^2-M_V^2)} & 0 \\ \frac{g}{\sqrt{2}\tilde{g}} & \frac{g^2M_V^2rs_\theta}{2\tilde{g}^2(M_V^2-M_A^2)} & \frac{1}{\sqrt{1+c_\theta^2}}(-1+\frac{g^2(3+c_{2\theta})}{8\tilde{g}^2}) & \frac{c_\theta}{\sqrt{1+c_\theta^2}} \\ \frac{gc_\theta}{\sqrt{2}\tilde{g}} & \frac{g^2M_V^2rs_{2\theta}}{4\tilde{g}^2(M_V^2-M_A^2)} & \frac{c_\theta}{\sqrt{1+c_\theta^2}}(-1+\frac{g^2(3+c_{2\theta})}{8\tilde{g}^2}) & \frac{-1}{\sqrt{1+c_\theta^2}} \end{pmatrix}. \tag{C.1}$$

The neutral eigenvectors up to $1/\tilde{g}^2$ and s_θ^2 are given by

$$B_\mu = \mathcal{N}_{1i} = \begin{pmatrix} -\frac{g\left(g'^2\left(\cos^2(\theta)-\left(r^2-2\right)\sin^2(\theta)\right)+g'^2-4\tilde{g}^2\right)}{4\tilde{g}^2\sqrt{g^2+g'^2}} \\ -\frac{g'\left(\sin^2(\theta)\left(2g^2\left(r^2-1\right)+g'^2r^2\right)+g'^2\cos^2(\theta)+g'^2-4\tilde{g}^2\right)}{4\tilde{g}^2\sqrt{g^2+g'^2}} - \frac{g'r\sin(\theta)}{\sqrt{2}\tilde{g}} \\ \frac{g'\sin^2\left(\frac{\theta}{2}\right)\left(\left(g^2+g'^2\right)(4\cos(\theta)+\cos(2\theta))+11g^2-5g'^2\right)}{8\tilde{g}(g'^2-g^2)} \\ \frac{g'\cos^2\left(\frac{\theta}{2}\right)\left(\left(g^2+g'^2\right)(\cos(2\theta)-4\cos(\theta))-5g^2+11g'^2\right)}{8\tilde{g}(g'^2-g^2)} \end{pmatrix}, \tag{C.2}$$

$$W_\mu^3 = \mathcal{N}_{2i} = \begin{pmatrix} \frac{g'\left(1-\frac{g^2\left(r^2\sin^2(\theta)+\cos^2(\theta)+1\right)}{4\tilde{g}^2}\right)}{\sqrt{g^2+g'^2}} \\ -\frac{g\left(1-\frac{g^2\left(r^2\sin^2(\theta)+\cos^2(\theta)+1\right)}{4\tilde{g}^2}\right)}{\sqrt{g^2+g'^2}} \\ \frac{gr\sin(\theta)}{\sqrt{2}\tilde{g}} \\ -\frac{g\cos^2\left(\frac{\theta}{2}\right)\left(\left(g^2+g'^2\right)(\cos(2\theta)-4\cos(\theta))+11g^2-5g'^2\right)}{8\tilde{g}(g^2-g'^2)} \\ -\frac{g\sin^2\left(\frac{\theta}{2}\right)\left(\left(g^2+g'^2\right)(4\cos(\theta)+\cos(2\theta))-5g^2+11g'^2\right)}{8\tilde{g}(g-g')(g+g')} \end{pmatrix}, \tag{C.3}$$

$$a^0_\mu = \mathcal{N}_{3i} = \begin{pmatrix} 0 \\ \frac{r\sqrt{g^2+g'^2}\sin(\theta)}{\sqrt{2}\tilde{g}} \\ 1 - \frac{r^2\left(g^2+g'^2\right)\sin^2(\theta)}{4\tilde{g}^2} \\ -\frac{M_A^2 r\sin(\theta)\left(\left(g'^4-g^4\right)\sin^2(\theta)-4\left(g^2-g'^2\right)^2+\cos(\theta)\left(-4g^4+\left(g^2+g'^2\right)^2\sin^2(\theta)+4g'^4\right)\right)}{8\sqrt{2}\tilde{g}^2(g^2-g'^2)(M_A^2-M_V^2)} \\ \frac{M_A^2 r\sin(\theta)\left(\left(g^4-g'^4\right)\sin^2(\theta)-4\left(g^2-g'^2\right)^2+\cos(\theta)\left(4\left(g^4-g'^4\right)+\left(g^2+g'^2\right)^2\sin^2(\theta)\right)\right)}{8\sqrt{2}\tilde{g}^2(g^2-g'^2)(M_A^2-M_V^2)} \end{pmatrix}, \tag{C.4}$$

$$v^0_{1\mu} = \mathcal{N}_{4i} = \begin{pmatrix} \frac{\sqrt{2}gg'}{\tilde{g}\sqrt{g^2+g'^2}} \\ \frac{g'^2-g^2}{\sqrt{2}\tilde{g}\sqrt{g^2+g'^2}} \\ \frac{M_V^2 r(g-g')(g+g')\sin(\theta)}{2\tilde{g}^2\left(M_V^2-M_A^2\right)} \\ -\frac{\left(g^2+g'^2-4\tilde{g}^2\right)\left(\left(g^2+g'^2\right)\sin^2(\theta)+4(g-g')(g+g')\right)+(g-g')(g+g')\cos(\theta)\left(\left(g^2+g'^2\right)\cos(2\theta)+7g^2-9g'^2\right)}{16\sqrt{2}\tilde{g}^2(g-g')(g+g')} \\ \frac{-\frac{\left(g^2+g'^2-4\tilde{g}^2\right)\left(\left(g^2+g'^2\right)\sin^2(\theta)-4g^2+4g'^2\right)}{g^2-g'^2}-2\cos(\theta)\left(\left(g^2+g'^2\right)\sin^2(\theta)+4(g-g')(g+g')\right)}{16\sqrt{2}\tilde{g}^2} \end{pmatrix}, \tag{C.5}$$

$$v^0_{2\mu} = \mathcal{N}_{5i} = \begin{pmatrix} 0 \\ -\frac{\sqrt{g^2+g'^2}\cos(\theta)}{\sqrt{2}\tilde{g}} \\ \frac{M_V^2 r\left(g^2+g'^2\right)\sin(2\theta)}{4\tilde{g}^2\left(M_V^2-M_A^2\right)} \\ \frac{\left(\frac{\left(g^2+g'^2\right)\sin^2(\theta)}{g'^2-g^2}+4\right)\left(1-\frac{\left(g^2+g'^2\right)\cos^2(\theta)}{4\tilde{g}^2}\right)}{4\sqrt{2}} \\ \frac{\left(\frac{\left(g^2+g'^2\right)\sin^2(\theta)}{g^2-g'^2}+4\right)\left(1-\frac{\left(g^2+g'^2\right)\cos^2(\theta)}{4\tilde{g}^2}\right)}{4\sqrt{2}} \end{pmatrix}. \tag{C.6}$$

D Additional material for Single Production Phenomenology

Here we state additional branching ratios and exclusion plots didn't made it into the main text.

D.1 Width & Branching ratios

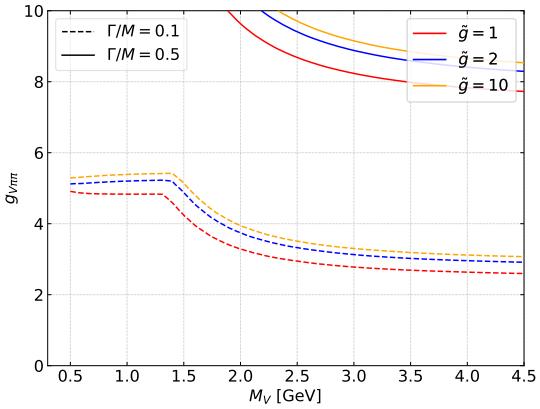

(a) Contour lines for $\Gamma/M = 0.1, 0.5$ in the $M_V - g_{V\pi\pi}$ plane for different values of $\tilde{g}$.

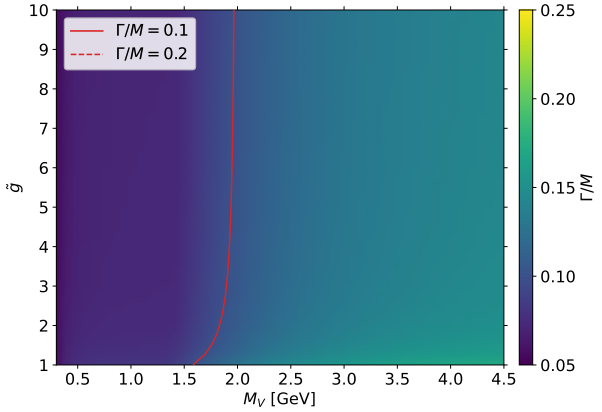

(b) Γ/M in the $M_V - \tilde{g}$ plane as colormap for fixed $g_{V\pi\pi} = 4$.

Figure D.1: Width Γ over mass M for the vector resonance $V^0_{2\mu}$ in the scenario of partial compositeness top coupling. The scalar masses are set as in eq. (4.7).

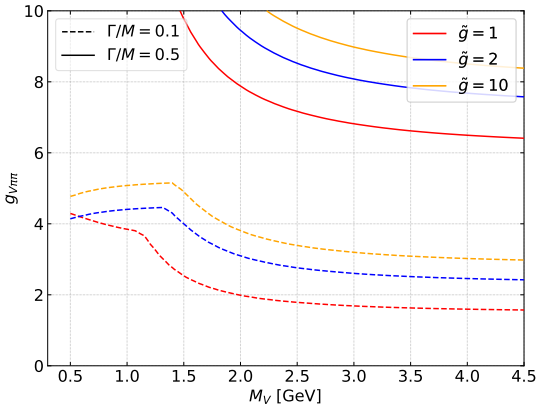

(a) Contour lines for $\Gamma/M = 0.1, 0.5$ in the $M_V - g_{V\pi\pi}$ plane for different values of $\tilde{g}$.

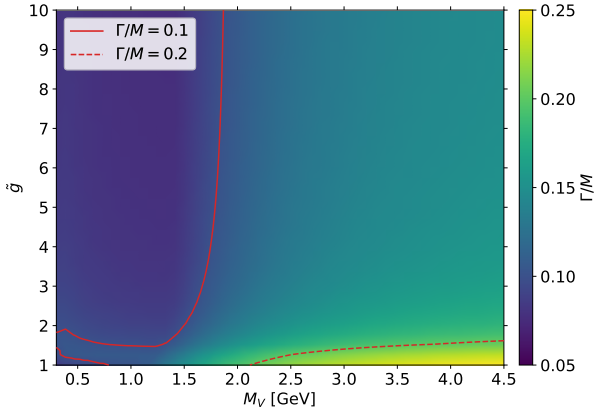

(b) Γ/M in the $M_V - \tilde{g}$ plane as colormap for fixed $g_{V\pi\pi} = 4$.

Figure D.2: Width Γ over mass M for the vector resonance $V^+_{1\mu}$ in the scenario of partial compositeness top coupling. The scalar masses are set as in eq. (4.7).

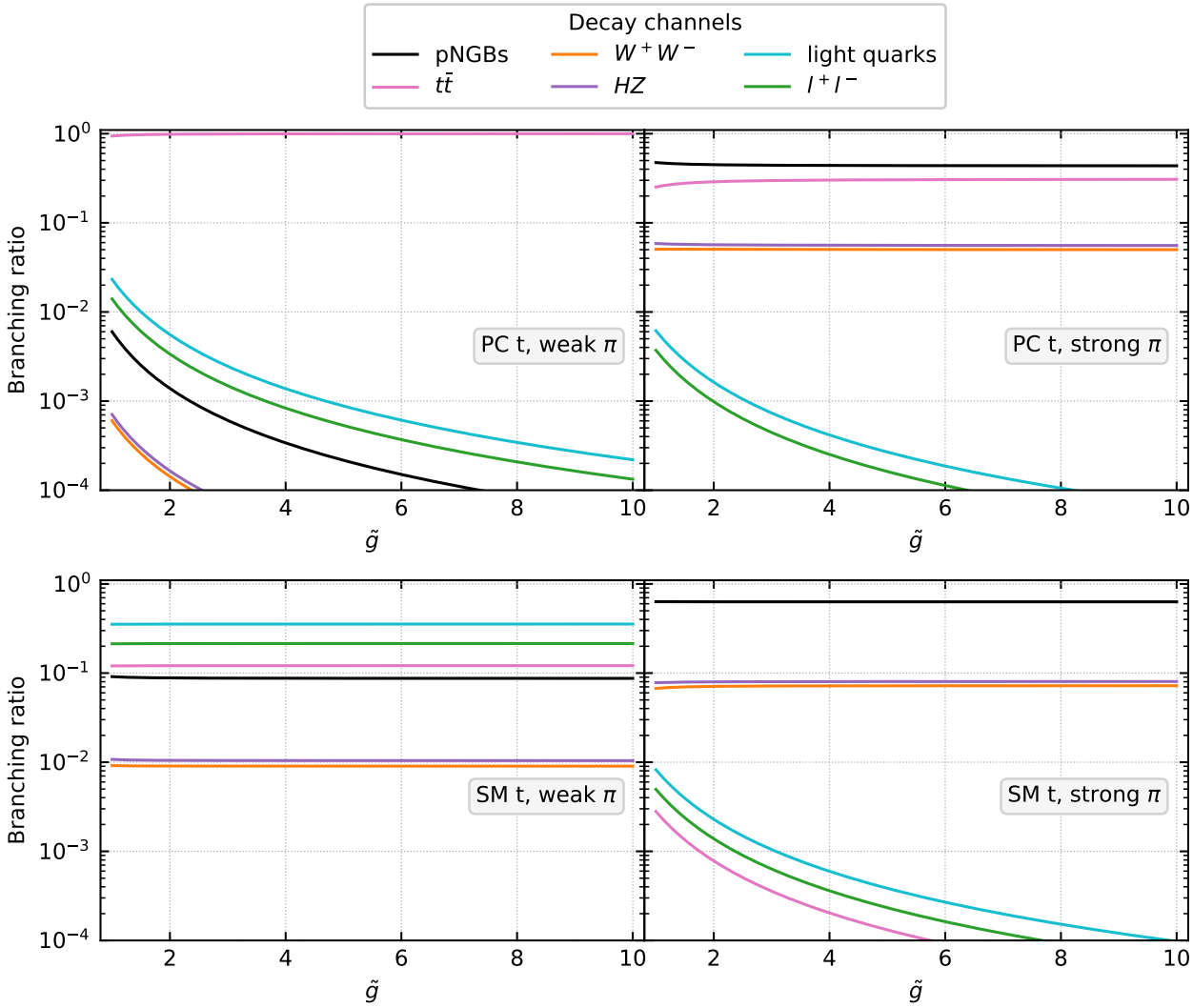

Figure D.3: Relevant branching ratios of $V^0_{2\mu}$ for $M_V = 3\,\text{TeV}$, $M_A/M_V = 1.4$ and $f = 1\,\text{TeV}$ in four benchmark scenarios defined in eqs. (4.5) and (4.6). The scalar masses are set as in eq. (4.7). We use here $l = e, \mu$ and the light quarks are u, d, s, c, b. The channel pNGB represents the sum of all decays into two pNGBs.

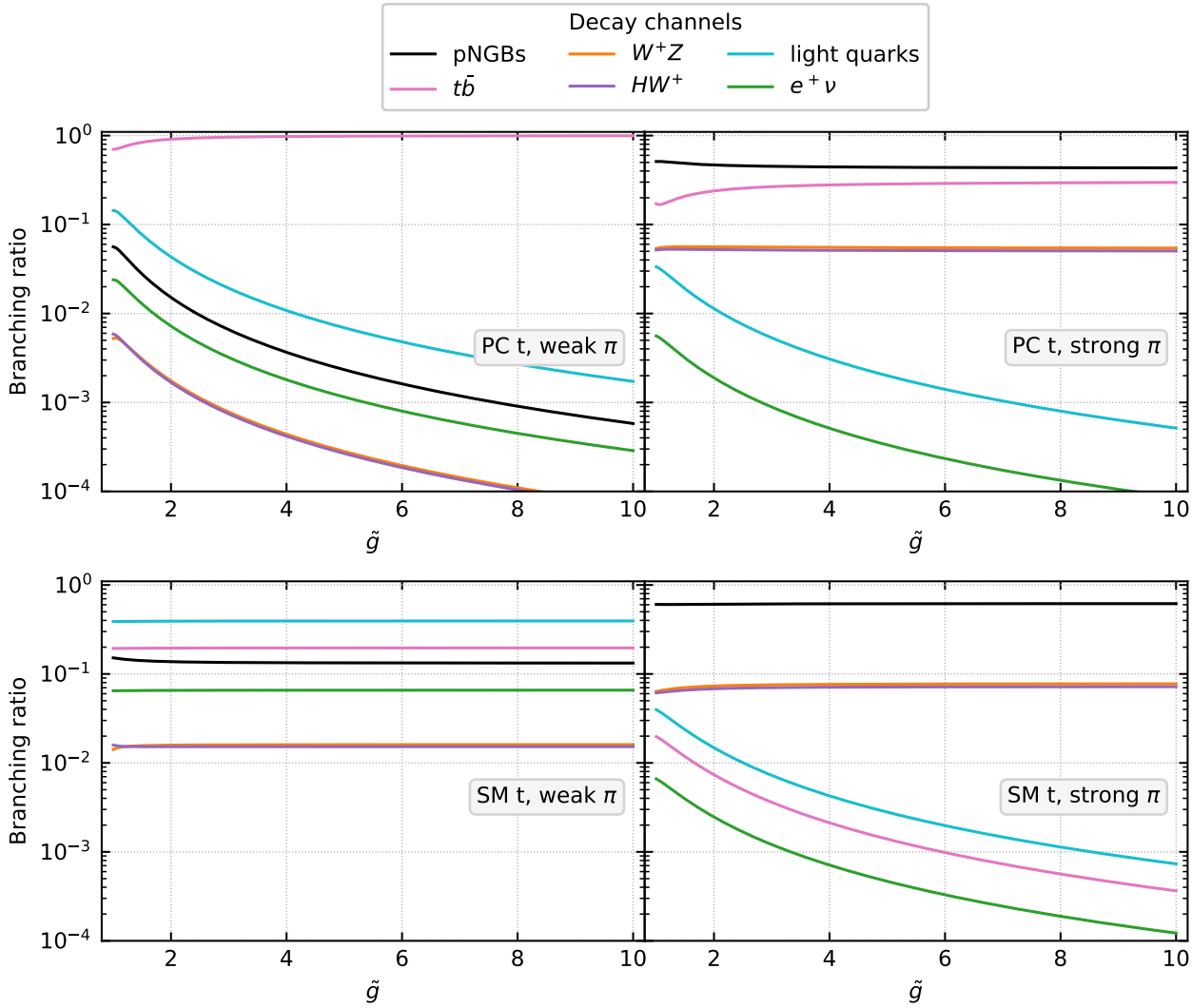

Figure D.4: Relevant branching ratios of $V_{1\mu}^{+}$ for $M_V = 3\,\text{TeV}$, $M_A/M_V = 1.4$ and $f = 1\,\text{TeV}$ in four benchmark scenarios defined in eqs. (4.5) and (4.6). The scalar masses are set as in eq. (4.7). The light quarks are u, d, s, c, b and the pNGB channel represents the sum of all decays into two pNGBs.

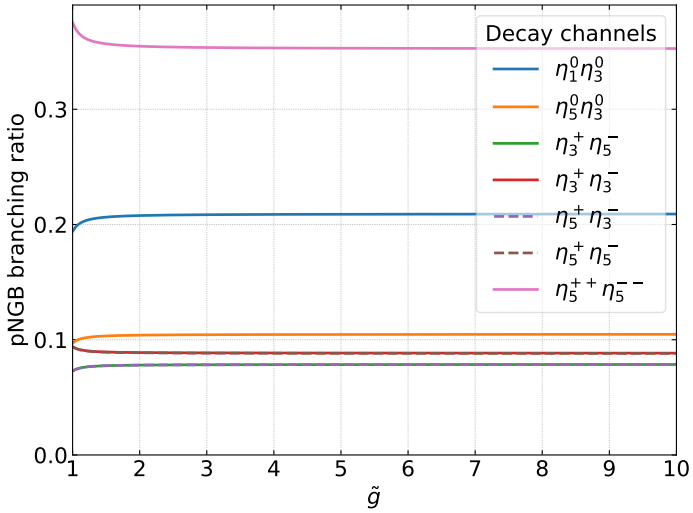

(a) pNGB decay channels of $V_{1\mu}^0$

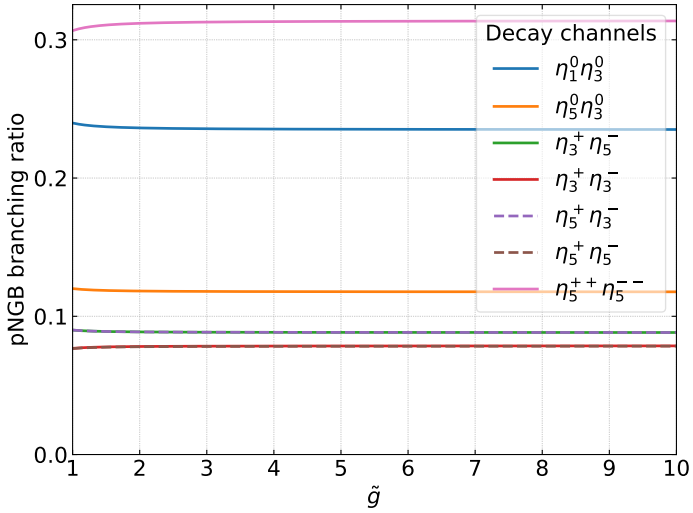

(b) pNGB decay channels of $V_{2\mu}^0$

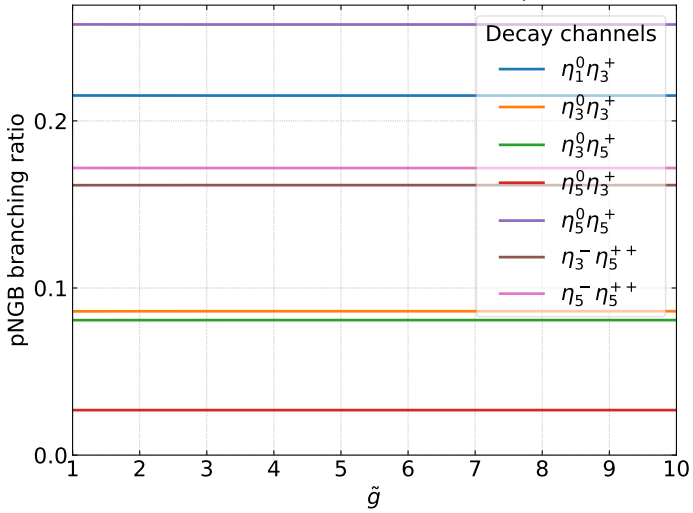

(c) pNGB decay channels of $V_{1\mu}^+$

Figure D.5: Shown are the relative widths of all decays into two pNGBs for $g_{V\pi\pi} = 4$ and $M_V = 3\,\text{TeV}$, which remain very stable while varying $\tilde{g}$.

D.2 Mass bounds

In fig. D.6 the 95% exclusion lines are shown derived from the channel $V^0_{1\mu} \to l^+l^-$ with $l = e, \mu$, while fig. D.7 shows the bound derived from $V^0_{2\mu} \to l^+l^-$. They were combined as function of the mass parameter M_V in fig. 4.7. fig. D.8 shows the bounds from $V^+_{1\mu} \to t\bar{b}$.
In fig. D.9, we combine the results from fig. 4.10 into one plot, which can be compared easily to bounds from other channels.
The recasting results for the decay into two pNGBs in a fermiophilic model with $M_\eta = 700\,\text{GeV}$ are shown in fig. D.10, where we also show the cross section as colormap in the background and the search which stated the strongest bounds are indicated for each grid point.

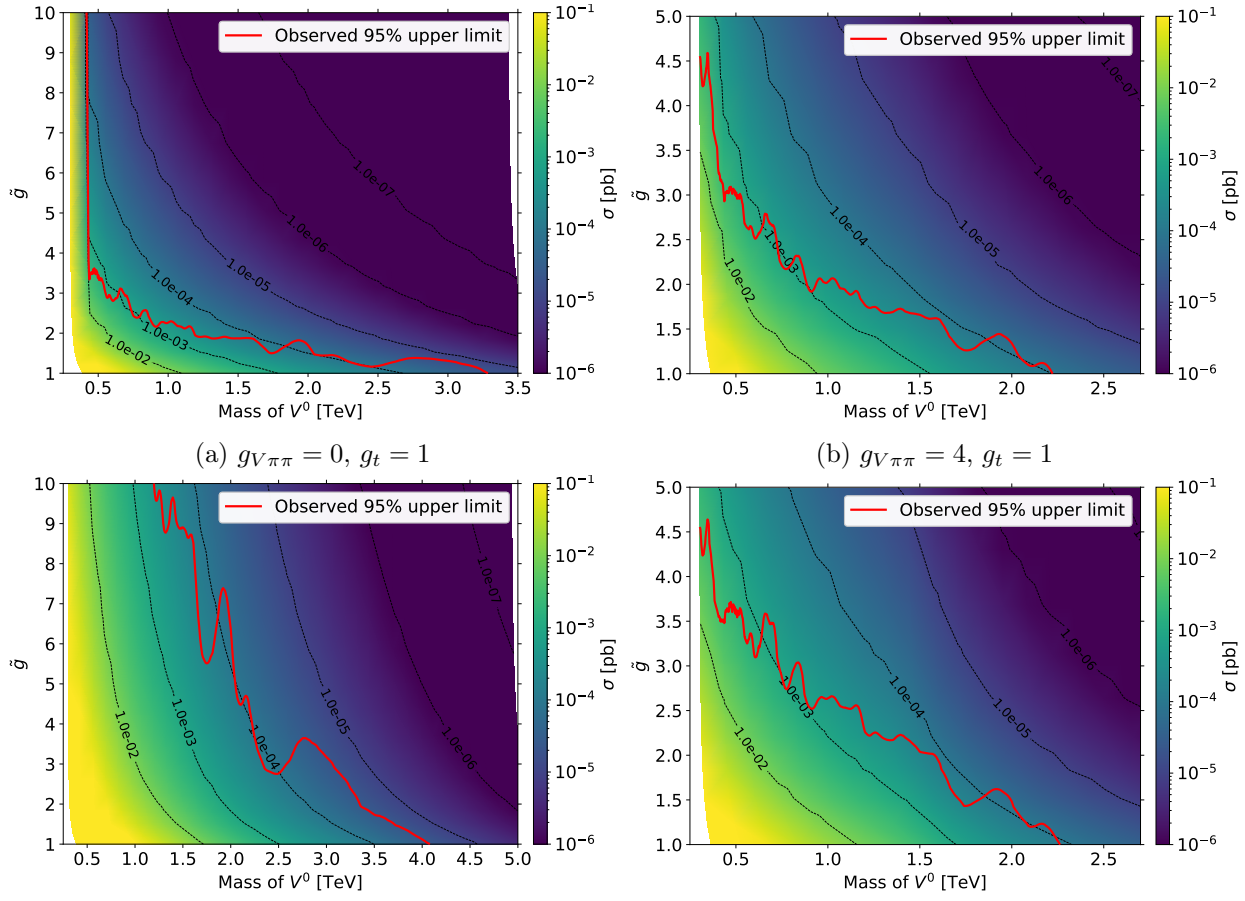

(a) $g_{V\pi\pi} = 0$, $g_t = 1$

(b) $g_{V\pi\pi} = 4$, $g_t = 1$

(c) $g_{V\pi\pi} = 0$, $g_t = g_t^{(\text{SM})}$

(d) $g_{V\pi\pi} = 4$, $g_t = g_t^{(\text{SM})}$

Figure D.6: Shown are the 95% CL exclusion lines derived from the channel $pp \to V^0_{1\mu} \to l^+l^-$ with $l = e, \mu$. The area below the red line is excluded, which was calculated from the upper limits on the cross section in [65]. The pNGB masses are defined as in eq. (4.7) and we fixed $M_A/M_V = 1.4$, $f = 1\,\text{TeV}$.

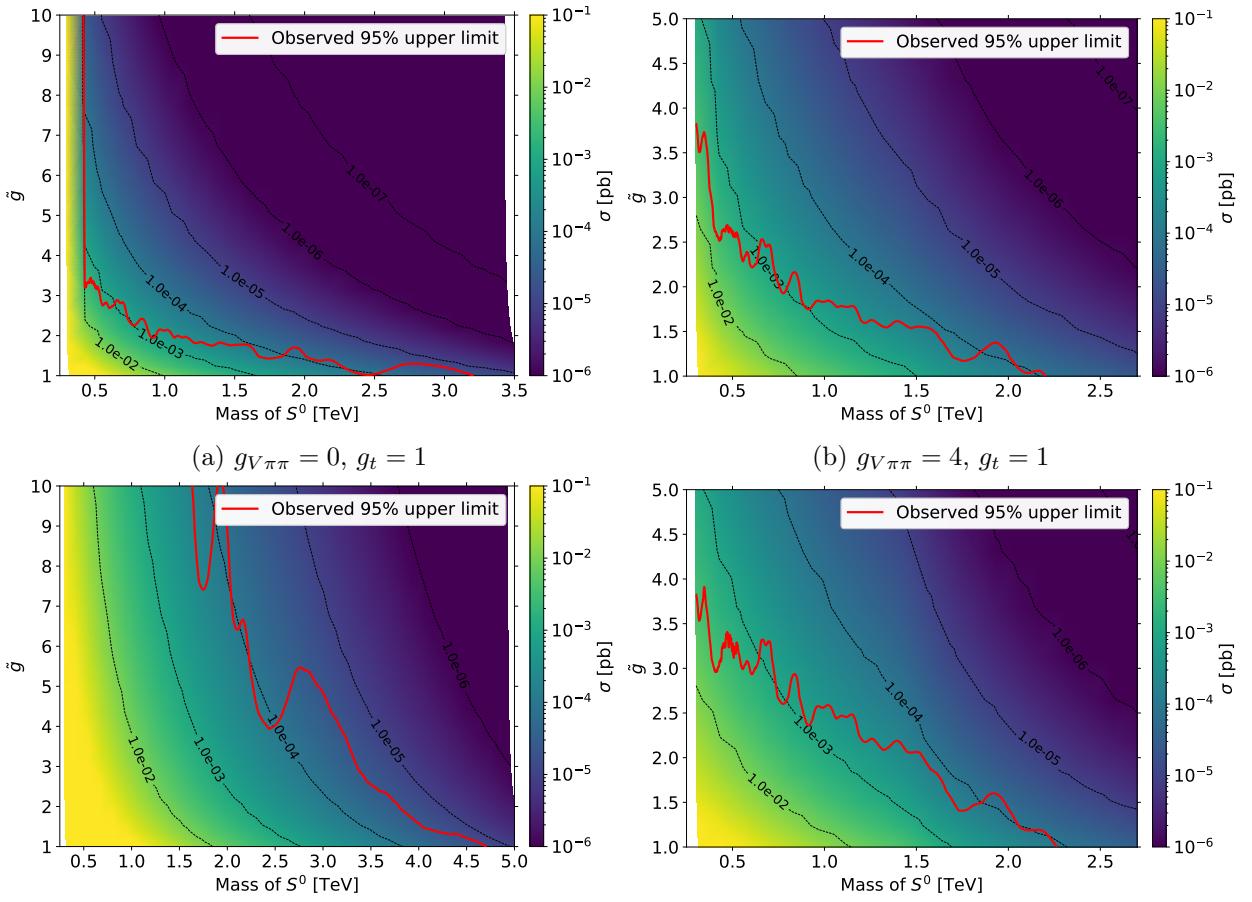

(a) $g_{V\pi\pi} = 0$, $g_t = 1$

(b) $g_{V\pi\pi} = 4$, $g_t = 1$

(c) $g_{V\pi\pi} = 0$, $g_t = g_t^{(\mathrm{SM})}$

(d) $g_{V\pi\pi} = 4$, $g_t = g_t^{(\mathrm{SM})}$

Figure D.7: Shown are the 95% CL exclusion lines derived from the channel $pp \to V_{2\mu}^0 \to l^+l^-$ with $l = e, \mu$. The area below the red line is excluded, which was calculated from the upper limits on the cross section in [65]. The pNGB masses are defined as in eq. (4.7) and we fixed $M_A/M_V = 1.4$, $f = 1\,\mathrm{TeV}$.

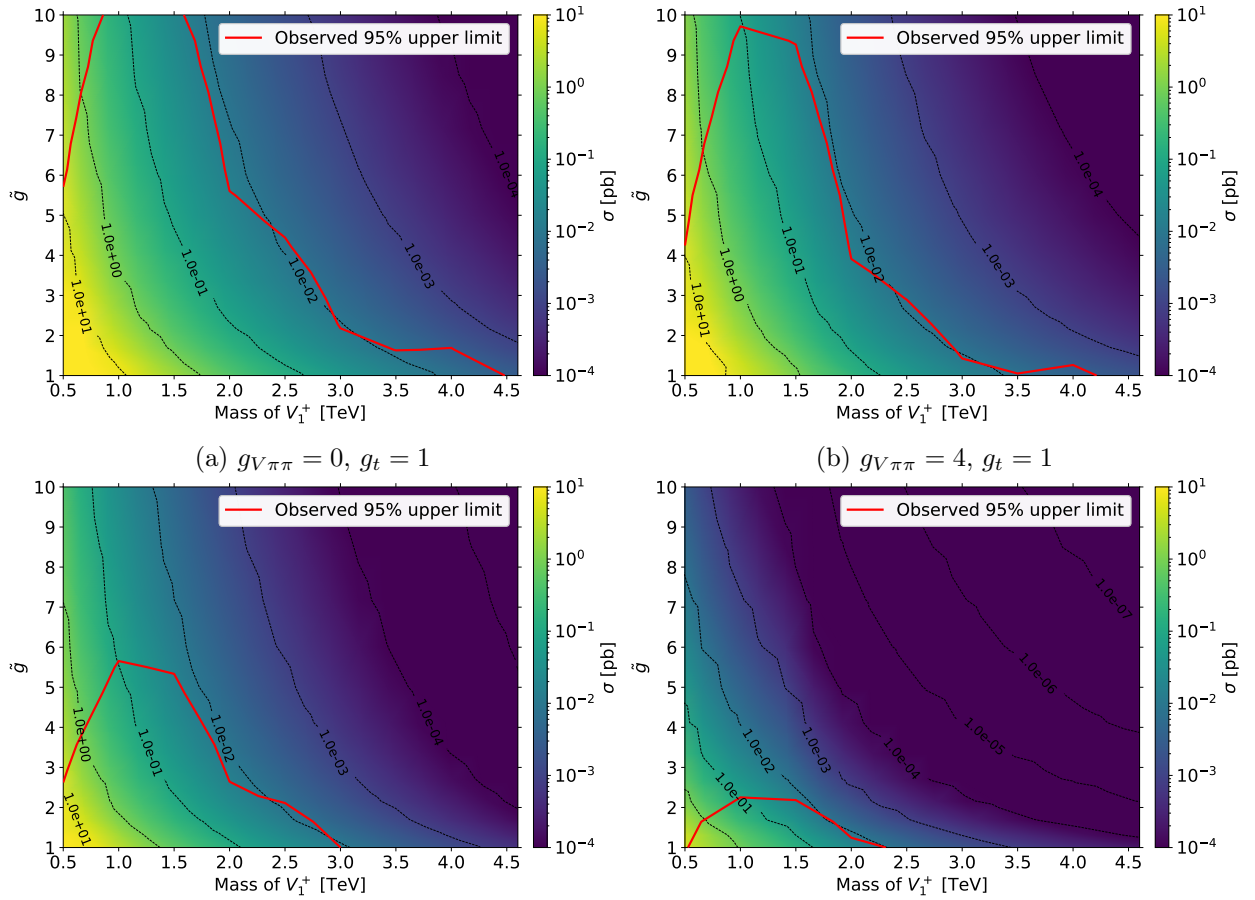

(a) $g_{V\pi\pi} = 0$, $g_t = 1$

(b) $g_{V\pi\pi} = 4$, $g_t = 1$

(c) $g_{V\pi\pi} = 0$, $g_t = g_t^{(\mathrm{SM})}$

(d) $g_{V\pi\pi} = 4$, $g_t = g_t^{(\mathrm{SM})}$

Figure D.8: Shown are the 95% CL exclusion lines derived from the channel $pp \to V_{1\mu}^+ \to t\bar{b}$. The area below the red line is excluded, which was calculated from the upper limits on the cross section in [67]. The pNGB masses are defined as in eq. (4.7) and we fixed $M_A/M_V = 1.4$, $f = 1\,\mathrm{TeV}$.

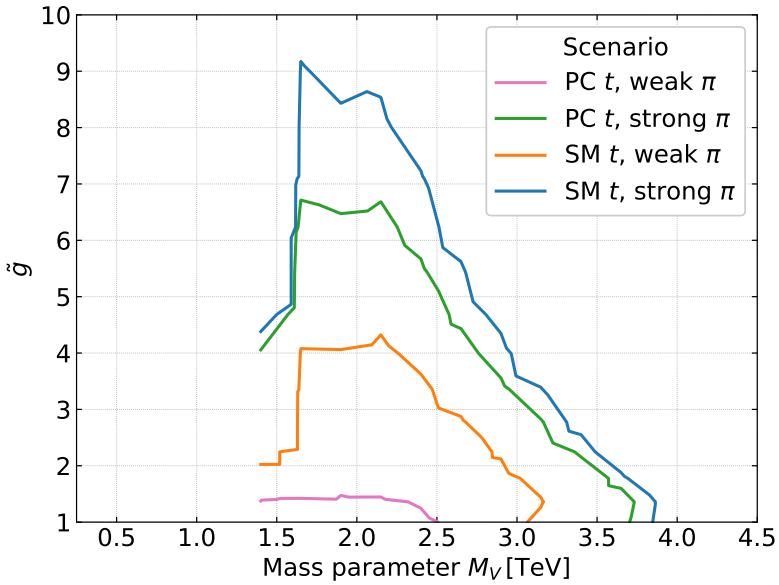

Figure D.9: Combined presentation of exclusion lines in fig. 4.10. The bounds were derived from single produced vector resonances decaying into a pair of pNGBs in a fermiophobic model. The benchmark scenarios were defined in eqs. (4.5) and (4.6).

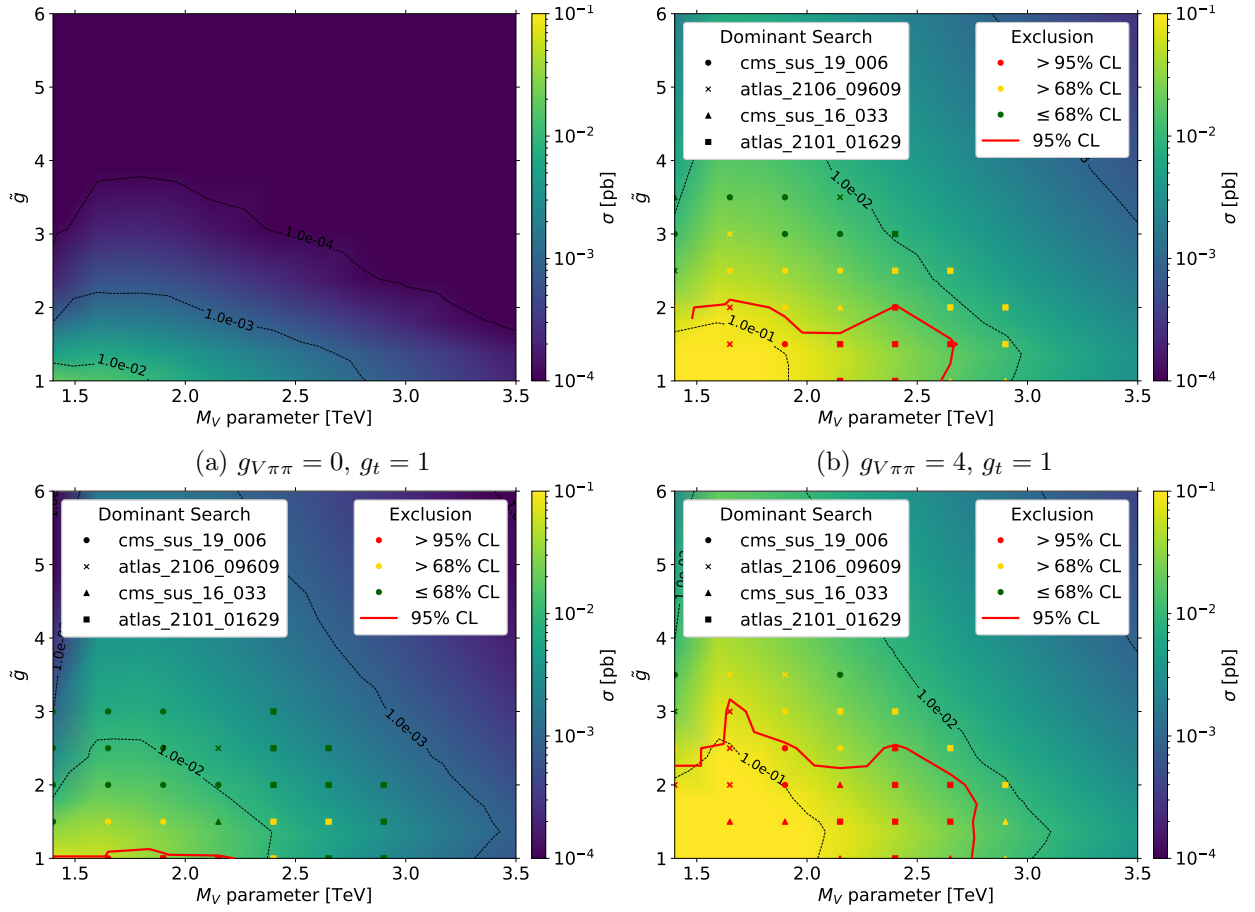

(a) $g_{V\pi\pi} = 0$, $g_t = 1$

(b) $g_{V\pi\pi} = 4$, $g_t = 1$

(c) $g_{V\pi\pi} = 0$, $g_t = g_t^{(\mathrm{SM})}$

(d) $g_{V\pi\pi} = 4$, $g_t = g_t^{(\mathrm{SM})}$

Figure D.10: Shown are the 95% CL exclusion lines derived from single produced vector resonances decaying into a pair of pNGBs in a fermiophilic model with pNGB masses as in eq. (4.7), $M_A/M_V = 1.4$ and $f = 1\,\mathrm{TeV}$. The bounds were derived using the recasted searches [70–73], where the area below the red line is excluded. Further, we show the cross section as colormap in the background and state the search which gave the strongest exclusion at each grid point.

List of Abbreviations

CHM Composite Higgs models

pNGB pseudo Nambu–Goldstone Boson

SM Standard Model

EW electroweak

irrep irreducible representation

VEV vacuum expectation value

CCWZ Callan-Coleman-Wess-Zumino

DOF degrees of freedom

WZW Wess-Zumino-Witten

QCD Quantum Chromo Dynamics

BSM Beyond the Standard Model

ABJ Adler-Bell-Jackiw

NWA Narrow-Width-Approximation

IR Infrared

UV Ultraviolet

References

[1] **ATLAS** Collaboration, G. Aad *et al.*, "Observation of a new particle in the search for the Standard Model Higgs boson with the ATLAS detector at the LHC," *Phys. Lett. B* **716** (2012) 1–29, arXiv:1207.7214 [hep-ex].

[2] **CMS** Collaboration, S. Chatrchyan *et al.*, "Observation of a New Boson at a Mass of 125 GeV with the CMS Experiment at the LHC," *Phys. Lett. B* **716** (2012) 30–61, arXiv:1207.7235 [hep-ex].

[3] P. W. Higgs, "Broken Symmetries and the Masses of Gauge Bosons," *Phys. Rev. Lett.* **13** (1964) 508–509.

[4] F. Englert and R. Brout, "Broken Symmetry and the Mass of Gauge Vector Mesons," *Phys. Rev. Lett.* **13** (1964) 321–323.

[5] G. S. Guralnik, C. R. Hagen, and T. W. B. Kibble, "Global Conservation Laws and Massless Particles," *Phys. Rev. Lett.* **13** (1964) 585–587.

[6] G. Panico and A. Wulzer, *The Composite Nambu-Goldstone Higgs*, vol. 913. Springer, 2016. arXiv:1506.01961 [hep-ph].

[7] S. Dimopoulos and L. Susskind, "Mass Without Scalars," *Nucl. Phys. B* **155** (1979) 237–252.

[8] L. Susskind, "Dynamics of Spontaneous Symmetry Breaking in the Weinberg-Salam Theory," *Phys. Rev. D* **20** (1979) 2619–2625.

[9] S. Weinberg, "Implications of Dynamical Symmetry Breaking," *Phys. Rev. D* **13** (1976) 974–996. [Addendum: Phys.Rev.D 19, 1277–1280 (1979)].

[10] T. Plehn, "Lectures on LHC Physics," *Lect. Notes Phys.* **844** (2012) 1–193, arXiv:0910.4182 [hep-ph].

[11] R. Contino, "The Higgs as a Composite Nambu-Goldstone Boson," in *Theoretical Advanced Study Institute in Elementary Particle Physics: Physics of the Large and the Small*, pp. 235–306. 2011. arXiv:1005.4269 [hep-ph].

[12] G. Ferretti, "UV Completions of Partial Compositeness: The Case for a SU(4) Gauge Group," *JHEP* **06** (2014) 142, arXiv:1404.7137 [hep-ph].

[13] L. Vecchi, "The Natural Composite Higgs," arXiv:1304.4579 [hep-ph].

[14] J. Goldstone, A. Salam, and S. Weinberg, "Broken Symmetries," *Phys. Rev.* **127** (1962) 965–970.

[15] M. E. Peskin, "The Alignment of the Vacuum in Theories of Technicolor," *Nucl. Phys. B* **175** (1980) 197–233.

[16] G. Cacciapaglia and F. Sannino, "Fundamental Composite (Goldstone) Higgs Dynamics," *JHEP* **04** (2014) 111, arXiv:1402.0233 [hep-ph].

[17] E. Katz, A. E. Nelson, and D. G. E. Walker, "The Intermediate Higgs," *JHEP* **08** (2005) 074, arXiv:hep-ph/0504252.

[18] A. Agugliaro, G. Cacciapaglia, A. Deandrea, and S. De Curtis, "Vacuum misalignment and pattern of scalar masses in the SU(5)/SO(5) composite Higgs model," *JHEP* **02** (2019) 089, arXiv:1808.10175 [hep-ph].

[19] D. Buarque Franzosi, "Towards the precise description of Composite Higgs models at colliders," arXiv:2302.02422 [hep-ph].

[20] S. R. Coleman, J. Wess, and B. Zumino, "Structure of phenomenological Lagrangians. 1.," *Phys. Rev.* **177** (1969) 2239–2247.

[21] C. G. Callan, Jr., S. R. Coleman, J. Wess, and B. Zumino, "Structure of phenomenological Lagrangians. 2.," *Phys. Rev.* **177** (1969) 2247–2250.

[22] A. Agugliaro, *Composite Higgs: Theory and Phenomenology*. PhD thesis, Florence U., 2019.

[23] M. Bando, T. Kugo, S. Uehara, K. Yamawaki, and T. Yanagida, "Is rho Meson a Dynamical Gauge Boson of Hidden Local Symmetry?," *Phys. Rev. Lett.* **54** (1985) 1215.

[24] M. Bando, T. Fujiwara, and K. Yamawaki, "Generalized Hidden Local Symmetry and the A1 Meson," *Prog. Theor. Phys.* **79** (1988) 1140.

[25] M. Bando, T. Kugo, and K. Yamawaki, "Nonlinear Realization and Hidden Local Symmetries," *Phys. Rept.* **164** (1988) 217–314.

[26] D. Buarque Franzosi, G. Cacciapaglia, H. Cai, A. Deandrea, and M. Frandsen, "Vector and Axial-vector resonances in composite models of the Higgs boson," *JHEP* **11** (2016) 076, arXiv:1605.01363 [hep-ph].

[27] R. M. Fonseca, "GroupMath: A Mathematica package for group theory calculations," *Comput. Phys. Commun.* **267** (2021) 108085, arXiv:2011.01764 [hep-th].

[28] X. Feng, K. Jansen, and D. B. Renner, "Resonance Parameters of the rho-Meson from Lattice QCD," *Phys. Rev. D* **83** (2011) 094505, arXiv:1011.5288 [hep-lat].

[29] G. Cacciapaglia, A. Deandrea, M. Kunkel, and W. Porod, "Coloured spin-1 states in composite Higgs models," *JHEP* **06** (2024) 092, arXiv:2404.02198 [hep-ph].

[30] D. B. Kaplan, "Flavor at SSC energies: A New mechanism for dynamically generated fermion masses," *Nucl. Phys. B* **365** (1991) 259–278.

[31] G. Ferretti and D. Karateev, "Fermionic UV completions of Composite Higgs models," *JHEP* **03** (2014) 077, arXiv:1312.5330 [hep-ph].

[32] G. Ferretti, "Gauge theories of Partial Compositeness: Scenarios for Run-II of the LHC," *JHEP* **06** (2016) 107, arXiv:1604.06467 [hep-ph].

[33] A. Belyaev, G. Cacciapaglia, H. Cai, G. Ferretti, T. Flacke, A. Parolini, and H. Serodio, "Di-boson signatures as Standard Candles for Partial Compositeness," *JHEP* **01** (2017) 094, arXiv:1610.06591 [hep-ph]. [Erratum: JHEP 12, 088 (2017)].

[34] M. J. Dugan, H. Georgi, and D. B. Kaplan, "Anatomy of a Composite Higgs Model," *Nucl. Phys. B* **254** (1985) 299–326.

[35] A. Banerjee *et al.*, "Phenomenological aspects of composite Higgs scenarios: exotic scalars and vector-like quarks," `arXiv:2203.07270 [hep-ph]`.

[36] G. Cacciapaglia, T. Flacke, M. Kunkel, W. Porod, and L. Schwarze, "Exploring extended Higgs sectors via pair production at the LHC," *JHEP* **12** (2022) 087, `arXiv:2210.01826 [hep-ph]`.

[37] A. Banerjee, D. B. Franzosi, and G. Ferretti, "Modelling vector-like quarks in partial compositeness framework," *JHEP* **03** (2022) 200, `arXiv:2202.00037 [hep-ph]`.

[38] W. Grimus and L. Lavoura, "The Seesaw mechanism at arbitrary order: Disentangling the small scale from the large scale," *JHEP* **11** (2000) 042, `arXiv:hep-ph/0008179`.

[39] E. Witten, "Global Aspects of Current Algebra," *Nucl. Phys. B* **223** (1983) 422–432.

[40] J. Wess and B. Zumino, "Consequences of anomalous Ward identities," *Phys. Lett. B* **37** (1971) 95–97.

[41] J. Davighi, *Topological effects in particle physics phenomenology.* PhD thesis, Cambridge U., DAMTP, 2020.

[42] W. Porod, "Zerfälle des Gluinos und der Squarks," Diplomarbeit, University of Vienna, July, 1993.

[43] N. D. Christensen and C. Duhr, "FeynRules - Feynman rules made easy," *Comput. Phys. Commun.* **180** (2009) 1614–1641, `arXiv:0806.4194 [hep-ph]`.

[44] C. Duhr, N. Christensen, and B. Fuks, "Standard Model - FeynRules," `https://feynrules.irmp.ucl.ac.be/wiki/StandardModel`, 2016. [Online; accessed 13-May-2024].

[45] J. Alwall, R. Frederix, S. Frixione, V. Hirschi, F. Maltoni, O. Mattelaer, H. S. Shao, T. Stelzer, P. Torrielli, and M. Zaro, "The automated computation of tree-level and next-to-leading order differential cross sections, and their matching to parton shower simulations," *JHEP* **07** (2014) 079, `arXiv:1405.0301 [hep-ph]`.

[46] R. D. Ball *et al.*, "Parton distributions with LHC data," *Nucl. Phys. B* **867** (2013) 244–289, `arXiv:1207.1303 [hep-ph]`.

[47] A. Buckley, J. Ferrando, S. Lloyd, K. Nordström, B. Page, M. Rüfenacht, M. Schönherr, and G. Watt, "LHAPDF6: parton density access in the LHC precision era," *Eur. Phys. J. C* **75** (2015) 132, `arXiv:1412.7420 [hep-ph]`.

[48] T. Sjöstrand, S. Ask, J. R. Christiansen, R. Corke, N. Desai, P. Ilten, S. Mrenna, S. Prestel, C. O. Rasmussen, and P. Z. Skands, "An introduction to PYTHIA 8.2" *Comput. Phys. Commun.* **191** (2015) 159–177, `arXiv:1410.3012 [hep-ph]`.

[49] M. Kunkel, "LHC Phenomenology of Top Partners in Models with SU(6)/Sp(6)," Master's thesis, University of Würzburg, September, 2021.

[50] E. Conte, B. Fuks, and G. Serret, "MadAnalysis 5, A User-Friendly Framework for Collider Phenomenology," *Comput. Phys. Commun.* **184** (2013) 222–256, `arXiv:1206.1599 [hep-ph]`.

[51] E. Conte, B. Dumont, B. Fuks, and C. Wymant, "Designing and recasting LHC analyses with MadAnalysis 5," *Eur. Phys. J. C* **74** no. 10, (2014) 3103, arXiv:1405.3982 [hep-ph].

[52] B. Dumont, B. Fuks, S. Kraml, S. Bein, G. Chalons, E. Conte, S. Kulkarni, D. Sengupta, and C. Wymant, "Toward a public analysis database for LHC new physics searches using MADANALYSIS 5," *Eur. Phys. J. C* **75** no. 2, (2015) 56, arXiv:1407.3278 [hep-ph].

[53] E. Conte and B. Fuks, "Confronting new physics theories to LHC data with MADANALYSIS 5," *Int. J. Mod. Phys. A* **33** no. 28, (2018) 1830027, arXiv:1808.00480 [hep-ph].

[54] D. Dercks, N. Desai, J. S. Kim, K. Rolbiecki, J. Tattersall, and T. Weber, "CheckMATE 2: From the model to the limit," *Comput. Phys. Commun.* **221** (2017) 383–418, arXiv:1611.09856 [hep-ph].

[55] **DELPHES 3** Collaboration, J. de Favereau, C. Delaere, P. Demin, A. Giammanco, V. Lemaître, A. Mertens, and M. Selvaggi, "DELPHES 3, A modular framework for fast simulation of a generic collider experiment," *JHEP* **02** (2014) 057, arXiv:1307.6346 [hep-ex].

[56] M. Cacciari, G. P. Salam, and G. Soyez, "The anti-k_t jet clustering algorithm," *JHEP* **04** (2008) 063, arXiv:0802.1189 [hep-ph].

[57] M. Cacciari and G. P. Salam, "Dispelling the N^3 myth for the k_t jet-finder," *Phys. Lett. B* **641** (2006) 57–61, arXiv:hep-ph/0512210.

[58] M. Cacciari, G. P. Salam, and G. Soyez, "FastJet User Manual," *Eur. Phys. J. C* **72** (2012) 1896, arXiv:1111.6097 [hep-ph].

[59] C. Bierlich *et al.*, "Robust Independent Validation of Experiment and Theory: Rivet version 3," *SciPost Phys.* **8** (2020) 026, arXiv:1912.05451 [hep-ph].

[60] J. Butterworth, "BSM constraints from model-independent measurements: A Contur Update," *J. Phys. Conf. Ser.* **1271** no. 1, (2019) 012013, arXiv:1902.03067 [hep-ph].

[61] A. Buckley *et al.*, "Testing new physics models with global comparisons to collider measurements: the Contur toolkit," *SciPost Phys. Core* **4** (2021) 013, arXiv:2102.04377 [hep-ph].

[62] A. L. Read, "Presentation of search results: The CL_s technique," *J. Phys. G* **28** (2002) 2693–2704.

[63] J. Erdmenger, N. Evans, W. Porod, and K. S. Rigatos, "Gauge/gravity dual dynamics for the strongly coupled sector of composite Higgs models," *JHEP* **02** (2021) 058, arXiv:2010.10279 [hep-ph].

[64] **ATLAS** Collaboration, G. Aad *et al.*, "Search for a heavy charged boson in events with a charged lepton and missing transverse momentum from pp collisions at $\sqrt{s} = 13$ TeV with the ATLAS detector," *Phys. Rev. D* **100** no. 5, (2019) 052013, arXiv:1906.05609 [hep-ex].

[65] **ATLAS** Collaboration, G. Aad *et al.*, "Search for high-mass dilepton resonances using 139 fb^{-1} of pp collision data collected at $\sqrt{s}$ =13 TeV with the ATLAS detector," *Phys. Lett. B* **796** (2019) 68–87, arXiv:1903.06248 [hep-ex].

[66] **CMS** Collaboration, A. M. Sirunyan *et al.*, "Search for high mass dijet resonances with a new background prediction method in proton-proton collisions at $\sqrt{s} = 13$ TeV," *JHEP* **05** (2020) 033, arXiv:1911.03947 [hep-ex].

[67] **ATLAS** Collaboration, G. Aad *et al.*, "Search for vector-boson resonances decaying into a top quark and a bottom quark using pp collisions at $\sqrt{s} = 13$ TeV with the ATLAS detector," *JHEP* **12** (2023) 073, arXiv:2308.08521 [hep-ex].

[68] **ATLAS** Collaboration, G. Aad *et al.*, "Search for $t\bar{t}$ resonances in fully hadronic final states in *pp* collisions at $\sqrt{s} = 13$ TeV with the ATLAS detector," *JHEP* **10** (2020) 061, arXiv:2005.05138 [hep-ex].

[69] **ATLAS** Collaboration, M. Aaboud *et al.*, "Search for photonic signatures of gauge-mediated supersymmetry in 13 TeV *pp* collisions with the ATLAS detector," *Phys. Rev. D* **97** no. 9, (2018) 092006, arXiv:1802.03158 [hep-ex].

[70] **ATLAS** Collaboration, G. Aad *et al.*, "Search for R-parity-violating supersymmetry in a final state containing leptons and many jets with the ATLAS experiment using $\sqrt{s} = 13TeV$ proton–proton collision data," *Eur. Phys. J. C* **81** no. 11, (2021) 1023, arXiv:2106.09609 [hep-ex].

[71] **ATLAS** Collaboration, G. Aad *et al.*, "Search for squarks and gluinos in final states with one isolated lepton, jets, and missing transverse momentum at $\sqrt{s} = 13$ with the ATLAS detector," *Eur. Phys. J. C* **81** no. 7, (2021) 600, arXiv:2101.01629 [hep-ex]. [Erratum: Eur.Phys.J.C 81, 956 (2021)].

[72] **CMS** Collaboration, T. C. Collaboration *et al.*, "Search for supersymmetry in proton-proton collisions at 13 TeV in final states with jets and missing transverse momentum," *JHEP* **10** (2019) 244, arXiv:1908.04722 [hep-ex].

[73] **CMS** Collaboration, A. M. Sirunyan *et al.*, "Search for supersymmetry in multijet events with missing transverse momentum in proton-proton collisions at 13 TeV," *Phys. Rev. D* **96** no. 3, (2017) 032003, arXiv:1704.07781 [hep-ex].

[74] **CMS** Collaboration, A. M. Sirunyan *et al.*, "Search for physics beyond the standard model in multilepton final states in proton-proton collisions at $\sqrt{s} = 13$ TeV," *JHEP* **03** (2020) 051, arXiv:1911.04968 [hep-ex].

[75] **CMS** Collaboration, A. Tumasyan *et al.*, "Search for new particles in events with energetic jets and large missing transverse momentum in proton-proton collisions at $\sqrt{s} = 13$ TeV," *JHEP* **11** (2021) 153, arXiv:2107.13021 [hep-ex].

[76] **ATLAS** Collaboration, G. Aad *et al.*, "Measurement of the $Z(\to \ell^+\ell^-)\gamma$ production cross-section in *pp* collisions at $\sqrt{s} = 13$ TeV with the ATLAS detector," *JHEP* **03** (2020) 054, arXiv:1911.04813 [hep-ex].

[77] S. Weinberg, *The Quantum theory of fields. Vol. 1: Foundations*. Cambridge University Press, 6, 2005.

Ich versichere, dass ich die vorliegende Masterarbeit selbstständig verfasst und nur die angegebenen Quellen und Hilfsmittel verwendet habe. Weiterhin versichere ich, dass ich die Arbeit bisher oder gleichzeitig keiner anderen Prüfungsbehörde zur Erlangung eines akademischen Grades vorgelegt habe.

Würzburg, den 01.08.2024

Acknowledgment

I am grateful for everybody who supported me through the past semesters of my Master's degree and in particular during the Master thesis. I especially would like to thank my supervisor Prof. Dr. Werner Porod for fascinating me for BSM physics and who always had an open door to discuss questions and problems that I had to face. Big thanks should also go to Manuel Kunkel who certainly was drilled with questions and was always able to help. In particular, your knowledge about simulation and recasting tools is invaluable.
Further, I'd like to acknowledge Christian Verollet for helping me out with the three-body decay calculation. I enjoyed working with you a lot! I am also thankful to Manuel Schmidt for explaining me how to use the julia cluster.
I would be remiss in not mentioning my parents, who supported me through the whole course of my studies and Felizitas for always covering my back.